RISK ASSESSMENT OF RADIOACTIVITY LEVELS IN NATURALLY OCCURRING RADIOACTIVE MATERIALS (NORM) ALONG THE NZIMA COASTLINE OF GHANA

A dissertation presented to the:

DEPARTMENT OF NUCLEAR SAFETY AND SECURITY

UNIVERSITY OF GHANA

By

BAAFI EUNICE NYARKO (ID: 10598881)

BSc (KNUST), 2014

MPhil (UG), 2018

In partial fulfilment of the requirements for the degree of

DOCTOR OF PHILOSOPHY

In

RADIATION PROTECTION

July, 2024

DECLARATION

I declare that this thesis is the outcome of the research work undertaken by Eunice Nyarko BAAFI in the Department of Nuclear Safety and Security, University of Ghana under the supervision of Prof. Augustine Faanu (Director, Radiological and Non-ionizing Radiation Directorate, NRA), Dr. Philip Deatanyah (Manager, HPC, Senior Research Scientist, RPI, GAEC) and Prof. David Okoh Kpeglo (Head, Department of Nuclear Safety and Security, SNAS; Manager, ERPC, Principal Research Scientist, RPI, GAEC).

Sign: 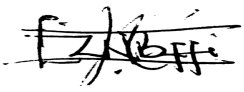

Baafi Eunice Nyarko (Student) Date: 08/11/2024.

Sign: 

Prof. David Okoh Kpeglo (Principal Supervisor) Date: 08/11/2024.

Sign: 

Prof. Augustine Faanu (Co-Supervisor) Date: 08/11/2024.

Sign: 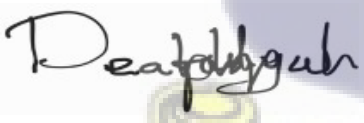

Dr. Philip Deatanyah (Co-Supervisor) Date: 08/11/2024.

ABSTRACT

Evaluation of naturally occurring radioactive material concentrations was conducted to establish the radioactivity levels of ^{238}U, ^{232}Th, ^{228}Th, ^{226}Ra, ^{228}Ra and ^{40}K in sea water, sand, and sediment along the coastal area of Western Ghana. The corresponding health hazards and risk associated with exposure to these radionuclides were also assessed. The findings from this study contributes to the environmental impact assessment and provide baseline information to assist in the selection of a site for the building of the planned nuclear power plant in Ghana. The radioactivity concentrations were determined by gamma and alpha spectrometry analyses using a high-purity germanium (HPGe) detector and an alpha analyst, respectively. The total samples collected were 80 beach sand samples, 80 sea sediment samples and 80 sea water samples. The results of activity concentration in the beach sand samples using the high- resolution gamma-ray spectrometry was 21.97±3.6 $Bqkg^{-1}$ for ^{238}U; 22.41±4.5 $Bqkg^{-1}$ for ^{232}Th; 344.98±90.7 $Bqkg^{-1}$ for ^{40}K and 21.31±1.8 $Bqkg^{-1}$ for ^{226}Ra; 20.65±6.4 $Bqkg^{-1}$ for ^{228}Ra and 20.42±2.4 $Bqkg^{-1}$ for ^{228}Th. The results of the sediment samples were 21.24±3.8 $Bqkg^{-1}$ for ^{238}U; 21.77±3.7 $Bqkg^{-1}$ for ^{232}Th; 305.54±68.4 $Bqkg^{-1}$ for ^{40}K and 19.00±1.4 $Bqkg^{-1}$ for ^{226}Ra; 16.54±4.6 $Bqkg^{-1}$ for ^{228}Ra and 26.86±2.9 $Bqkg^{-1}$ for ^{228}Th. The sea water samples also provided values of 1.55±0.6 BqL^{-1} for ^{238}U; 2.05±0.5 BqL^{-1} for ^{232}Th; 11.83±1.6 BqL^{-1} for ^{40}K and 0.86±0.1 BqL^{-1} for ^{226}Ra and 2.65±0.4 BqL^{-1} for ^{228}Th. The calculated average activity concentration of beach sand samples using alpha spectrometry analysis for ^{232}Th, ^{238}U, ^{234}U and ^{230}Th were 1.10 ±0.3 $Bq.kg^{-1}$, 2.02±0.6 $Bq.kg^{-1}$, 1.34±0.7 $Bq.kg^{-1}$, and 1.66±0.8 $Bq.kg^{-1}$, respectively. That of the sea sediment were estimated to be 2.69±0.4 $Bq.kg^{-1}$, 3.11±0.8 $Bq.kg^{-1}$, 1.53±0.6 $Bq.kg^{-1}$, and 2.23±0.8 $Bq.kg^{-1}$ for ^{232}Th, ^{238}U, ^{234}U and ^{230}Th, respectively.

The estimated average absorbed dose rate (D), radium equivalent activity ($Raeq$) and the annual gonadal dose (AGD), for beach sand samples were 36.62 $nGyy^{-1}$, 77.12 $Bqkg^{-1}$, and 259.85 μSvy^{-1}, respectively. The estimated average annual effective dose (AED) from soil samples was 0.11 mSv y^{-1}, which is below the recommended value of 1 mSv y^{-1} for the public. The external hazard index (H_{ext}) and the internal hazard index for beach sand were 0.21 and 0.27, respectively. The activity utilization index and the representative level index also gave average values of 0.47 and 0.11, respectively. The estimated mean cancer risk for beach sand was 0.17×10^{-3}. The estimated absorbed dose rate (D) for sea sediment was 35.41 $nGyy^{-1}$, while the mean value obtained for radium equivalent activity ($Raeq$) was 75.29 $Bqkg^{-1}$. The average estimated annual effective dose (AED) from soil samples was 0.11 mSv y^{-1}. The average estimated annual gonadal dose (AGD) was 250.55 μSvy^{-1}. The external hazard index (H_{ext}) and the internal hazard index recorded mean values of 0.20 and 0.26, respectively. On the other hand, the activity utilization index and the representative level index recorded average values of 0.48 and 0.12, respectively. All the hazard indices show that the samples from the western coast area do not pose any significant hazard. The Excess Lifetime Cancer Risk (ELCR) of sea sediment was 0.15×10^{-3} which is within the globally accepted reference level of 0.29×10^{-3} as recommended by UNSCEAR. These values suggest that the risk of cancer due to exposure to these radionuclides is minimal for the coastal population.

An empirical model was developed using statistical techniques in R programming to assess the risk of exposure to Naturally Occurring Radioactive Materials (NORM) along the coastal areas of Western Ghana. The analysis focused on determining the relationships between key radionuclides, using a multiple linear regression approach. The ^{228}Ra radionuclide was set as the dependent variable, while ^{232}Th, ^{228}Th, and ^{40}K were the independent variables. R code scripts were employed for data manipulation, regression analysis, and diagnostic checks. The output of the model provided

the intercept and coefficients for the predictor variables, highlighting that ^{232}Th had the strongest positive influence on ^{228}Ra levels, while ^{40}K had an insignificant impact. Statistical diagnostics such as p-values, R-squared, and adjusted R-squared values were calculated to evaluate the model's fit, revealing that the model explained 99.36% of the variability in ^{228}Ra concentrations which suggests its close relationship to the predictor variables. Residual diagnostics, correlation tests, and multicollinearity assessments were also performed to ensure the model's validity and to interpret the relationships among radionuclides accurately. The overall codebase supported effective data analysis, provided a robust predictive model for radiation risk assessment, and stressed on the need for targeted monitoring of key radionuclides, particularly ^{232}Th, to ensure effective management of NORM-related risks in the western coast of Ghana.

DEDICATION

This research work is dedicated to my loving husband, children, and parents.

ACKNOWLEDGEMENTS

Am most grateful to God for the successful completion of this research work. My utmost appreciation goes to my supervisors (Prof. Augustine Faanu, Dr. Philip Deatanyah and Prof. David Okoh Kpeglo) for their constructive criticisms, encouragement, and insightful contributions towards this research work.

Lastly, I express my profound gratitude to the management of the Radiation Protection Institute (RPI), Ghana Atomic Energy Commission (GAEC), the gamma spectrometry and alpha spectrometry laboratory and all who assisted me in various ways till the completion of this thesis.

LIST OF ABBREVIATIONS

AED	-	Annual Effective Dose
APPEA	-	Australian Petroleum Production and Exploration Association
AGD	-	Annual Gonadal Dose
AUI	-	Activity Utilization Index
ASTM	-	American Society for Testing and Materials
CNSC	-	Canadian Nuclear Safety Commission
CCME	-	Canadian Council of Ministers for the Environment
ELCR	-	Excess Lifetime Cancer Risk
GPS	-	Global Positioning System
GSS	-	Ghana Statistical Services
H_{ex}	-	External Hazard Index
H_{in}	-	Internal Hazard Index
IAEA	-	International Atomic Energy Agency
ICRP	-	International Commission on Radiological Protection
IARC	-	International Agency for Research on Cancer
MCA	-	Multi-Channel Analyzer
MDA	-	Minimum Detectable Activity

NEA-OECD	-	Nuclear Energy Agency-Organization for Economic Co-operation and Development.
NCRP	-	National Council on Radiation Protection and Measurement
NORM	-	Naturally Occurring Radioactive Material
NPG	-	Nuclear Power Ghana
NPP	-	Nuclear Power Plant
NRC-NAS	-	National Research Council-National Academy of Sciences
PIPS	-	Passivated Implanted Planar Silicon
Ra_{eq}	-	Radium Equivalent Activity
RLI	-	Representative Level Index
SAEPA	-	South Australian Environmental Protection Authority
TEN	-	Tweneboah, Enyera and Ntomme
USEPA	-	United States Environmental Protection Agency
UNSCEAR	-	United Nations Scientific Committee on the Effects of Atomic Radiation
WAINPG	-	West African Integrated Nuclear Power Group
WERF	-	Water Environment Research foundation

TABLE OF CONTENTS

LIST OF TABLES

LIST OF FIGURES

LIST OF PLATES

CHAPTER ONE

INTRODUCTION

1.1 Background

Human beings are constantly exposed to different sources of radiation. Radiation refers to the emission of energy in the form of waves or particles from a source which travels through space or other mediums. The sources of radiation can be natural or artificial. Artificial radiation comes from a number of sources, including medical applications to cure patients, and industrial and nuclear applications to satisfy the demand or need for alternative sources of energy (UNSCEAR, 2000). Natural radioactive materials are ubiquitous in the environment, and as a result, they are known to be the major source of natural radiation. A substantial quantity of them has been found in the earth's crust, in soil, water and air (Vearrier et al., 2009). According to (UNSCEAR, 2000), they are the obvious source of radiation to which human beings are most exposed. Therefore, health protection measures need to be considered, as humans are at risk of exposure to the effects of radiation.

Natural radionuclides occur in different concentrations and there are two types of sources. They are the primordial (^{238}U, ^{235}U and ^{232}Th decay series, ^{40}K, ^{87}Rb) and cosmic ray interactions (^{3}H, ^{14}C, ^{7}Be). The primordial radionuclides that are of significant interest are uranium (^{238}U, ^{235}U), thorium (^{232}Th) and potassium (^{40}K) (Thorne, 2003). Cosmic radiation emitted from space is the other naturally occurring radioactive source. The basic cosmic radiation particles have high energies which produce secondary particles in the upper atmosphere and subsequently enter the earth's atmosphere to ground level (Santawamaitre, 2007).

The concentrations of primordial radionuclides are known to depend on the geological nature of the local area and as such differ with location (Faanu et al., 2012). Most reservoir rocks contain

a variable amount of naturally occurring primaeval radioactive materials. Natural radioactive materials which occur in reservoir rocks have minute quantities of natural uranium and thorium (Smith, 1992). Uranium is found in rocks in concentrations of approximately 4 ppm. Thorium on the other hand, is about three times as prevalent as uranium. Alluvial formations comprising black shale, common shale, orthoquartzites, claystone, siltstones, sandstones, carbonates, carbonate rocks, halite, bentonites, anhydrite, chert, and phosphate rock, can contain uranium and thorium according to (Alnabhani et al., 2015). The concentration of radionuclides varies depending on the kind of rock. For instance, black shale, like that found in the Marcellus, frequently has higher amounts of ^{238}U, ^{235}U, ^{232}Th, and ^{40}K than grey shale, limestone, or sandstone which have less organic content. Additionally, geological formations, oil and natural gas also contain a variety of radionuclides. (Chambers, 2015).

About 80% of human exposure to radiation emanate from radioactive sources that occur naturally (Adebiyi et al., 2021) with a greater amount coming from oil and gas production (Avwiri and Ononugbo, 2012). Oil and gas exploration activities have been ongoing in different areas along the west coast of Ghana for several years. Some of the oil fields that have emerged since that time include the TEN oil field, Jubilee, Odum, Saltpond, etc. Natural radionuclide concentrations in the area near oil and gas plants may rise, raising additional concerns about potential effects on people and the environment. The daily production of crude oil from offshore and onshore drilling activities contains radioactive materials which undoubtedly have a high level of risk and as such may harm people and the environment. Offshore activities of the oil and gas industry, as argued (Ite et al., 2013), have a very high probability of exposing the inhabitants of communities along the coastal areas to high levels of radioactivity.

The intake of seafood caught in sea waters for sustenance and plants gathered from the shore increases the risk of radiation exposure. The risk of radiation exposure may be through ingestion of contaminated sea food, water or crops which is one of the environmental pathways of radiation exposure. The basic natural radionuclides of concern in this case, which are very detrimental to health are ^{226}Ra and ^{228}Ra (Kpeglo, 2015). These isotopes are the decay products of ^{238}U and ^{232}Th. Other radionuclides that may be of interest, particularly in gas processing are ^{210}Pb and ^{222}Rn, which are occasionally present in natural gas (Ahmad et al., 2021). Produced water is created during the reservoir formation process and is produced along with the oil or gas. Individuals who ingest large quantities of sea food harvested from areas closest to produced water discharge points have the potential to risk exposure to particularly radium (Kpeglo, 2015). Produced water for sea discharge is known to contain up to 48 ppm of petroleum (Emam et al., 2014). Heavy metals and a sizable number of hydrocarbons are present in these discharges, which can have an impact on the marine ecosystem. In the case of oil spillage, marine organisms and their habitats (ecosystems) would be exposed to the detrimental effects of the naturally occurring radionuclides (Ajayi et al., 2009).

Exploration into additional non-fossil fuel forms of energy has increased due to the demand for a reliable, secure source of energy (Agyekum et al., 2021). Nuclear energy has some benefits over conventional electricity generation methods, such as having no carbon emissions, minimal operational and fuel expenses, a distribution of fuel sources that is balanced globally and lengthy operational times (Baskurt and Aydin, 2018).

The energy demand for industrialization purposes has resulted in many countries in Africa, including Ghana, exploring the need to consider nuclear energy according to the World Nuclear Association. Consequently, Ghana has ramped up its efforts to incorporate nuclear power into its

energy mix by the year 2030 to aid the country's industrialization drive. The Nuclear Power Ghana, the body mandated to oversee the deployment of nuclear power in Ghana has identified four candidate sites for the nuclear plant (Nuclear Power Ghana, 2022). According to (Ennison et al, 2013) the preferred location for the deployment of a power plant has been limited to areas along the west coast (Western Region) of Ghana due to the availability of water for cooling. With this anticipation, it raises radiation protection concerns, as the potential releases of radioactive materials from the nuclear plant could have a negative effect on the public and the environment. In addition, Ghana's oil rig is also located offshore of the western coast and the possible contamination from waste materials arising from the oil and gas production and unintended spills and chemical pollution from the activities of the petroleum industry cannot be overruled. It is, therefore, imperative that an evaluation of the risk of exposure to radiation of the critical group on the west coast is undertaken. Establishing the radioactivity levels of the sea water, sea sediment, sand and their related hazards along the west coast is relevant. This data can also serve as a reference for further research in the future.

1.2 Problem Statement

About 23 to 60% of the world's population are inhabitants of coastal areas. In Ghana, 25% of its population live along the coastal area due to its multiple use (Boye & Fiadonu, 2020) . The increased population growth of the coast and infrastructural development along the coast has the potential to elevate levels of radioactivity in the coastal environment. Consequently, the health of the human and marine ecosystems may be negatively impacted by radionuclide contamination of the coastal environment (Nyarko et al., 2011). This is especially so with the envisaged development of the nuclear power infrastructure in the study area which has the potential to

produce large volumes of wastes which could contain high concentrations of naturally occurring radionuclides.

Whilst a limited number of studies have been conducted along parts of the coastal areas and specifically near the production site of oil fields in Saltpond and have established some preliminary data for the coastal communities the area (Kpeglo, 2015) , more extensive studies is necessary to cover the entire stretch of the area.

The above reasons and in addition to the intention of Ghana to include nuclear power in its energy mix, make it imperative to establish radiological data which will be needed as part of the site characterization for siting of a facility such as the nuclear power plant. This information will be helpful for future evaluations of potential environmental evolutions of the study area possibly due to the pollution and spills arising from human activities including the extractive industry as well as for assessing the current radiological state of the coastal environment.

Furthermore, modeling of the impact of spillage of materials into the coastal areas will be carried out to ascertain the radiological risk of the long-term consumption of seafood in the study area based on hypothetical levels of exposure since fish is the single most important low-cost animal protein source in Ghana (Amoasah, 2010; Hasselberg et al., 2020). Radionuclides may enter the food chain and through bioaccumulation effects with the potential to cause chronic diseases in humans.

Currently, there is very little information available on the radiation levels along the coastal area of Ghana and other coastal areas of West Africa, and this is the motivation for this study. A study by Botwe et al. (2017) on natural radioactivity levels in Ghana's coastal environment covered only the beach sediments.

This study focused on determining the radioactivity levels of the natural radionuclides, ^{238}U and ^{232}Th and their decay series radionuclides in sea water and soil/sand along the coast (beach sand), and sea sediment. The data from the radioactivity concentration levels will be used to assess the radiological risks of exposure to natural radionuclides to the environment and inhabitants of the study area. The modeling of the risk of exposure will be done using the R software for the data analysis to predict the exposure rate of the population.

1.3 Objectives of Research

This research work aims to establish the radioactivity levels of ^{238}U, ^{40}K, ^{228}Th, ^{228}Ra, ^{226}Ra and ^{232}Th in sea water, beach sand, and sediment as well as assess the human health risk of the exposure to these radionuclides along the coastal area of Western Ghana.

The specific objectives of this research work are to:

i. Determine the activity concentration levels of ^{238}U, ^{40}K, ^{228}Th, ^{228}Ra, ^{226}Ra and ^{232}Th radionuclides in sea water, beach sand, and sea sediment along a portion of the coastal areas of western Ghana.
ii. Evaluate the radiation hazard indices, annual effective dose, the radium equivalent activity, activity utilization index and gamma representative level index.
iii. Estimate the Excess Lifetime Cancer Risk (ELCR) of the reference group.
iv. Assess the exposure rate of the critical population using a predictive model.

1.4 Relevance of the Study

The spread of radioactivity in the environment and its levels is investigated to offer crucial radiological data for future use. Ghana's west coast has had considerable exploration activity,

including sand mining for construction, oil and gas exploration, and many other uses of the coastal area by indigenes. Nonetheless, the coastal zone has been subjected to only a few radionuclide assessments and analyses.

Reference data describes the natural environmental variation. It is used to assess the current radiological condition of the coastal environment as well as subsequent assessments of potential environmental contamination owing to extractive industry activities including nuclear power plants, oil, gas, etc. This data will be useful to oil field operators, policy makers and other stakeholders as reference information to assess any future differences in the background radioactivity level because of geological processes and artificial influences from industries in the environment, as well as for compliance.

Finally, this work will serve as a blueprint for radioactivity concentration mapping along the west coast of Ghana.

1.5 Scope of Research

This study was limited to measurements of the activity concentrations of ^{238}U, ^{40}K, ^{228}Th, ^{228}Ra, ^{226}Ra and ^{232}Th in sea water, beach sand and sea sediment along the coastal areas of the Western region of Ghana. The health risk assessment was done using the activity concentrations obtained from the analysis of the radionuclides.

1.6 Presentation of Dissertation

There are six chapters in this work. The historical setting is described in Chapter One along with the purpose, significance, and boundaries of the study. The review of radioactivity in the environment, its effects, and related scholarly study are the main topics of Chapter Two. The study

region is described in full in Chapter Three, and the methodology and resources used are also covered. Chapter Four highlights the findings and the debates that go along with them. Chapter Five discusses the findings. The study's summary results, key findings, and suggestions for important stakeholders are presented in Chapter Six, the last chapter.

CHAPTER TWO

LITERATURE REVIEW

2.1 Radioactivity

The term "radioactivity" is used to characterize the spontaneous atomic transitions that involve changes in the nuclei of atoms and emit energy and particles of ionizing radiation. Each nucleus releases a charged particle as it disintegrates to form a more stable combination. Because of its kinetic energy, this charged particle can penetrate solid objects. Such a transition releases energy that is emitted as electromagnetic radiation and particles of considerable penetrating power (Al Nabhani, 2021).

The three most prevalent types of radiation are generally categorized as alpha, beta, and gamma radiation. Other types of nuclear radiation include neutron or proton emission, as well as the spontaneous fission of large nuclei. All forms of radiation are energy transfers from the emitting source to the intervening medium, where they may interact to varying degrees depending on the radiation's properties and the structure of the medium.

2.2 Sources of Radiation

Humans are inevitably exposed to ionizing radiation from the environment. Radioactive sources outside the body can cause external exposure, while radioactive substances inside the body can cause internal exposure (UNCSEAR, 2008). Humans are mostly exposed to radiation internally and externally through natural sources. In addition to natural sources, human activities that involve the use of radiation and radioactive materials also expose people to radiation (Martin

and Harbison, 2006). Humans are also exposed to radiation through medical treatments as well as laboratory activities involving the use of radioactive material.

2.2.1 Natural sources

Naturally occurring radioactive elements are found in soils, rocks, water, air, vegetation, the human body, and all living tissues in different concentrations (SAEPA, 2017). The sources of natural radioactivity can be categorized as terrestrial and cosmic radiation. In nature, there are more than sixty (60) radionuclides that fall into two categories: primordial and cosmic radionuclides. The primordial radionuclides include ^{232}Th, ^{238}U, ^{235}U, and ^{40}K, while the cosmic radionuclides include ^{36}Cl, ^{32}Si, ^{7}Be, ^{14}C, ^{10}Be, ^{26}Al, and ^{3}H (Adebiyi et al., 2021; Khandaker et al., 2012).

2.2.1.1 Cosmic Radiation

Cosmic radiation continuously bombards the Earth's outer atmosphere. Cosmic radiation typically consists of swiftly moving particles that are present in space and come from a range of sources, such as the sun and other celestial occurrences in the universe. Mostly protons, cosmic rays can also be other particles or wave energy. Natural radiation exposure happens when ionizing radiation enters the Earth's atmosphere and is absorbed by people (CNSC, 2019). These radiations are responsible for producing various radionuclides in the environment such as ^{7}Be, ^{14}C, and ^{3}H. Cosmic radiation from space and radioactive compounds found in the environment at large, including the human body, are the main causes of natural radiation exposure. The distribution of these natural radiation sources accounts for approximately 85% of the average yearly dosage of 2.4 mSv that the global population receives (Dołhańczuk-Śródka, 2012). Cosmic ray interactions

account for 15% of the overall dose from natural sources at sea level, but latitude and especially altitude are the variables that lead to dose rate changes from these environmental exposures (UNSCEAR, 2008). At the cruising altitude of commercial aircraft, cosmic ray exposure is much more than at sea level (UNSCEAR, 2000). Primordial radionuclides constitute a major contributor to the annual dosage of naturally occurring radiation in addition to cosmic - ray produced radiation. Table 2.1 shows the radiation levels at different altitudes.

Table 2.1: Levels of radiation at different altitudes (UNSCEAR, 2000)

Altitude (km)	Exposure Rate (μSvh^{-1})
15	10.0
10	5.0
6.7	1.0
2	0.01
Sea level	0.03

2.2.1.2 Terrestrial Radiation

The materials that make up the earth's crust are a significant source of natural radiation. Natural uranium, potassium, and thorium deposits that naturally decay and generate trace amounts of ionizing radiation are the principal contributors. Thorium and uranium can be found almost anywhere. Natural radiation exposure can occur indoors as well as outside because traces of these minerals are present in building materials (CNSC, 2019). Terrestrial radiations are released into the environment by the decay of primordial radionuclides like ^{40}K, naturally existing radionuclides of the ^{238}U and ^{232}Th series, and their offspring in the earth's crust. As a result of inhaling radon

and its breakdown products, a person living in an area with reasonably high soil radium content may receive a dosage of up to 100 mSv annually, whereas the ICRP has set a 1 mSv annual exposure limit for the general population (UNSCEAR, 2000).

2.2.1.3 Inhalation and Ingestion

The body absorbs radioactivity from the environment through air intake, food and water consumption, and skin contact. Natural radioactive nuclides (^{40}K, ^{238}U, and ^{232}Th) series, fission or activation products, and cosmogenic nuclides (^{3}H, ^{14}C, and ^{22}Na) make up most of the causes of internal exposure (^{131}I, ^{134}Cs, ^{137}Cs, ^{90}Sr and ^{60}Co). The radioactive decay of ^{238}U results in the production of radon, an odorless and colorless gas. As an inert gas, it does not react with the environment in any way or with surrounding matter. It readily moves up through the ground and into the atmosphere since it does not react. Thorium produces a radioactive gas known as thoron. Depending on the composition of the soil and bedrock, radon and thoron levels may vary widely from place to place. These gases are generally discharged into the air and diluted to safe levels in the atmosphere, but occasionally they are trapped and built up inside buildings, where they are inhaled by residents. If radon gas is allowed to build up in homes, it can be harmful to homeowners (Stanley et al., 2019). It exposes them to the largest source of natural radiation, on average.

According to (UNSCEAR, 2000), ordinary foods such as vegetables, cereals, fruit, and milk also contain some form of radioactivity. Naturally occurring radioactive materials can be found in trace concentrations in certain foods and water sources. For instance, soil and groundwater that contain radioactive elements are often used to grow crops. Internal radiation hazards are caused by this radioactivity, which is deposited in several important human organs. ^{40}K and ^{14}C, two naturally occurring radioactive isotopes, share the same chemical and biological characteristics as their non-

radioactive isotopes. Our bodies are built and maintained using these radioactive and non-radioactive components. With the basis of the International Commission on Radiological Protection, ICRP-30 statistics (ICRP, 1979), Table 2.2 shows the estimated activity that results in internal exposure to a 70 kg adult because of inhalation or ingestion of the sources.

Table 2.2: Estimated activity levels of naturally occurring radionuclides in ICRP Reference Man (ICRP, 2007)

Nuclide	Mass of nuclide	Activity	Daily intake
Uranium	90 µg	1.1 Bq	1.9 µg
Thorium	30 µg	0.11 Bq	3 µg
Potassium	17 mg	$4.4 * 10^3$ Bq	0.39 mg
Radium	31 pg	1.1 Bq	2.3 pg
Carbon-14	95 µg	$15 * 10^3$ Bq	1.8 µg
Tritium	0.06 pg	23 Bq	0.003 pg
Polonium	0.2 pg	37 Bq	0.6 µg

2.2.2 Artificial Sources

People are exposed to radiation from different man-made sources of radioactivity, as reported by UNSCEAR, 2000, in addition to background radiation from the environment. Most of these activities result in enhanced levels of radioactivity. Some of the typical instances in industrial, medicinal, and nuclear applications include:

2.2.2.1 Atmospheric Testing of Nuclear Weapons and Accidents

Radioactive material, known as fallout, was released into the atmosphere during atmospheric testing of atomic weapons from the conclusion of World War II until 1980. The fallout was absorbed into the environment as it settled on the ground. Additionally, the Chernobyl and Fukushima nuclear plant catastrophes contributed to the fallout's global dispersal (UNSCEAR,

2008). Some of the fallout continues to decay to date even though a large portion had short half-lives and no longer exists. Doses to people and the environment from fallout progressively reduce from year to year (Bourguignon & Scholz, 2016).

2.2.2.2 Medicine

Radiation is widely used in medical procedures. The use of X-rays, radioisotopes, and other contemporary procedures in medical diagnostics is seen as being second in importance only to background radiation from the environment (Donya et al., 2014). The most well-known application of radiation is in X-ray equipment, which employ it to discover broken or shattered bones and identify disease. The trend is anticipated to continue because radioisotopes are widely used in nuclear medicine for diagnostic or therapeutic purposes, even if the doses delivered in various types of X-ray scans range from a small fraction of a m Gy to tens of m Gy (ICRP, 2021).

2.2.2.3 Industrial Sources

From nuclear gauges used to build highways to density gauges used to measure material flow via pipes in factories, radiation is employed in industry for a variety of objectives. Additionally, it is used to estimate oil field reserves as well as in computers, televisions, smoke alarms and some glow-in-the-dark exit signs. Sterilization is another radiation application, in which large, heavily shielded irradiators are utilized. Radioactive components found in building materials, phosphate fertilizers, crushed rock, and other consumer goods are a few less major sources of radiation (Razak, 2015).

2.2.2.4 Nuclear Applications

In nuclear power reactors, most of the radiation produced is safely controlled. Nuclear power plants (NPPs) use uranium to fuel a sequence of processes that result in steam, which drives turbines to produce electricity. Humans are exposed to low levels of radiation because of the routine emission of radioactive material from nuclear power facilities (IAEA, 2011). A minuscule section, nevertheless, does escape as stack gas or liquid effluent and could potentially contaminate the air and water sources. Similar discharges from nuclear fuel reprocessing facilities add to the background radiation level globally. The population receives a dose of radioactivity from uranium mines and facilities that handle radioactive waste.

According to UNSCEAR (2000), the average annual radiation exposure from man-made and natural sources is 2.4 mSv. However, this amount varies by a factor of several hundred percent depending on the location. Figure 2.1 displays the distribution of radiation doses from several natural and man-made sources. It demonstrates that radon accounts for 82% of the overall average yearly effective dosage that comes from natural radiation sources. The majority of the remaining 18% comes from medical diagnosis and treatments, with less than 1% coming from nuclear power and fallout.

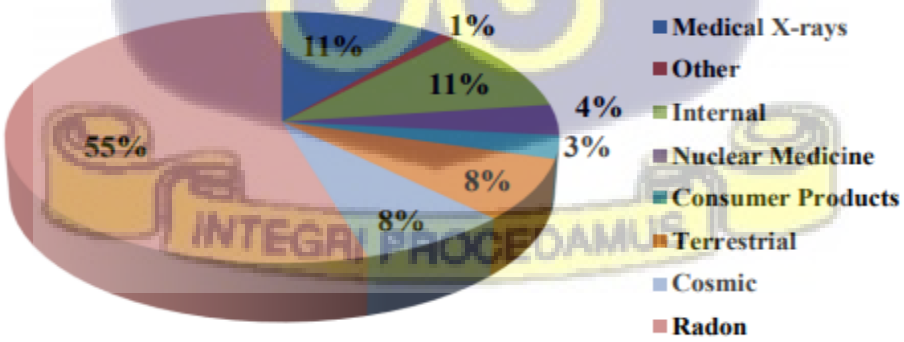

Figure 2.1: Contributions of radiation sources to annual effective dose (UNSCEAR, 2000).

Table 2.3: Ranges and averages of the concentrations of ^{40}K, ^{232}Th and ^{238}U in rocks and soils (UNSCEAR 2000)

Radionuclide	Median activity concentration ($Bqkg^{-1}$)	Population-weighted average ($Bqkg^{-1}$)	Typical global range ($Bqkg^{-1}$)
^{40}K	400	420	100 – 700
^{238}U	35	33	10 – 100
^{232}Th	30	45	7 – 200

2.3 Exposure to Environmental Radiation

The maximum radiation that people are typically exposed to comes from natural sources. According to studies, more than 80 % of the environmental radiation in the world comes from natural sources (Doyi, 2015). The interaction between primordial radionuclides in the earth's crust and atmospheric cosmic rays is the primary cause of environmental radiation exposure (UNSCEAR 2008; Jasaitis et al., 2020). They are found in various forms of media in the environment such as in sand, water, air, sediment, and many others. Geological processes such as weathering, erosion, and the dissolution of rocks in groundwater can cause primordial radionuclides to be distributed across the natural environment like streams, rivers, and seas, as such uranium, potassium and thorium can be found everywhere. More than 40% of the world's population, according to the United Nations Mission in South Sudan, live within 100 kilometers of the coast due to the multiple uses of the coast and coastal resources. Therefore, they are radiologically exposed to the detrimental effects of natural radionuclides. Beach dwellers and fishermen are constantly exposed to gamma radiation directly from beach sands.

Studies on natural radionuclides in soil and water media from coastal areas have been undertaken in great numbers, and these studies have provided information on the type and levels

of background radiation as well as changes in radioactivity levels in that area. Most investigations indicate that ^{40}K and nuclides from the uranium and thorium series are present in most soils and sediments, though their amounts can vary greatly. The amounts and distributions of these radionuclides are important because they give useful information for monitoring natural radioactivity contamination in the environment (Yii et al., 2009).

The narrative is also true for sea water, sediments and sea sand which are known to hold a variety of pollutants, including radionuclides. The radioactivity level in marine environments has been influenced by anthropogenic activities. The main causes of high radioactivity levels in various marine habitats have been identified as nuclear accidents, industrial discharges, and the release of nuclear waste. Numerous studies conducted all over the world (Al-Mur & Gad, 2022) have seen human nuclear-related activities which have left uranium footprints in the sediments of the Baltic Sea, uranium discharged from the phosphate plant and Sellafield nuclear-fuel reprocessing facility which has led to the enrichment of ^{238}U, ^{236}U, and ^{234}U in the sea sediment from Loch Etive in Scotland, and mining-related activities that have elevated values of ^{226}Ra and ^{235}U in Stratoni port, Greece. The background levels of ^{226}Ra and ^{40}K in Bafa Lake in Turkey, were found to have increased dramatically, according to Aközcan et al., (2018). These hot spots were attributed to agricultural and industrial activity.

In Ghana, the baseline data on radionuclide activity concentrations of ^{210}Pb, ^{137}Cs and ^{226}Ra in coastal sands along the Ghanaian coast were determined by Nyarko et al., (2011) using gamma spectrometry. From the study, the beach sand was found to contain very low levels of ^{210}Pb and ^{226}Ra, while activity concentrations of ^{137}Cs were below the detection limit of 0.4 $Bqkg^{-1}$. Comparatively, the levels of radionuclides measured in the study were lower with results obtained from similar studies in other countries like Turkey, Egypt, and Brazil. However, continuous

monitoring of radionuclides in all compartments of the coastal environment of Ghana from this study was recommended.

In other studies, (Lawluvi, 2016) suggested beach sand does not pose a significant radiological hazard to fishermen and beach users. The corresponding values obtained from the study, which was conducted using gamma spectrometry, for the beaches of the Volta region, were below the average background doses obtained for terrestrial radionuclides worldwide. This was ascribed to the samples' low gamma dose rates, which were measured in relation to the public dose limit of 1mSv y^{-1}. With an average value of 0.18 mSv y^{-1}, the estimated yearly external effective dose rates ranged from 0.05 to 0.40 mSv y^{-1}.

Although a series of studies on natural radioactivity have been conducted along the coast of Ghana, radiological data in the country is limited, especially applying analytical techniques other than gamma spectrometry. Lots of studies which have been conducted on natural radioactivity levels in the environment have focused on the mining areas (Nyarko et al., 2011). However, data on radionuclides in the coastal environment of Ghana are only a few.

Some coastal communities in Ghana such as Saltpond, which is nearest to the production site of oil fields have been assessed for naturally occurring radionuclides (Kpeglo, 2015), and the radioactivity concentrations which were recorded were lower compared to international standards. This study, therefore seeks to assess the radioactivity levels of other coastal communities as the exponential growth of coastal population and development in infrastructure could lead to significantly increased levels of radioactivity in the coastal environment (Nyarko et al., 2011). This is to add to the blueprint of radioactivity along the coast of Ghana.

In other jurisdictions, oil exploration and production activity in Egypt's Gulf of Suez (Diab et al. 2019) has led to a modest increase in ^{238}U and ^{232}Th levels along its coast. Al-Mur & Gad,

(2022) again reported that the Gulf of Bothnia, the Swedish coast, the Amvrakikos Gulf (Greece), Vefsnfjord (Norway), the Black Sea, and the Baltic Sea are only a few of the European locations where Chernobyl's effects may still be seen in marine sediments. The Fukushima accident unleashed radionuclides that have traveled over a large portion of the Pacific Ocean and are now being stored in marine sediments.

A study was conducted in Chittagong, Bangladesh, for instance, on the investigation of the concentrations and distribution of radionuclides in coastal soils and river sediments by Chowdhurry et. al. (1999) found the activity concentrations of ^{40}K, ^{232}Th and ^{238}U to be higher than the average international values of 400 $Bqkg^{-1}$, 30 $Bqkg^{-1}$, and 35 $Bqkg^{-1}$ (UNSCEAR, 2000), respectively.

The radioactivity levels of the soil and sediment in Turkey, Firtina Valley, were measured by a research group from Karadeniz University of Rize, Cekmece Nuclear Research and Training and Technical University, according to Kurnaz et al., (2007), the mean activity concentrations of ^{232}Th, ^{40}K, ^{238}U, and ^{137}Cs in the study area were found to be 38, 573, 39, and 6 $Bq.kg^{-1}$ in sediment and 42, 643, 50, and 85 $Bqkg^{-1}$ in soil samples.

Investigation of sediment samples from the region of the Upper Egypt Nile River by El-Gamal et. al., (2007) produced ranges of activity concentrations of 3.83-34.94, 2.88-30.10 and 112.31-312.98 Bq.kg-1 for ^{238}U, ^{232}Th and ^{40}K respectively.

In other investigations conducted by Ahmed et al., (2014), the average and total activity concentrations of ^{226}Ra, ^{232}Th and ^{40}K in the sediments of Indus, Hunza, and Gilgit Rivers in Northern Pakistan were higher than the globally reported mean values. These findings indicated that sediments of the Hunza, Gilgit and Indus Rivers pose a radiological threat to locals and tourists who visit Northern Pakistan for trekking and pose a radiological threat if the river sediments are

used as a building material for construction purposes. Also, the excessive lifetime cancer risk factor was 3.21×10^{-3} which is higher than the world's range of values. Therefore, numerous cancer deaths were annually reported in the Northern area of Pakistan.

Additionally, gamma-ray spectrometry was used to determine the natural radioactivity levels of ^{238}U, ^{232}Th, and ^{40}K in surface water from coastal settlements in Ndokwa East in the Delta State of Nigeria as reported by Ononugbo and Anyalebechi (2018). In that study, the activity concentrations of ^{232}Th and ^{40}K in natural water were greater than their required acceptable values of 1.0 and 10.0 Bql^{-1}, respectively. The total effective doses due to radionuclide ingestion of water for infants, children, and adults, respectively, were 58.483, 3.195, and 6.243 $mSvy^{-1}$, which are higher than the accepted reference levels of 0.26, 0.2, and 0.1 mSv of committed effective dose from one-year ingestion of water for infants, children, and adults, respectively. Regarding the projected lifetime fatality cancer risk for adults, roughly 442 out of 10,000,000 may have cancer fatality, and approximately 274 out of 1000,000,000 may experience some genetic consequences. The findings of this study revealed that petroleum production activities, together with other human activities along the coast, resulted in the radioactive build-up in the surface water of the five coastal settlements of Ndokwa East.

Due to the activities of humans, the activity concentrations of natural radionuclides have increased significantly. Artificial sources such as fallout radionuclides like ^{90}Sr, ^{137}Cs, ^{239}Pu and ^{240}Pu account for 0.4% of the global testing of nuclear weapons (Botwe et al., 2017). The operation of nuclear power plants, manufacturing and utilization of radioactive sources, mining and processing of uranium ores and mineral sands, burning of fossil fuels, manufacturing of fertilizers, refining of metals, exploration, drilling and processing of oil and gas are also major contributors (Adukpo et al., 2015). Some studies have shown that artificial radioactive nuclides such as ^{137}Cs

can be detected in some areas (Chowdhurry et al, 1999; Kurnaz et al, 2007). All these sources account for the significant increase in radioactivity.

In several nations around the world, nuclear energy has been used to generate power since the 1950s. According to reports from the IAEA, 456 nuclear power stations were active worldwide in 2019. Around 10% of the world's electricity production as of 2020 came from nuclear power plants. There are over fifty additional nuclear reactors in various phases of construction around the world, which is comparable to about 15% of the current capacity according to the World Nuclear Association (2020). Several African countries signed an agreement in July 2015 with a 3-year action plan to build a collaborative nuclear power program in West Africa. Benin, Ghana, Mali, Burkina Faso, Niger, Nigeria, and Senegal are among the nations that took part in this cooperation agreement in July 2015. Collectively, these nations make up the West African Integrated Nuclear Power Group (WAINPG) (World Nuclear Association, 2020).

Due to industrialization, population increase, and urbanization, energy demand has risen throughout time (Agyekum and Velkin, 2020; Agyekum, 2020). As a result, nuclear power has been added to the mix of sources used to generate electricity worldwide. However, unlike other power plants, the development and usage of nuclear facilities and nuclear power plants require a special safety approach. During operation and in the event of an accident, the radiological impact of Nuclear Power Plants on the environment and people should be maintained to a minimum (Baskurt and Aydin, 2018). To reduce the harmful effects on the environment, environmental capability evaluation is crucial when choosing a location for a nuclear power plant. During the planning and construction stages, environmental factors must be considered as they could negatively impact the environment through radioactive compound pollution (Barzehkar et al., 2016).

Additionally, the routine operation of nuclear power facilities and the disposal of radioactive waste add up to radiation in the environment even though these are only minor sources (Tadmor, 1986). Nuclear power plants typically emit very small amounts of radioactive materials into the environment. Less than 0.1% of the annual dosage from natural radiation is, on average, the total annual exposure from all processes in the nuclear fuel cycle. However, these materials can remain radioactive and dangerous to human health for thousands of years. Radioactive wastes are subject to special regulations that govern their handling, transportation, storage, and disposal to protect human health and the environment (Iqbal et al., 2021).

Numerous nations, including China and others, as stated by (Cao et al., 2022), have researched the impact of nuclear power plants while they are in operation. These studies concentrate on a variety of topics, including public health risks and cancer incidence, as well as radioactivity levels in environmental samples, including drinking water, food, soil, and air. All these studies have indicated the level of risk the public is exposed to.

Internal and external radiation exposure are the two ways that people who are in the vicinity of a nuclear power plant can be exposed to radiation. The ingestion of drinking water is one of the dose contributors to internal radiation exposure. Exposure to the ambient environment represents the dominant pathway for external radiation exposure (Hamlat et al, 2018).

The levels of exposure to persons working at the various nuclear power industry plants vary significantly. The largest doses are received by the maintenance and repair staff at nuclear power plants. Radon and its daughters present radiation risks to uranium miners, particularly those working underground. Additionally, the fuel-cycle processes release radionuclides with a substantially longer half-life that persist in the environment for thousands of years. The collective dose commitment, if these radionuclides provide doses over an illogically endless period, is 69

manSv per gigawatt-year of power produced. Only 10% of this total will be delivered over the next 100 years, though. Radon exposure from mill tailings would commit as much as 150 man Sv per gigawatt year of electricity generated (Gonzales & Anderer, 1989).

2.4 Radiation Protection and Safety

Biological organs in the human body can be harmed by ionizing radiation. The biological consequences of radiation have been the subject of several investigations. To safeguard radiation workers and the public from radiation exposure, these investigations seek to determine whether dose limits are exceeded. Many of the facts about how radiation affects people have been learned from survivors of atomic bombs as well as occupationally exposed workers through everyday activities or accidents (Lilley, 2001).

Two classifications of the effects of radiation exposure are known. They are deterministic effects and stochastic effects (Cember and Johnson, 2009; Noz and Maguire, 2007). The observable effect when the body receives an amount of dose above a certain threshold is known as a deterministic effect. Detrimental effects are not seen below this threshold. However, the magnitude of the effect increases with an increased dose. The probability of a stochastic effect occurring, on the other hand, is dependent on the amount of dose. Also, its occurrence is random (Martin and Harbison, 2006; Cember and Johnson, 2009). These kinds of effects are regarded to have the potential to induce cancer and have genetic effects on future generations.

The ICRP radiation protection system is built on three key principles: justification, optimization, and dose limitation. The justification principle asserts that any decision that alters a radiation exposure situation must result in more benefits than harm. Essentially, the introduction of a radiation source must provide enough advantages to individuals or society to outweigh its

potential harm. The optimization principle dictates that exposure likelihood, the number of people exposed, and the magnitude of each exposure should be kept as low as reasonably achievable while considering economic and societal factors. As part of this process, the ICRP recommends applying dose constraints to limit the amount of radiation an individual can receive from a specific source.

The third principle, dose limitation, ensures that individual radiation doses from planned exposures (excluding medical treatments) do not exceed the limits recommended by the Commission. The ICRP recognizes three types of exposure situations: planned exposure (deliberate introduction and operation of sources), emergency exposure (requiring immediate action to mitigate harm), and existing exposure (such as prolonged post-emergency exposure). These are outlined in ICRP Publication 103 (ICRP, 2007).

The ICRP also identifies three categories of exposed individuals: workers (occupational exposure), patients (medical exposure), and the public (public exposure). Occupational exposure refers to radiation exposure encountered during work, while public exposure covers any radiation that is neither medical nor occupational.

While dose limitations apply only to planned exposures, the principles of justification and optimization are relevant across all exposure types—planned, emergency, and existing. An exception is medical exposure in planned scenarios, where dose limits do not apply, and dose constraints become vital.

In planned exposures, the optimization process involves applying dose constraints, which set an individual dose level not to be exceeded under normal conditions. These constraints serve as a planning tool, but they do not represent a strict boundary between safe and dangerous levels. For exposures with associated dose limits, dose constraints should always be below the relevant limit.

Table 2.4 shows the dose limits as recommended by ICRP.

Table 2.4: Recommended ICRP 103 dose limits in planned exposure situations (ICRP 2007).

Type of limit	Occupational, mSv per year	Public, mSv per year
Effective Dose	20, averaged over 5 years, with no more than 50 mSv in any one year	1 (exceptionally, a higher value of effective dose could be allowed in a year provided that the average over 5 years does not exceed 1 mSv in a year)
Equivalent dose (lens of the eye)	150	15
Equivalent dose (skin)	500	50
Equivalent dose (hands and feet)	500	-

To reduce the likelihood of stochastic effects, the annual effective dosage for occupational exposure is restricted to 20 mSv averaged over a specified period of 5 years. The dose may be greater than 20 mSv, but it cannot be greater than 50 mSv in a single consecutive year. The annual dosage limit for a member of the public is 1 mSv, which is lower than the annual dose limit for a group of occupationally exposed workers. The recommended occupational equivalent dose limits for the skin, hands and feet, and eye lens, respectively, are 500, 500, and 150 mSv per year. These limits are intended to prevent deterministic consequences. Fifteen millisieverts for the eye lens and 50 mSv for the skin are the maximum annual equivalent doses that any one member of the public may receive (Noz and Maguire, 2007, ICRP, 2007; Martin and Harbison, 2006).

Natural radiation sources are difficult to control, and it is impossible for the public to completely avoid being exposed to them. Additionally, there has always been a keen understanding

of the possible risks associated with nuclear criticality and the emission of radioactive materials throughout the process of producing electricity using nuclear power. Nuclear power plant design and operation strive to reduce the likelihood of accidents and minimize any negative effects on people should an accident occur. In the history of civil nuclear power, there have been two significant reactor accidents: Chernobyl and Fukushima Daiichi. Fukushima Daiichi rigorously tested the containment, allowing some radioactive to leak out, while Chernobyl entailed a major fire without a plan for containment. In the more than 18,500 total reactor years of commercial nuclear power operation in 36 nations, these are the only significant incidents that have happened. The information gathered over the past six decades demonstrates that nuclear power is a secure way to produce electricity. Nuclear power facilities have a low and reduced accident risk. Compared to other widely acknowledged dangers, the effects of an accident or terrorist attack are negligible.

In nuclear power facilities, the safety of the operating team is of utmost importance. For many tasks in the reactor's core, remote handling equipment is used to reduce radiation exposure. Physical protection and restricting the amount of time employees spend in regions with high radiation levels are further control measures that can be taken. This can be supported by continuous monitoring of individual doses and the workplace environment, which ensures very low radiation exposure compared to other industries.

The fundamental principle of the operation nuclear power plants globally, is that the operator is responsible for safety. The national regulator has the responsibility of ensuring that the plants are operated safely by the licensee and that the design is approved. A second important concept is that a regulator’s mission is to protect people and the environment.

According to the IAEA, dose limitation should be applied to doses due to occupational exposures incurred in nuclear power plants by the employees of the operating organizations, doses due to occupational exposures incurred in all plants and facilities by contractors and doses due to exposures incurred by members of the public as a result of activities in radioactive waste management and effluent discharges deriving from the nuclear power plant (IAEA, 2012). Public exposure could occur from direct irradiation from the nuclear power plant itself, gaseous or liquid discharges of radioactive elements from the facility, or both. Discharges must be managed in line with regulatory body-issued authorizations such that radiation doses to the most exposed members of the public (the critical group) near the plant are within the dose constraint. The dose constraint assigned by the regulatory body to this source of exposure should be a fraction of the dose limit for the public. The authorized discharge level should be set by using environmental modeling techniques to establish the relationship between the release level and the potential dose to the critical group, with due account taken of all expected pathways of exposure (external or internal).

2.5 Exposure Pathways of Radionuclides

An exposure pathway describes the process through which contaminants such as radionuclides are transported through the environment to their receptors (humans). It is of utmost importance to know how much of each radionuclide moves through the environment and into the human body. Exposure may result from natural radionuclides or from human activities that release radionuclides into the environment. Fentiman et al., (2004) reported that radionuclides travel through the environment along pathways as other materials. They travel through the air, water, and eventually through the food chain. Radionuclides may enter the human body through ingestion or inhalation (internal), or the skin (external exposure). Figure 2.2 shows the major exposure pathways of radionuclides.

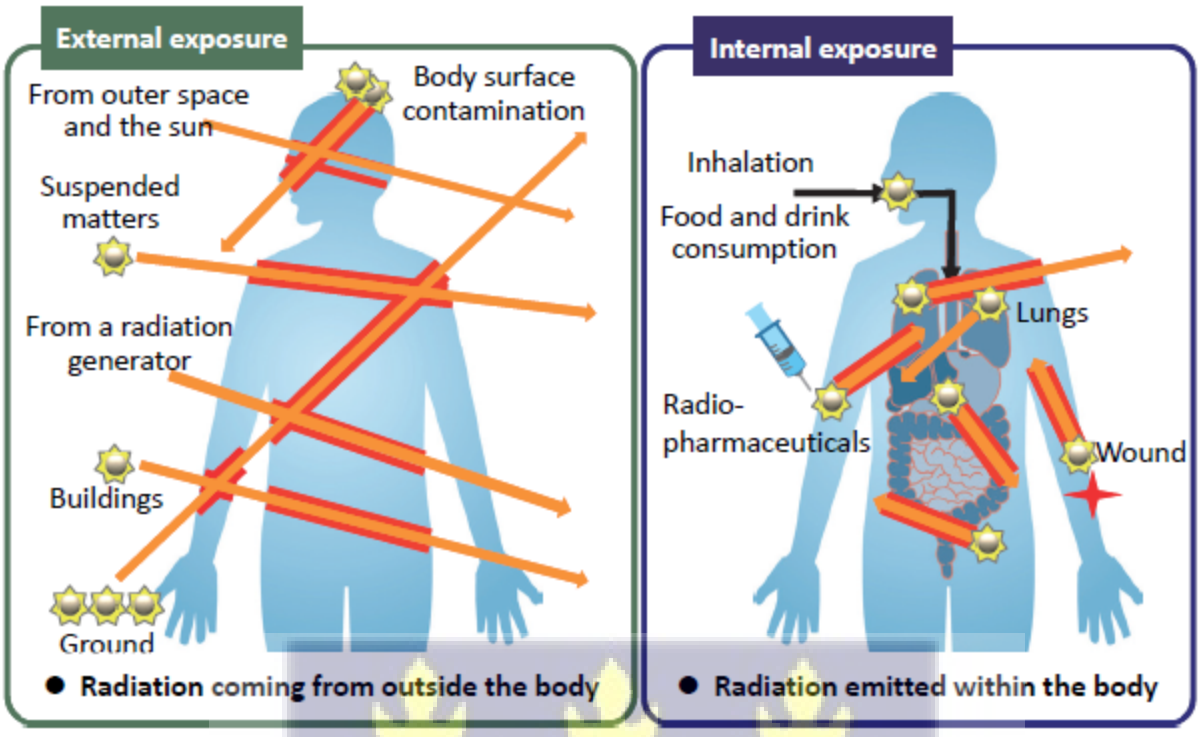

Figure 2.2: A schematic illustration of possible exposure pathways (Source: Ministry of The Environment Government of Japan, 2018).

Following atmospheric releases of radionuclides, plants are the main source of radioactive contamination in the food chain. The use of contaminated sources as a water supply for agricultural purposes, such as watering or irrigation of vegetables, fruits, and grains; and irrigation of pasture grass may be consumed by livestock. Animals that eat plants or other animals are secondary consumers of food chain pollution. Animal food chains are involved in several significant radionuclides transfer channels to humans, including milk, eggs, and meat or flesh from fish and other animals. Milk consumption is the primary animal channel for radiologically significant radionuclides such as ^{90}Sr, ^{131}I, and ^{137}Cs to reach humans. Cesium is transported to animals' soft tissues, particularly muscle, through its chemical congener potassium. Like calcium, strontium is mostly transported to the bone. Radionuclides are taken up by fish and shellfish both directly from

sea water and through their food. Aquatic animals may contain high concentrations of radionuclides that are not a problem in the food chains of terrestrial species because of low absorption efficiency in humans. This is true, for instance, of polonium, which is concentrated in fish and shellfish as well as crustaceans.

The radionuclides that are a part of our environment can deliver doses both internally and externally. The common radionuclides include ^{226}Ra, ^{238}U, ^{40}K, and their offspring. Ingestion, inhalation, and cutaneous absorption through the skin are the three main ways that radionuclides enter the body.

2.6 Detrimental Effects of Radionuclides on Humans and the Environment

The primary health concern associated with radioactive materials is the increased risk of developing cancer. While many radioactive materials occur naturally, others are produced through various nuclear reactions, such as those in nuclear reactors (World Nuclear Association, 2022). For instance, ingested radium has been linked to bone cancer, bone sarcoma, and head carcinoma, with the latter likely caused by the accumulation of radon gas in head cavities (Mays et al., 1985). Radon, a decay product of radium, exists as a gas and is closely associated with lung cancer (Wanty and Schoen, 1993). When inhaled, radon's immediate decay products, which have short half-lives, attach to fine particles in the air and irradiate lung tissues with alpha particles, thereby increasing lung cancer risk.

Radon has long been recognized as a radiation hazard, particularly for underground miners, and has been classified as a human carcinogen (ICRP, 1981; IARC, 1988). Since the 1970s, evidence has shown that radon can pose significant health risks even outside of mining environments (WHO, 1993; ICRP, 1993). As radon exposure accounts for approximately half of

all radiation exposure from natural sources (Kathren, 1998), there has been increasing concern over radon-related health risks in the general populations.

Radionuclides such as ^{137}Cs and ^{90}Sr from nuclear reactor waste are very dangerous to health. Exposure to ^{137}Cs can increase the risk of cancer because of exposure to high-energy gamma radiation. Internal exposure to ^{137}Cs, through ingestion or inhalation, enables the radioactive material to be disseminated in soft tissues, particularly muscle tissue, subjecting these tissues to beta particles and gamma radiation and increasing the risk of cancer. ^{90}Sr also causes severe damage or even death once inhaled or ingested. Once in the body, ^{90}Sr acts like calcium and is readily incorporated into bones and teeth, where it can cause cancers of the bone, bone marrow, and soft tissues around the bone (World Nuclear Association, 2022) .

The current approach to environmental radiation protection for flora and fauna is based on the ICRP's recommendations (ICRP, 2007), which do not set specific radiation dose limits for plants or animals. According to ICRP assumptions, protecting humans under certain radiological standards inherently ensures the protection of biota. This means that if public exposure to radiation from radioactive waste discharges is kept below the 1 mSv/y limit, the radiation doses absorbed by flora and fauna would also remain within acceptable levels. This concept of environmental radiation protection is particularly relevant in the petroleum industry, where both radioactivity levels and potential discharge rates of naturally occurring radioactive materials are typically low (APPEA, 2002).

Natural radioactive materials released to the environment can lead to an increase in human radiation doses through different pathways as earlier mentioned, and the potentially highest radiation exposures are estimated to be received by the “critical group of the public” (APPEA, 2002).

2.7 Human Health Risk Assessment

Risk assessment for human health is the process of determining the nature and likelihood of harmful health effects in potential human exposure to pollutants in the environment. Additionally, it is a method for estimating health consequences that could be caused by exposure to both cancer-causing and non-cancerous substances or contaminants (USEPA, 2001; Kamunda & Madhuku, 2017). According to USEPA (2001), the risk assessment process involves hazard identification, exposure assessment, toxicity (dose-response) assessment, and risk characterization.

Estimates of human health risk are based on variables such as environmental concentrations, body weight, absorption rates, exposure scenarios, and other factors, all of which can vary between locations. There are two primary ways to describe the likelihood that exposure to a hazardous agent will cause harm. The first is individual lifetime cancer risk, which estimates the increased probability that an individual will experience a specific adverse health effect due to exposure over their lifetime. The second is population risk, which estimates the number of deaths in the exposed population (Meinhold & Hamilton, 1993). The outcomes of a risk assessment are used by risk managers to determine whether regulation or remediation is necessary.

Human health risk assessment models are extensively applied in the decision-making process for dealing with radiologically contaminated soil, water, or air. Researchers have created new methods for a better representation of human health risk due to the complexity of real-world data used for risk assessment. The simplification and imprecision of the information that is currently available allow the risk assessment models to consider parameters that are typically subject to uncertainty (Ferson, 1996). Uncertainty is an essential and inescapable ingredient of the evaluation of risk. Two categories of uncertainty are known. They are type A uncertainty and type B uncertainty; Type A is induced by natural variability and cannot be reduced, while type B uncertainty results from a lack of proper knowledge or partial ignorance of information. Both

"Type A" and "Type B" uncertainty occur when the assessment objective is to estimate the distribution of individual doses or risks within an exposed population group where the true shape and spread of this distribution is uncertain or unknown (Roucher et al., 2002; Hammonds et al., 1994). To characterize the uncertainties in natural processes, a variety of technical methods are available, such as the probabilistic approach, mathematical and numerical modeling, interval analysis, convex modeling, fuzzy set theory, possibility theory, and evidence theory (Kpeglo, 2015). There is no single approach that provides thorough answers to every kind of uncertainty. Each strategy has a unique set of benefits and drawbacks (Zimmermann, 2001).

Monte Carlo (MC) simulation is the most used method for describing uncertainty in risk assessment research. (USEPA, 1996). The Monte Carlo methods need information on statistical dependencies among the variables; distributions of input parameters; and information on the model structure to evaluate any environmental scenario. Low probability parameter values in MC simulation have fewer odds of being randomly chosen, hence certain possibilities might be disregarded. (Guyonnet et al., 1999). Moreover, based on the regulatory limit or target value, Monte Carlo methods provide a single line for exceedance risk. The exceedance risk is not a single line, but rather a range showing the lower and upper bounds (Ferson, 1996). Monte Carlo computation cannot be used to analyze data that is insufficient or inaccurately informative (Chowdhury et al., 2004).

Various organizations offer well-established methodologies for risk assessment. Most notable among them are the models from the National Research Council of the National Academy of Sciences (NRC-NAS) (1992), US EPA (1998), Council of Ministers of the Environment (CCME) 1996, and WERF (1999). In terms of both individuals and the population, the NRC-NAS model identifies risks and quantifies their severity (NRC, 1992). The Ecological Risk Assessment Model

of the US EPA is comprehensive (US EPA, 1998). Problem formulation is the first of the model's four fundamental steps. It is followed by analysis, risk characterization, risk management, and risk communication. Problem formulation involves evaluation criteria, conceptual models, and analysis strategies. Measurement, testing, and mathematical modeling are used during the risk assessment process to calculate the link between the initial event and any negative impacts (Kpeglo, 2015).

In this research, the R statistical package was used for statistical computing and graphics to assess the exposure rate of the critical population. It provided a wide variety of statistical (linear and non-linear modelling, classical statistical tests, time-series analysis, classification, clustering) and graphical techniques and is highly extensible. This research presents a linear and or non-linear modeling procedure from the data that were obtained for health risk assessment of exposure to radioactivity. The primary objective was to estimate radiation doses and cancer risks to humans using the R software package to develop a mathematical model and obtain vital information from the data.

CHAPTER THREE

MATERIALS AND METHODS

3.1 Description of the Study Area

The Western Region of Ghana stretches from the Ivory Coast (Comoé District) in the west to the Central region in the east and covers a land size of 13,842 sq. km (GSS, 2021), as shown in Figure 3.1. It lies within latitudes 4º 40′ and 5º 10′ north and longitudes 3º 07′ and 1º40′ west. The region has a lengthy stretch of coastline that runs from Southern Ghana's border with the Ivory Coast to its eastern border with the Central Region which stretches to about 192 km constituting about 35% of the Ghana coastline. The coast has a wide continental shelf with 200 nm extending to about 80 km off Cape Three Points. (Boye and Fiadonu, 2020), with a generally low-lying topographic elevation not exceeding 30 m above mean sea level. The region is in the equatorial climate zone, which is characterized by mild temperatures, receives the highest rainfall, and has fertile soils and green hills. About 75% of its vegetation is found in Ghana's high forest zone. With an average annual rainfall of 1,600 mm, it is also the wettest region in Ghana.

Sekondi-Takoradi, and the coastal communities of Axim, Beyin, Atuobo, Half Asini, New Town and Elubo are some of the various communities in the region. It also includes Cape Three Points, Ghana's southernmost point.

3.2 Geology of the Study Area

Approximately 2 391 km^2 (or 10% of Ghana's total land area) is covered by the Western Region (GSS, 2012). About 60% of the coastline is made up of sand beaches, and 40% is made up of composite rock and rocky headlands alternating with sandy bays. The western region has coastal

materials which can be characterized as heterogeneous, with different types of coastal rock including granitoids, shales, sandstones, and soils.

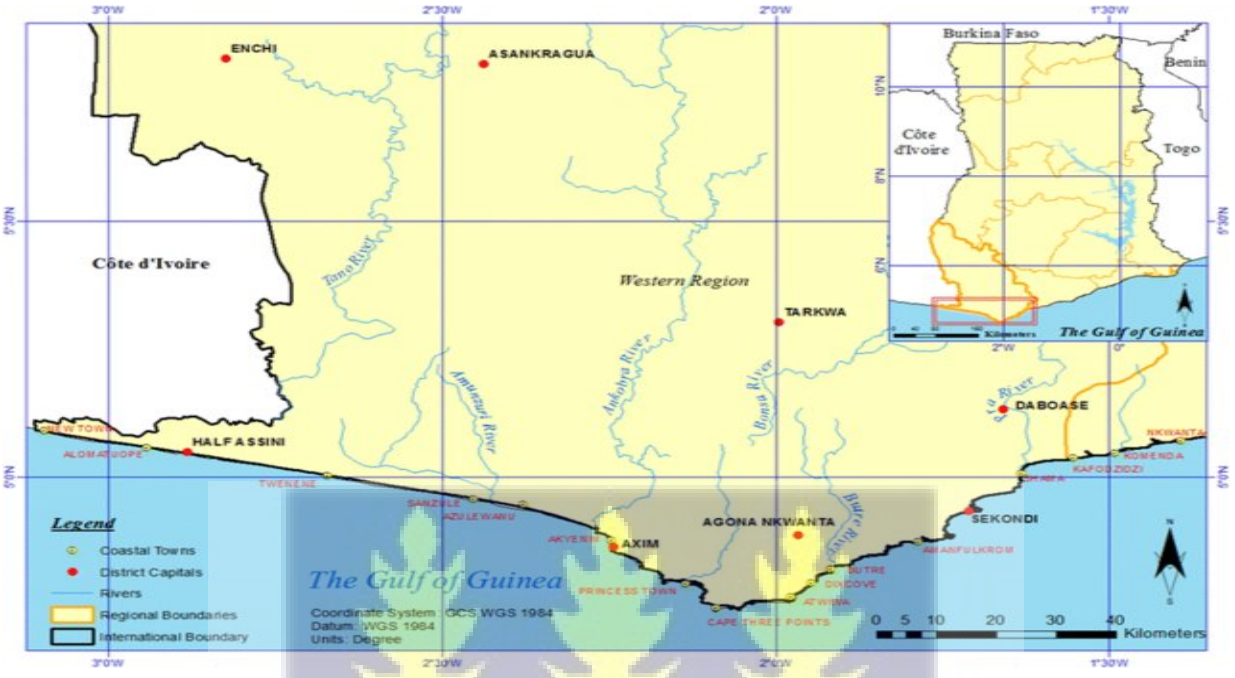

Figure 3.1: Map of the Coast of the Western Region of Ghana (source: SMD, Lands Commission, Ghana)

The research area has uniform coastal materials and is made up primarily of sandy beaches that are sporadically cut through by estuaries and lagoons. Eocene and Cretaceous Appolonian strata make up the subsurface of the Western Region, which is located inside the Tano Basin. Rapidly alternating sands and clays, with sporadic thin layers of gravel and fossiliferous limestone, make up the Appolonian. At depth, the clays and sands become denser and transform into sandstones and shales. The clays and shales frequently include pyrite or marcasite nodules, while some of the sand strata frequently have muscovite nodules (Boye, 2015).

3.3 Sample Collection

Samples were collected from four (4) selected communities along the west coast of Ghana; Half Asini, Beyin, Axim and Takoradi (Figure 3.2). A total of two hundred and forty (240) samples were collected for laboratory analysis. They comprised twenty (20) samples of beach sand and sea sediment for each location and 80 samples of seawater. Geographical coordinates of the sampling areas were recorded using a Garmin Global Positioning System (GPS). The beach sand samples were collected at random positions from each site at depths between 5 and 25 cm using a hand coring tool. Plate 3.1 shows the dose rate measurements that were taken 1 m above the surface of the coast before the sampling was done. The hand coring tool has a diameter which typically ranges from 100 mm to 200 mm with weight varying from 7 kg to 7.8 kg. Sediment samples were collected using a 3.5-L Ekman bottom grab sampler. The Ekman grab sampler is made of stainless steel with dimensions of 152 mm × 152 mm × 152 mm and a cable length of 30 m. The sampling locations were approximately 200 m apart, covering a wide area and range of water depths to provide representative data on the radionuclide distribution in the coastal area. On the other hand, seawater samples were collected using a Niskin bottle also at locations 200 m apart (Plate 3.2). At each sampling point, the physicochemical parameters such as temperature, pH, total dissolved solids (TDS) and conductivity were measured *in situ* using a Hanna multi-parameter probe meter (HI9129, Hanna Instruments, USA.

Plates 3.3 and 3.4 shows the evidence of the use of the beach sand for construction purposes by the inhabitants of the coast.

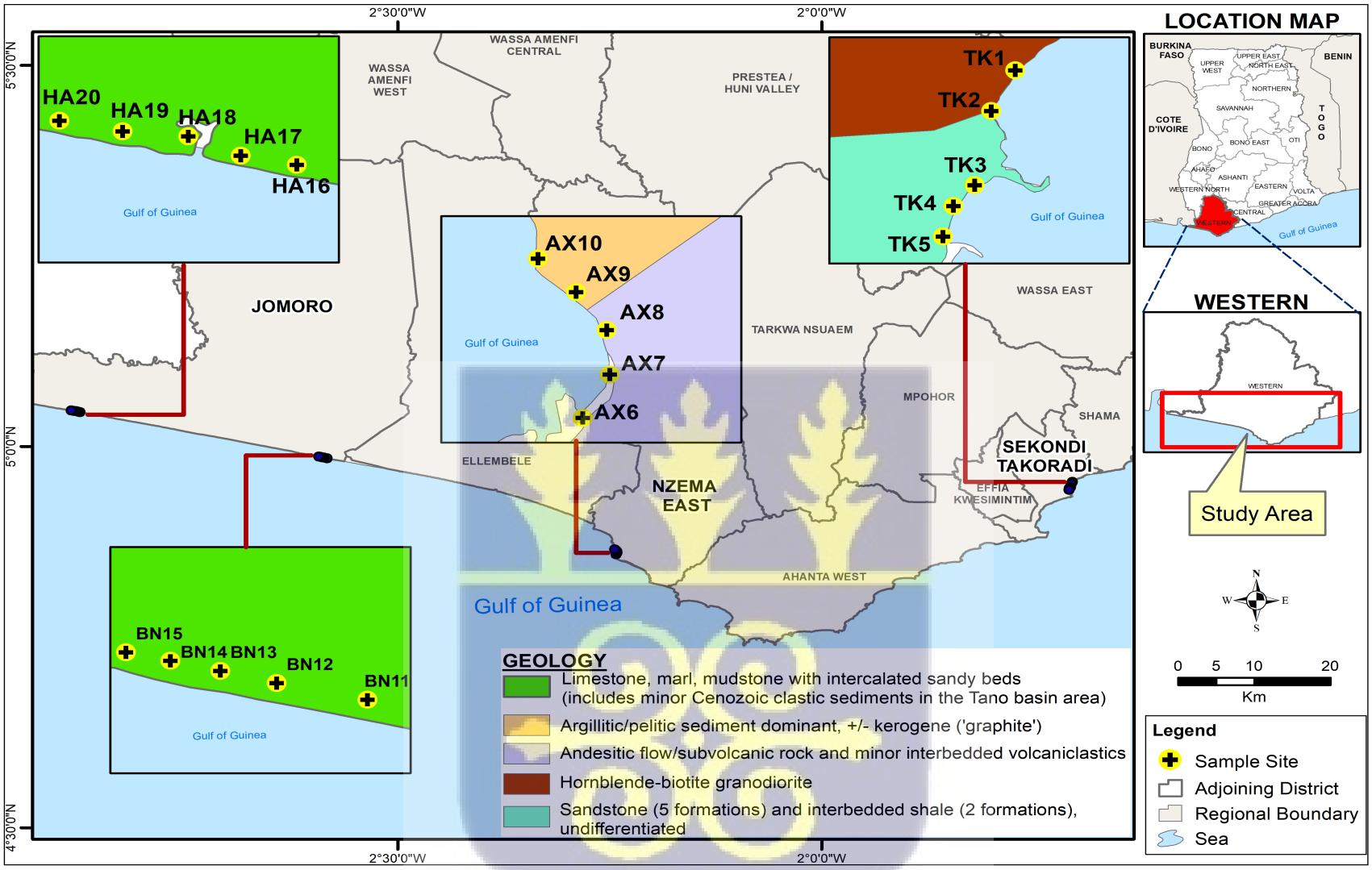

Figure 3.2: Geological map of the western coast of Ghana showing the sampling points.

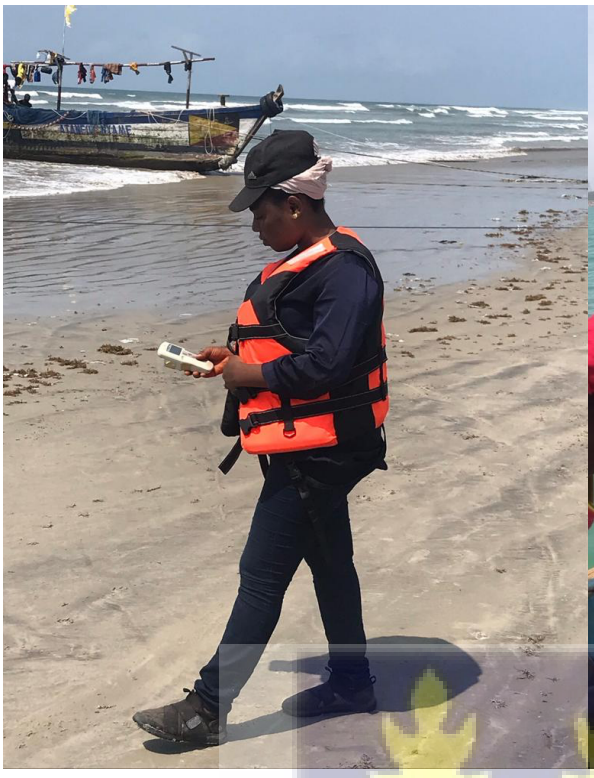

Plate 3.1: Dose rate measurement at 1m above ground surface on the coast.

Plate 3.2: Seawater sampling with a Niskin bottle

Plate 3.3: Beach sand used for sand-crates for building at Half-Asini

Plate 3.4: Indigenes of Half-Asini mixing beach sand and adhesive for construction purposes.

3.4 Sample Preparation and Measurement by Gamma Spectrometry.

3.4.1 Sample Preparation

In the laboratory, sand and sediment samples were spread on trays and air-dried at room temperature for 7 days to remove excess moisture. They were then oven-dried at 50°C for 24 hours, ground into fine powder using a ball mill, homogenized, and screened with a 500-µm mesh before being transferred into selected geometries and containers. The containers were completely sealed with radon-impermeable tape and stored for 1 month to allow the short-lived daughters of the ^{238}U and ^{232}Th decay series to attain secular equilibrium with their long-lived parent radionuclides (Tracerco, 2007; ASTM, 1983; 1986). The sealed samples were weighed and radioactivity measured using a high purity Germanium detector. Sea water samples were transferred into 1-liter Marinelli beakers and sealed with a radon-impermeable tape.

3.4.2 Gamma Spectrometry Measurement

3.4.2.1 Instrumentation

A high-resolution gamma spectrometry system with a p-type extended range germanium coaxial detector (XtRa) was used to non-destructively analyze all the samples (Figure 3.3). The detector has a relative efficiency of 37.1% and an energy resolution of 1.8 keV for gamma-ray energy of 1332 keV of ^{60}Co. It is enclosed in a 10-cm thick passive lead shield, and on top of the lead shield is a Bicron BC-418 organic scintillation detector that operates in anticoincidence mode with the Ge detector. This guarantees a remarkable degree of precision in environmental gamma-radiation measurements, due to the incredibly low background. For each sample, the counting period lasted 36,000 s. Using the Genie 2000 gamma acquisition and analysis software program, radionuclides were quantitatively analyzed after being identified individually using their distinctive gamma-ray energies. The net peak area of gamma rays of the detected isotopes was corrected using the background spectra that were acquired. At the 95% confidence level, the background spectrum was also used to calculate the minimum detectable activity of ^{226}Ra, ^{232}Th, and ^{40}K. ^{214}Pb and ^{214}Bi's respective γ-yields at 351.9 keV (35.8%) and 609.3 keV (44.8%) were used to calculate the activity concentrations of ^{226}Ra.

The activity concentrations of ^{228}Ra and ^{228}Th were estimated using the gamma emissions of ^{228}Ac at 911 keV (26.6%) and ^{212}Pb at 238.6 keV (43.3%), ^{208}Tl at 583 keV (30.1%), and 2614.7 keV (35.3%), respectively, while considering a branching ratio of 33.7% from ^{212}Bi to ^{208}Tl. While the ^{210}Pb activity concentration was directly determined from the gamma emission line at 46.5 keV (4.3%), the ^{40}K activity concentration was directly determined from its emission line at 1460.8 keV (10.7%). The self-absorption correction factor for the low energy photo peak ^{210}Pb was considered while computing the activities (Chu et al., 1999; Kpeglo et al, 2019).

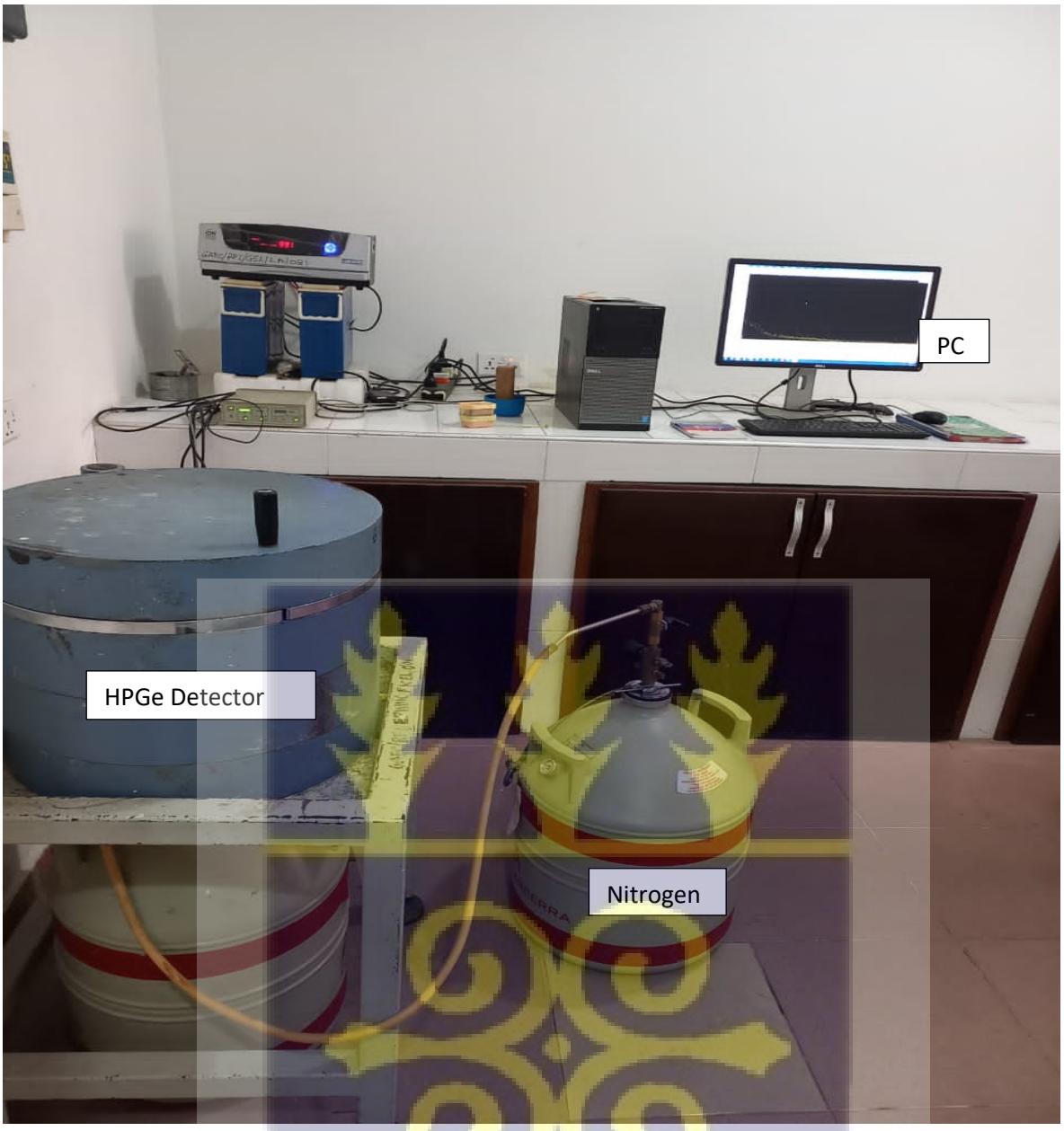

Figure 3.3: Setup of High Purity Germanium detector system

3.4.2.2 Energy Calibration of the γ-Spectrometer

In nuclear spectrometry measurement, one of the essential requirements is the ability to identify the photo peaks present in a spectrum produced by the detector system (IAEA, 1989). This is achieved by carrying out energy calibration of the detection system. A collection of standard point

sources with well-defined energies between 46.5 keV and 2000 keV was used for the calibration. To create a linear curve with a second-order polynomial, the channel number that corresponds to the centroid of each complete energy event on the Multi-Channel Analyzer was recorded and plotted. An indicator that the system is functioning properly is the linear curve produced from the data points (IAEA, 1989). By measuring and plotting at least two separate gamma energies, the system was examined every day it was in use to ensure the stability of the slope and intercept. The standard was counted on the gamma detector until the count rate of total absorption could be computed with an accuracy of 95% confidence and a statistical uncertainty of 5%. Following the calibration of energy, the calibration of resolution would be the next procedure in the spectrum analysis sequence. The parameter FWHM (full width at half maximum) of the photopeak determines the resolution and if the photopeak fits a Gaussian, the value will take this parameter FWHM = 2.35σ being assigned the standard deviation σ from software to the Gaussian distribution.

The resolution of Ge detectors typically comes with initial specifications since it gives the spacing capacity of the photopeak presenting a specific system. The most typical nominal resolutions to cover various energy intervals are: ^{55}Fe (5.9 keV), ^{57}Co (122 keV) and ^{60}Co (1333 keV).

3.4.2.3 Efficiency Calibration of the γ-Spectrometer

The photopeak efficiency of the detector is the ratio of the number of actual events that the detector records at each photopeak to the total number of events with a specified energy that is emitted by the radiation source. To quantify radionuclides in the sample, a precise photopeak efficiency calibration of the instrument is required.

Efficiency calibration was done by counting well-defined reference radionuclides from known activities with energies between 60 and 2000 keV. Standard radionuclides that were evenly

dispersed in solid water and had a volume and density of 1000 cm^3 and 0.98 gcm^{-3}, respectively, were used to calibrate the efficiency for the analysis of water samples (Source number: AJ-9177 and manufactured by Eckert & Ziegler Nuclitec GmbH).

The expression used to determine the efficiencies is given as follows (Darko et al., 2007)

$$\eta(E) = \frac{N_\tau - N_B}{P_E A_{STD} T_{STD}} \qquad (3.1)$$

where P_E is gamma emission probability for energy (E); η (E) is the photopeak efficiency of the detector; N_τ is the total counts under a photopeak; N_B is the background count; A_{STD} is the activity (Bq) of the radionuclide in the calibration standard at the time of calibration; T_{STD} is the counting time of the standard.

3.4.2.4 Determination of Minimum Detectable Activity in Gamma Spectrometry

The smallest amount of radioactivity that could be measured under specific circumstances is known as minimum detectable activity (MDA). The determination of MDA is crucial in low-level counting, especially in environmental-level systems where a sample's count rate is nearly identical to the background count rate. "In this scenario, the background is counted with a blank, such as a sample holder, whereby everything else that may be counted with an actual sample is counted with a blank. As described by Hartwell (1975), Equation 3.2 was used to determine the minimum detectable activity (MDA) from the background spectrum for gamma measurements".

$$MDA = \frac{\left(2.71 + 4.65\sqrt{N_{TB}\left(\frac{t_T}{t_B}\right) + N_C}\right)}{t_T . I . \varepsilon} \qquad (3.2)$$

N_{TB} is the background count for the region of interest of each radionuclide; t_T is the sample measurement time; t_B is the background counting time; N_C is an integral; I is the gamma emission

probability (gamma yield) of each radionuclide, ε is the photopeak efficiency for the measured gamma-ray energy.

3.5 Sample Preparation and Measurement by Alpha-Particle Spectrometry Analysis

3.5.1 Sample Preparation

Alpha-particle spectrometry requires the isolation and purification of radionuclides by utilizing numerous radiochemical procedures before measurement on the detector to determine the concentration of the radionuclides. This process of sample preparation and conditioning prior to the measurement is laborious and expensive. The radiochemical separation of the radionuclides is important to avoid self-absorption effects of the radionuclides in the sample matrix. The preparation of liquid and solid matrix samples for U and Th analysis in alpha-particle spectrometry involves three main processes. These include pre-concentration, radiochemical separation, and electrodeposition (Figure. 3.4).

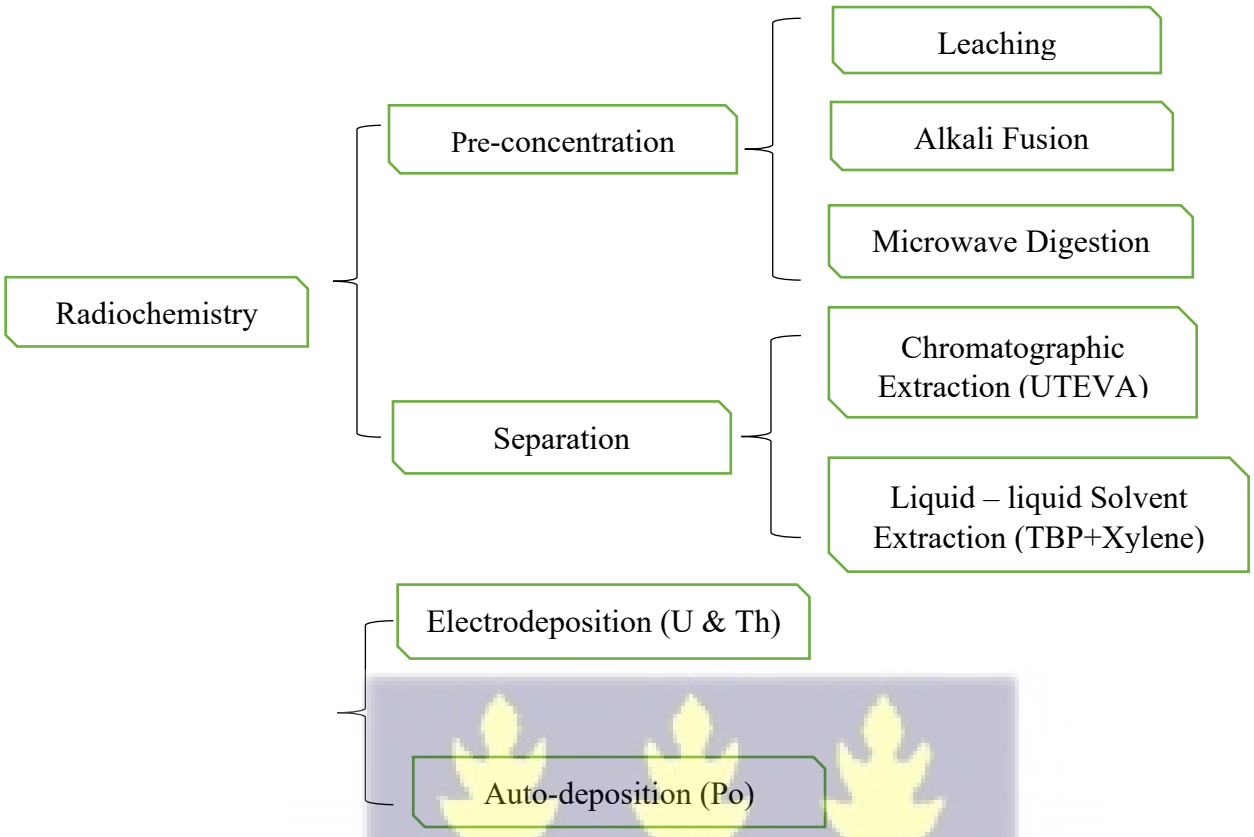

Figure 3.4: Summary of analytical steps in Alpha spectrometry.

3.5.1.1 Liquid Matrix Sample

For water samples, uranium and thorium were pre-concentrated through co-precipitation with iron hydroxide. To inhibit microbial growth and minimize interactions with the walls of the storage containers prior to laboratory analysis, the liquid samples were acidified to a pH of 2-3 using concentrated HNO_3 (65%). After homogenization, 0.5 L of the water sample was taken and filtered. Following the filtration, tracers with known concentrations of 0.1137 Bqg^{-1} for ^{229}Th and 0.352 Bqg^{-1} for ^{232}U were added while gently heating the sample to 30°C and stirring to ensure complete mixing. Then, 2 ml of an Fe^{3+} carrier (5 mg/mL solution) was added. The pH was adjusted to 8.0-8.5 using concentrated NH_3 (25%), causing the co-precipitation of iron hydroxides

along with the actinides. After the precipitate settled, the supernatant was decanted, and the remaining fraction was centrifuged at 4500 rpm for 10 minutes. The precipitate, containing U and Th, was dried, and dissolved in 5 ml of 3M HNO_3, marking the beginning of the radiochemical separation process.

3.5.1.2 Solid Matrix Sample

Between 0.5g and 1g of dried and homogenized mass of soil and sea sediment samples was taken and calcinated at 600ºC for 24 hours after the addition of the same tracers mentioned earlier. The ashed material was then wet digested with aqua regia using the leaching method for 4 hours at 50ºC. Twelve milliliters of H_2O_2 was added dropwise with an additional 45 mL of concentrated HNO_3 (65%) while the sample was stirred for 12 hours at constant room temperature. Thirty milliliters of 8M HNO_3 was added and finally filtered. The filtrate was evaporated to 10 mL, and then distilled water was added to top up to the 50 mL mark. The 50-mL final solution was then subjected to the earlier described actinides co-precipitation iron hydroxide technique for water samples (Lehritani et al, 2012).

U and Th sources were individually electrodeposited onto stainless steel discs. Th was electroplated for two hours at 1.5 A whereas the U isotopes were electroplated for one hour at 1.2 A. With 450 mm^2 active surface PIPS detectors in an 8-chamber Alpha Analyst System (Canberra)., U and Th isotopes electroplated on stainless steel discs were counted for 3 to 4 days.

3.5.2 Instrumentation and Calibration of the Alpha Spectrometry System

An 8-chamber Alpha Analyst system (Canberra) was used for the alpha-spectrometric system in this study (Figure 3.5). To prevent cross-contamination, each chamber has a PIPS detector that was only used to measure one element.

Measurements must span an energy range of between 4 and 6 MeV. A dissolution containing ^{239}Pu, ^{242}Pu, and ^{243}Am was electrodeposited in a circular stainless steel planchet with a diameter of 25 mm to carry out the energy-channel calibration in this energy interval for each chamber. The various radionuclides that are present in the analyzed samples can be identified when the energy-channel calibration has been completed.

In this experiment, all sample measurements were conducted at a source-to-detector distance of 0.5 cm, and efficiency values for all alpha chambers were calculated using this distance. Using the Genie 2000 software, the alpha spectra were accumulated and analyzed for 200,000s.

The background spectrum was utilized to determine the minimum detectable activity (MDA) of U and Th with a measurement duration of two to three days.

Figure 3.5: Alpha analyst system (Canberra)

3.5.2.1 Calculation of Minimum Detectable Activity in Alpha Spectrometry

For alpha measurements, the MDA was calculated using Equation (3.3), (Hartwell, 1975).

$$MDA = \frac{1}{I.\varepsilon.C_1.t_T}\left(2.71 + 3.29\sqrt{N_B + \frac{N_B.t_B}{t_T}}\right) \quad (3.3)$$

N_B refers to the background count for the region of interest for each radionuclide; t_T represents the sample measurement time; t_B denotes the background counting time; C_1 is the radiochemical yield calculated for the tracer; I represent the intensity of alpha emission for each radionuclide; and ε is the detector efficiency for the measured alpha particle energy within the same chamber.

3.6 Calculation of Activity Concentration and Estimation of Doses

3.6.1 Calculation of Specific Activity

The activity concentrations of radionuclides in the soil, sea sediments and water for gamma measurements were calculated from the expression as shown below.

$$A_{sp} = \frac{N.e^{\lambda pTd}}{p.T_c.\eta.m} \quad (3.4)$$

where A_{sp} represents the activity concentration, N is the net count of the radionuclide in the samples, T_d is the delay time between sampling and measurement, p denotes the gamma emission probability (gamma yield), η is the absolute counting efficiency of the detector system, T_c is the sample counting duration, m is the mass of the sample (kg) or volume (L), $e^{\lambda pTd}$ is the decay correction factor accounting for the delay between sampling and counting, and λp is the decay constant of the parent radionuclide.

For alpha measurements, activity concentrations were determined using isotopic dilution techniques, while the yield was calculated using Equation (3.5) (Kpeglo, 2015).

$$A(Bq) = \frac{N}{t.\varepsilon.I.C_1} \qquad (3.5)$$

where A is the activity of the tracer, N is the net counts of the tracer peak in the samples, t is the sample measurement time, I is the Intensity of alpha emission, ε is the detector efficiency for the measured alpha ray energy for the same chamber, C_1 is the radiochemical yield calculated for tracer (%).

3.6.2 Estimation of Doses

3.6.2.1 Absorbed Gamma Dose Rate

The outdoor air-absorbed dose rates caused by terrestrial gamma rays at 1 m above the ground were estimated based on the concentrations of ^{226}Ra, ^{232}Th, and ^{40}K in sand. The following equation was used to calculate the absorbed dose rate:

$$D_R\ (nGyh^{-1}) = 0.0417\ A_K + 0.462\ A_{Ra} + 0.604\ A_{Th} \qquad (3.6)$$

where A_{Ra}, A_{Th} and A_K are the mean activity concentrations of ^{226}Ra, ^{232}Th, and ^{40}K in $Bqkg^{-1}$. The dose conversion factors that were used in the estimation for ^{226}Ra, ^{232}Th, and ^{40}K were 0.462, 0.604 and 0.0417 in $nGyh^{-1}$ per $Bqkg^{-1}$ respectively, as have been used in other dose rate calculations (Ravisankar et al, 2015; Lawluvi, 2016).

3.6.2.2 Annual Effective Dose (AED)

The absorbed dose rate in air at 1 m above ground level does not reflect the radiological risk to which a person is exposed. The absorbed dose from terrestrial gamma radiation can be converted into the annual effective dose equivalent using three variables: the conversion coefficient from the absorbed dose in air to effective dose, the indoor occupancy factor, and the outdoor occupancy factor. The annual effective dose (AED) can be computed using the formula below (UNSCEAR, 2000).

For outdoor: $AED = D(nGyh^{-1}) \times 8760\ h \times 0.2 \times 0.7\ SvGy^{-1}$ (3.7)

where 8760 is the number of hours in a year, and the occupancy factor for outdoor areas is 0.2, D is the absorbed gamma dose rate, respectively. The external gamma radiation conversion factor is 0.7 $SvGy^{-1}$.

3.6.6.3 Annual Gonadal Dose (AGD)

The measurement of the genetic importance of the annual dose equivalent that the population's reproductive organs receive is crucial to determine risk of exposure of the specific organs. In the same context, UNSCEAR regards the activity of bone marrow and bone surface cells as being relevant organs. To compute the annual gonadal dose (AGD) resulting from the activities of ^{226}Ra, ^{232}Th, and ^{40}K, the following formula was used (Mamont-Ciesla et al., 1982; Ravisankar et al., 2015).

$$AGDE = 3.09A_{Ra} + 4.18A_{Th} + 0.314A_K \quad (3.8)$$

where, A_{Ra}, A_{Th} and A_K are the activity concentrations of ^{226}Ra, ^{232}Th, and ^{40}K in $Bq\,kg^{-1}$, respectively. The conversion factors used to convert the activity concentrations of ^{226}Ra, ^{232}Th,

and ^{40}K into the total dosage absorbed by the target organs are 3.09, 4.18, and 0.314 in μSv y^{-1} per Bq kg^{-1}, respectively.

3.6.3 Calculation of Radium Equivalent Activity and Hazard Indices

3.6.3.1 Radium Equivalent Activity

The radiological risk of NORM in sand from the study area, which could be used for road construction, housing, cement manufacturing, block production, and other applications, was assessed by calculating the radium equivalent activity (Ra_{eq}) as well as the external and internal hazard indices (OECD/NEA, 1979; Beretka and Mathew, 1985; Kpeglo, 2015).

The Ra_{eq} is a commonly used hazard index for assessing the potential radiological effects on human health under the assumption that the gamma dose rate from 370 $Bqkg^{-1}$ of ^{226}Ra, 260 $Bqkg^{-1}$ of ^{232}Th, or 4810 $Bqkg^{-1}$ of ^{40}K would be the same. It was calculated using Equation (3.9).

$$Ra_{eq}=C_{Ra}+1.43C_{Th}+0.077C_{K} \quad (3.9)$$

where, C_{Ra}, C_{Th} and C_K are the activity concentrations of ^{226}Ra, ^{232}Th and ^{40}K, respectively. The maximum suggested value of Ra_{eq} for raw building materials and products should be less than 370 $Bqkg^{-1}$ for safe use. Thus, the external gamma dose must be less than 1.5 $mSvy^{-1}$.

3.6.3.2 External Hazard Index

Another criterion for determining the amount of gamma radiation related to naturally occurring radionuclides in certain building materials is the external hazard index (H_{ex}). It is described in Equation (3.10).

$$H_{ex} = \frac{C_{Ra}}{370} + \frac{C_{Th}}{259} + \frac{C_K}{4810} \quad (3.10)$$

where C_{Ra}, C_{Th} and C_K are the activity concentrations of ^{226}Ra, ^{232}Th and ^{40}K, respectively. The external hazard index must be less than one for the risk from gamma radiation to be deemed insignificant. Exposure to radiation due to the radioactivity from building materials has a limit of 1.5 $mSvy^{-1}$.

3.6.3.3 Internal Hazard Index

Equation (3.11) was also used to compute the internal hazard index (H_{in}) caused by radon and its offspring. This is because radon and its short-lived byproducts are also harmful to the respiratory system.

$$H_{in} = \frac{C_{Ra}}{185} + \frac{C_{Th}}{259} + \frac{C_K}{4810} \qquad (3.11)$$

where C_{Ra}, C_{Th} and C_K are the activity concentrations of ^{226}Ra, ^{232}Th and ^{40}K, respectively. The internal hazard index of building materials must be less than one for it to be deemed safe for use in the construction of homes.

3.6.3.4 Gamma Representative Level Index (*Iγr*)

The level of gamma radiation hazard associated with natural gamma emitters in sediments can be estimated using the representative level index *Iγr* of the sediment. This index serves as a screening tool for detecting materials that can become health concerns when utilized as construction materials and is used to correlate the annual dose rate due to the excess external gamma radiation created by surface materials. The formula based on the radiation hazard index *Iγr* (NEA-OECD, 1979; Alam et al., 1999) was used to determine the gamma radiation hazard level of the sediment samples linked to natural radionuclides (Ravisankar et al., 2015; Penabei et al., 2018).

$$\mathbf{I\gamma r} = \frac{1}{150A_U} + \frac{1}{100A_{Th}} + \frac{1}{1500A_K} \qquad (3.12)$$

where A_U, A_{Th} and A_K are the activity concentrations of ^{238}U, ^{232}Th and ^{40}K respectively. To keep the radiation, hazard insignificant, the representative level index (Iγr) must be less than unity.

3.6.3.5 Activity Utilization Index (AUI)

An activity utilization index is used to determine if construction materials from the sea sediments are safe. This is to facilitate the calculation of dose rates in air from the combination of the three different radionuclides in sediments by using the appropriate conversion factors. It is given by the formula:

$$AUI = \left(\frac{A_U}{50Bqkg^{-1}}\right)f_U + \left(\frac{A_{Th}}{50BqKg^{-1}}\right)f_{Th} + \left(\frac{A_K}{500Bqkg^{-1}}\right)f_K \qquad (3.13)$$

where A_U, A_{Th} and A_K are activity concentrations (in $Bqkg^{-1}$) of ^{238}U, ^{232}Th and ^{40}K and f_U, f_{Th}, and f_K are the fractional contributions to the total dose rate in air due to gamma radiation from the actual concentrations of these radionuclides. Typical activities per unit mass of ^{238}U, ^{232}Th, and ^{40}K in sediments A_U, A_{Th} and A_K are referred to be 50, 50 and 500 $Bqkg^{-1}$, respectively (NEA-OECD, 1979).

3.6.3.6 Excess Lifetime Cancer Risk (ELCR)

Estimating the likelihood of cancer occurrence in a population of people for a certain lifetime using estimated intakes and exposures and chemical-specific dose-response data allows us to identify potential carcinogenic effects (i.e., slope factors). During a person's lifetime, exposure to

harmful substances increases their risk of developing cancer (Ravisankar et al., 2014). The following equation is used to compute the excess lifetime cancer risk (ELCR):

$$ELCR = AEDE \times DL \times RF \qquad (3.14)$$

where AEDE, DL and RF are the total annual effective dose equivalent, duration of life (70 y) and risk factor (0.057 Sv^{-1}), that is, fatal cancer risk per sievert, respectively (Taskin et al., 2009).

3.7 Statistical Approach

R is a programming language and environment for statistical computing and graphics. It provides a wide variety of statistical (linear and non-linear modeling, classical statistical tests, time-series analysis, classification, clustering) and graphical techniques and is highly extensible. This research presents a linear and or non-linear modeling procedure from the data which was used to develop an empirical model. The model was based on correlations obtained from analysis of the experimental data obtained for assessment of the risk of exposure to naturally occurring radioactive materials. The model was used to fit the data using regression analysis to reflect all data points in a mathematical form. At a 95% confidence level, a p-value of 0.5 was set for all the statistical analyses conducted.

CHAPTER FOUR

RESULTS OF DATA ANALYSIS

4.1 Analytical Quality Control Procedures

Before the analysis, quality control procedures were carried out for both alpha and gamma spectrometry systems to verify the accuracy and dependability of the measurements.

4.1.1 Gamma Spectrometry System

For liquid matrix samples, the gamma system was efficiently calibrated using a multi-gamma certified cocktail standard (^{109}Cd, ^{139}Ce, ^{241}Am, ^{113}Sn, ^{85}Sr, ^{57}Co, ^{88}Y, ^{60}Co, and ^{137}Cs), which was uniformly distributed in solid water with volume and density of 1000 cm^3 and 0.98 gcm^{-3}, respectively. On the other hand, the solid matrix samples were prepared similarly to the mean densities (1.33 ± 0.03 gcm^{-3}) of the IAEA reference materials IAEA-RGU-1(U-ore), IAEA-RGTh-1 (Th-ore) and IAEA-RGK-1 (K-ore).

Figures 4.1 and 4.2 display the results of the energy and efficiency calibration for the gamma spectrometry system.

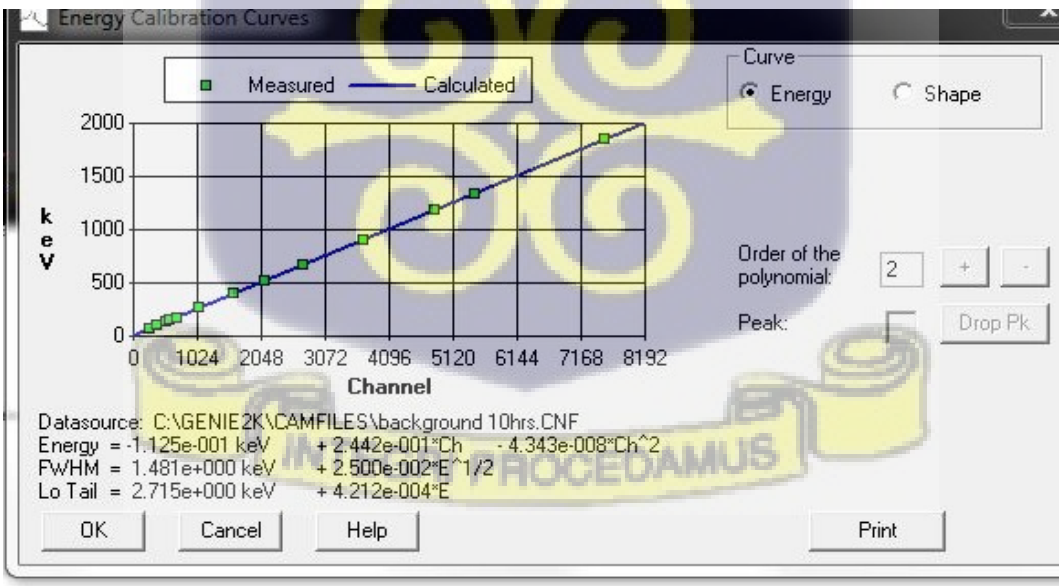

Figure 4.1: Energy calibration curve for gamma spectrometry system.

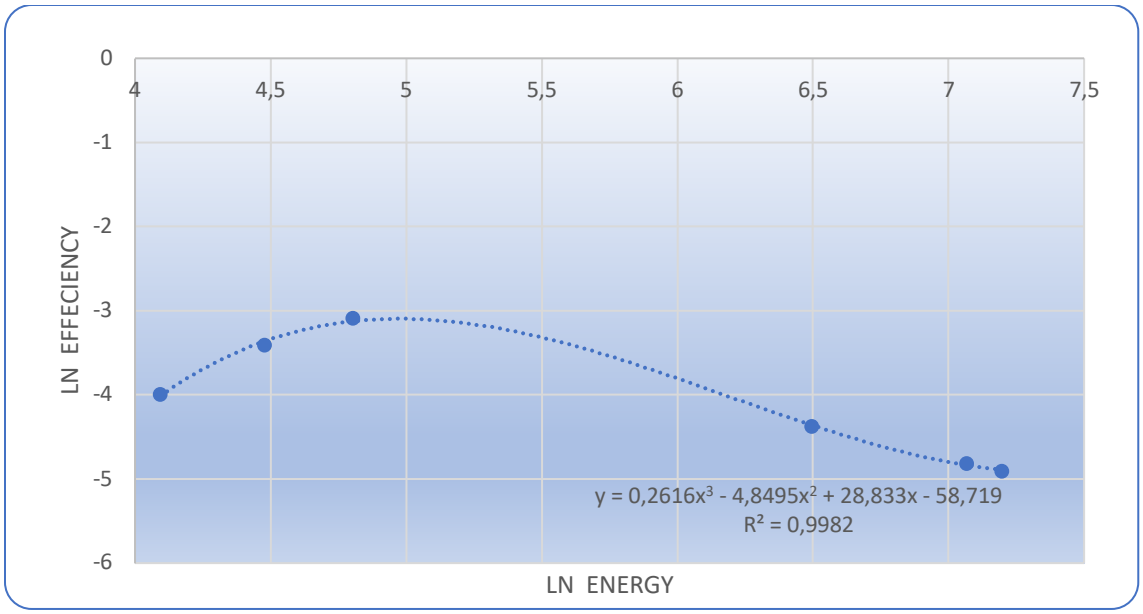

Figure 4.2: Efficiency calibration curve for the gamma spectrometry system.

4.1.2 Alpha Spectrometry System

The efficiency values for all alpha chambers as shown in Table 4.1 were measured at a source-to- detector distance of 0.5 cm and the same source-to-detector distance was used for measurements of samples in this study. However, these efficiency values were only used for the estimation of the radiochemical yields.

Table 4.1: Results of experimental efficiencies for the alpha chambers at a source-to-detector distance of 0.5 cm

Chamber	1A	1B	2A	2B	3A	3B	4A	4B
E (%)	20.1±1.2	19.5±1.1	19.0±1.2	19.9±1.1	18.9±1.3	19.3±1.3	19.5±1.3	19.4±1.3

An Eckert & Ziegler Certified mixed standard radionuclide calibration source (^{238}U, ^{234}U, ^{241}Am, and ^{239}Pu) in a 24.1 mm diameter by 0.65 mm thick stainless steel disc shape (the same geometry

utilized for samples in alpha measurements) was utilized to do the energy calibration (Figure 4.3) for the alpha system.

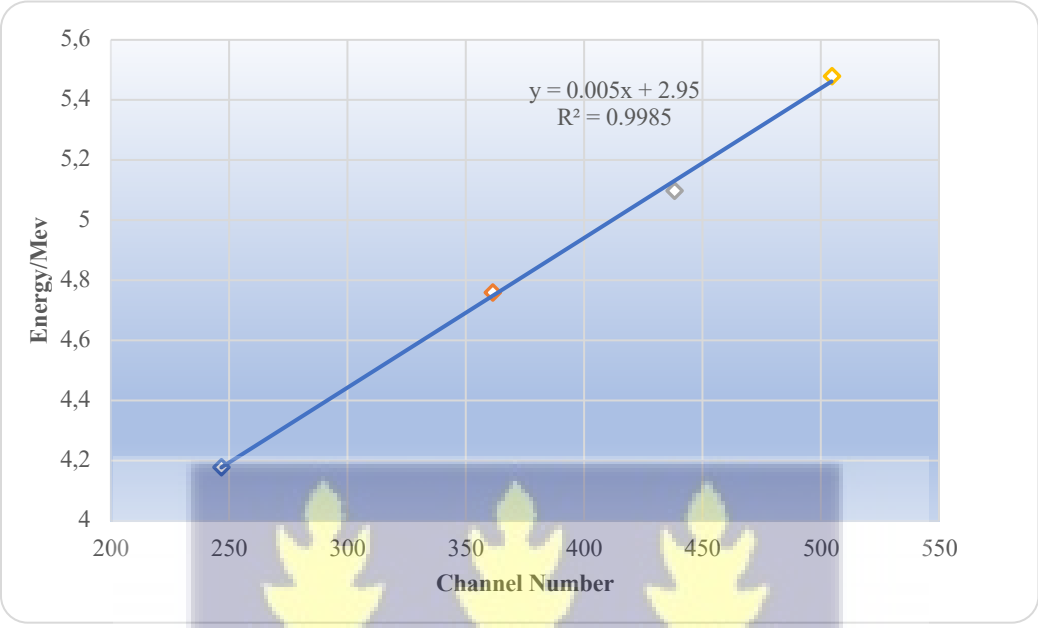

Figure 4.3: Energy calibration curve for alpha spectrometry system with PIPS detection system.

4.2 Results of Activity Concentrations Measured by Gamma Spectrometry Analysis.

The activity concentrations of the radionuclides in coastal soil and sediment for each of the four locations determined by gamma spectrometry are presented in Tables 4.2 to 4.9.

4.2.1 Activity Concentration Results of NORM in Beach Sand

The calculated activities of ^{40}K, ^{232}Th, ^{238}U, ^{226}Ra, ^{228}Ra, and ^{228}Th for coastal sand in Sekondi-Takoradi are shown in Table 4.2. The average values of ^{40}K, ^{232}Th, ^{238}U, ^{226}Ra, ^{228}Ra, and ^{228}Th were 649.8±172 $Bqkg^{-1}$ (in the range 564.4–865.6 $Bqkg^{-1}$), 25.25±6.3 $Bqkg^{-1}$ (in the range 14.8 – 32.5 $Bqkg^{-1}$), 21.23±2.1 $Bqkg^{-1}$ (in the range 13.7 – 27.5 $Bqkg^{-1}$), 21.87±2.9 $Bqkg^{-1}$ (in the range 16.8 – 28 $Bqkg^{-1}$), 25.22±11.4 $Bqkg^{-1}$ (in the range 12.5 – 35.4 $Bqkg^{-1}$), and 25.3±2.1 $Bqkg^{-1}$ (in the range 15.9 – 30.7 $Bqkg^{-1}$), respectively.

Table 4.2: Activity concentrations of radionuclides in coastal sand from Sekondi-Takoradi determined by gamma spectrometry analysis.

Sample ID	Activity Concentration ($Bqkg^{-1}$)					
	^{238}U	^{232}Th	^{40}K	^{226}Ra	^{228}Ra	^{228}Th
TK 1	15.8±4.8	20.9± 5.7	864.4±257.7	23.2±2.0	16.5± 10	25.3±1.3
TK 2	13.8± 3.8	18.2± 4.3	754.9± 200.4	20.3± 1.5	14.4±7.8	22.1±0.9
TK 3	21.1± 0.1	14.8±7.2	636.2± 138.8	26.7± 3.2	13.7± 9.8	15.9±4.6
TK 4	25.9± 5.2	24.1± 5.8	564.4± 153.3	20.7± 1.3	26.4± 10.3	21.8± 1.2
TK 5	22.4±6.2	29.5± 7.2	603± 162.6	19.2± 2.6	32.2± 13.6	26.8± 0.9
TK 6	24.6± 7.4	32.4± 8.7	663.1± 194.1	21.1± 3.1	35.4± 16.4	29.5± 1.0
TK 7	21.4± 5.7	28.2±6.6	575.7±149.3	18.3±2.4	30.8± 12.4	25.6±0.8
TK 8	21.7± 5.8	28.5± 6.8	582.9±152.8	18.5±2.4	31.1± 12.7	25.9± 0.8
TK 9	23.5±6.8	31± 7.9	633.1±178	20.1± 2.8	33.8±15.0	28.1±0.9
TK 10	13.7± 3.0	24.4±3.7	617.5± 129.3	26.7± 2.7	19.3± 5.1	29.5± 2.2
TK 11	17.9 ± 3.2	19.8±4.5	865.6±259.4	24.3±3.0	14.6±8.6	26.5±2.8
TK 12	15.2± 5.8	17.2±3.2	756.3±201.6	21.9±2.6	13.1±9.0	23.7±2.0
TK 13	23.0± 4.7	15.9±8.4	637.7±140.4	27.8±2.0	12.5±8.6	17.7±5.8
TK 14	27.5± 6.0	26.1±7.0	565.5±154.6	21.8±2.8	24.8±12.0	23.1±3.2
TK 15	24.2± 7.7	28.0±5.2	604.7±164.6	20.8±4.1	30.5±14.8	28.3±2.1
TK 16	25.7± 8.6	30.4±7.3	664.5±192.6	22.6±4.2	34.3±15.3	30.6±2.3
TK 17	22.7± 4.6	29.7±5.4	577.3±150.9	17.0±3.9	32.3±11.4	23.8±2.0
TK 18	23.2± 7.0	30.1±5.8	581.6±151.4	16.8±3.7	32.9±11.2	24.5±2.4
TK 19	25.4± 5.7	32.5±9.5	631.3±179.3	21.6±3.9	35.2±17.0	26.5±2.1
TK 20	15.8± 4.5	23.2±4.9	616.3±128	28.0±4.3	20.6±6.7	30.7±3.6
Mean	21.23±2.1	25.25±6.3	649.8±172	21.87±2.9	25.22±11.4	25.3±2.1
Max	27.5±6.0	32.5±9.5	865.6±259.4	28.0±4.3	35.4±16.4	30.7±3.6
min	13.70±3.0	14.8±7.2	564.4±153.3	16.8±3.7	12.5±8.6	15.9±4.6

The calculated activity concentrations of ^{40}K, ^{232}Th, ^{238}U, ^{226}Ra, ^{228}Ra, and ^{228}Th for coastal sand in Axim are presented in Table 4.3. The average values of ^{40}K, ^{232}Th, ^{238}U, ^{226}Ra, ^{228}Ra, and ^{228}Th were 199.09±53.5 $Bqkg^{-1}$ (in the range 132.5–238.5 $Bqkg^{-1}$), 14.34±3.61 $Bqkg^{-1}$ (in the range 10.4 – 20.3 $Bqkg^{-1}$), 23.84±2.67 $Bqkg^{-1}$ (in the range 18 – 29.1 $Bqkg^{-1}$), 15.86±0.88 $Bqkg^{-1}$ (in the range 7 – 27.1 $Bqkg^{-1}$), 14.95±4.29 $Bqkg^{-1}$ (in the range 6.4 – 20.5 $Bqkg^{-1}$), and 15.09±2.6 $Bqkg^{-1}$ (in the range 8.2 – 26.2 $Bqkg^{-1}$), respectively.

It is observed from Table 4.3 that all the radionuclides of interest, especially ^{238}U, ^{232}Th and ^{40}K are all within globally accepted levels of 35 $Bqkg^{-1}$, 30 $Bqkg^{-1}$ and 400 $Bqkg^{-1}$.

Table 4.3: Activity concentration of radionuclides in coastal sand from Axim determined by gamma spectrometry analysis.

Sample ID	Activity Concentration (Bqkg^{-1})					
	^{238}U	^{232}Th	^{226}Ra	^{228}Ra	^{228}Th	^{40}K
AX 1	18.9± 0.9	10.8± 3.9	12.8± 2.4	14.7±4.9	7.1± 3.0	237.3± 66.3
AX 2	18± 3.9	14.4± 2.7	6.4± 0.8	9.6± 4.1	19.2± 1.3	132.5± 27.9
AX 3	27.9± 6.8	11.6± 1.8	18± 0.2	8.2± 3.3	14.9± 0.4	167.8± 44.3
AX 4	23.4± 0.4	20.3± 3.1	20.5± 0.1	13.5± 4.8	27.1± 1.5	137± 29.6
AX 5	20.4± 7.9	18.3± 0.4	16.3± 1.5	16.3±1.7	20.3± 2.6	235.6±64.8
AX 6	19.3± 0.7	19.9± 0.4	14.6± 1.1	12.8± 1.4	26.9± 2.1	201.7± 48.4
AX 7	23.3± 0.9	14± 4.2	15.5± 0.3	17.8± 4.6	10.2± 3.7	205.6± 57.6
AX 8	25.7± 1.1	15.5± 5.0	17.1± 0.4	19.7± 5.4	11.2± 4.6	226.9± 69.1
AX 9	27.7± 0.8	10.9± 4.3	16.6± 0.1	14.6± 4.8	7.1± 3.8	218± 63.7
AX 10	29± 0.9	11.4± 4.7	17.5± 0.1	15.3± 5.2	7.4± 4.2	228.7± 69.7
AX 11	19.9±1.9	10.4±5.1	14.0±2.0	15.9±5.1	8.2±3.6	238.5±67.0
AX 12	19.0±4.2	13.2±4.7	7.6±0.8	11.1±5.1	20.4±3.2	133.6±26.6
AX 13	29.1±8.0	10.6±3.0	19.1±0.6	9.4±4.5	16.5±1.5	166.9±42.8
AX 14	24.6±1.4	19.2±3.5	21.5±0.5	12.2±6.0	26.2±1.1	138.5±28.0
AX 15	21.6±7.0	16.8±1.6	17.6±2.5	14.5±2.9	19.4±2.6	237.2±62.9
AX 16	20.7±0.9	18.0±1.6	16.1±1.4	14.0±2.6	26.1±1.2	200.8±46.6
AX 17	24.9±1.1	12.8±4.8	16.7±0.9	16.0±5.8	11.5±2.3	206.8±56.0
AX 18	27.0±1.3	14.0±6.0	18.8±0.5	17.9±3.6	12.6±2.8	225.5±67.9
AX 19	29.1±2.1	12.1±5.5	17.8±0.6	16.4±3.6	9.1±4.2	216±62.5
AX 20	27.2±1.2	12.6±5.9	16.6±0.7	16.2±6.4	9.3±2.2	226.8±68.0
mean	23.84±2.67	14.34±3.61	15.86±0.88	14.95±4.29	15.09±2.6	199.09±53.5
Max	29.1±8	20.3±3.1	21.4±0.5	19.7±5.4	26.9±2.1	238.5±67
min	18±3.9	10.4±5.1	7.6±0.8	9.4±4.5	7.1±3.0	132.5±27.9

The calculated activities of ^{40}K, ^{232}Th, ^{238}U, ^{226}Ra, ^{228}Ra, and ^{228}Th for coastal sand in Beyin are shown in Table 4.4. The average values of ^{40}K, ^{232}Th, ^{238}U, ^{226}Ra, ^{228}Ra, and ^{228}Th were 221.12±65.3 Bqkg^{-1} (in the range 139.1–353.3 Bqkg^{-1}), 32.52±4.57 Bqkg^{-1} (in the range 12.8 – 33.3 Bqkg^{-1}), 21.04±5.4 Bqkg^{-1} (in the range 12.8 – 30.9 Bqkg^{-1}), 24.29±2.9 Bqkg^{-1} (in the range 5.1 – 41 Bqkg^{-1}), 25.31±6.74 Bqkg^{-1} (in the range 11.8 – 46.3 Bqkg^{-1}), and 23.45±2.64 Bqkg^{-1} (in the range 6.2 – 44.9 Bqkg^{-1}), respectively.

Table 4.4: Activity concentration of radionuclides in coastal soil from Beyin determined by gamma spectrometry analysis.

Sample ID	Activity Concentration (Bqkg^{-1})					
	^{238}U	^{232}Th	^{226}Ra	^{228}Ra	^{228}Th	^{40}K
BN 1	15.9±4.9	18.7± 4.6	18± 0.1	15.5± 5.2	22±5.2	147.8± 44.6
BN 2	21.2± 5.3	33.3± 3.9	32.5± 0.6	36.9± 5.2	29.7±2.7	183± 43.9
BN 3	23.5±6.5	24± 0.1	40± 0.8	31.8± 1.5	16.3± 1.4	229± 61.8
BN 4	24.2± 0.6	15.9± 2.5	24.4± 3.3	12.9± 4.6	18.9±0.4	212.6±65.2
BN 5	30.9± 9.1	29.7± 5.3	21.9± 3.1	30.7± 9.6	28.6±1.1	259± 74
BN 6	16.6± 5.2	30.9± 8.8	29.9±3.9	44.9± 14.3	16.8± 3.3	215.6±65.6
BN 7	12.8± 3.9	24.6± 0.8	30.7± 9.6	16.8± 1.9	32.3± 3.5	352± 103.6
BN 8	25.7± 7.7	12.8± 5.6	17.8± 0.6	20.4± 7.3	5.1±3.9	139.1± 40.6
BN 9	17.9± 5.5	19.1± 5.4	20.3± 2.5	15.9± 9.8	22.5± 1.0	281± 84.9
BN 10	22.5± 0.3	19.5±4.2	22.2±3.1	12.6± 5.9	26.4± 2.6	222.9± 65.4
BN 11	15.4±6.1	19.9±5.8	19.1±0.1	17.0±5.4	24.0±5.2	149.3±45.8
BN 12	20.0±6.3	32.8±5.2	34.5±1.6	38.9±5.8	30.9±2.8	184.2±44.0
BN 13	22.3±7.0	25.2±1.1	41.0±0.6	32.7±2.0	17.6±1.6	230.6±62.8
BN 14	22.2±1.6	17.0±3.5	25.5±3.5	13.8±5.2	20.4±0.6	214.6±66.2
BN 15	30.0±9.2	30.8±6.3	23.4±3.4	32.1±10.0	29.8±1.0	260.3±75.0
BN 16	15.5±6.4	32.4±10.0	30.8±4.2	46.3±14.6	17.0±4.5	353.5±66.6
BN 17	14.2±5.2	26.6±1.8	31.9±10.4	17.6±2.2	33.3±3.7	140.3±104.6
BN 18	26.9±8.9	14.2±6.8	19.4±1.0	21.6±8.6	6.2±4.1	140.0±39.6
BN 19	19.0±6.5	20.2±5.4	18.7±2.7	16.7±10.2	23.5±1.2	283.0±86.0
BN 20	24.0±1.3	21.0±4.2	22.8±3.7	11.8±5.4	27.8±3.0	224.5±66.2
mean	21.04±5.4	32.52±4.57	24.29±2.9	25.31±6.74	23.45±2.64	221.12±65.3
Max	30.9±9.1	33.3±3.9	41.0±0.6	46.3±14.6	30.9±2.8	353.5±66.6
min	12.8±3.9	12.8±5.2	17.8±0.6	11.8±5.4	5.1±3.9	139.1±40.6

The calculated activities of ^{40}K, ^{232}Th, ^{238}U, ^{226}Ra, ^{228}Ra, and ^{228}Th for coastal sand in Half Asini are shown in Table 4.5. The average values of ^{40}K, ^{232}Th, ^{238}U, ^{226}Ra, ^{228}Ra, and ^{228}Th were 309.89±71.88 Bqkg^{-1} (in the range 252.8 – 376.6 Bqkg^{-1}), 17.53±3.4 Bqkg^{-1} (in the range 13.2 – 23 Bqkg^{-1}), 20.75±4.13 Bqkg^{-1} (in the range 11 – 28.5 Bqkg^{-1}), 23.23±0.92 Bqkg^{-1} (in the range 19 – 37.2 Bqkg^{-1}), 17.13±3.8 Bqkg^{-1} (in the range 10.6 – 31 Bqkg^{-1}), and 17.84±2.14 Bqkg^{-1} (in the range 8.8 – 21.6 Bqkg^{-1}), respectively.

Table 4.5: Activity concentration of radionuclides in coastal soil from Half-Asini determined by gamma spectrometry analysis.

Sample ID	Activity Concentration ($Bqkg^{-1}$)					
	^{238}U	^{232}Th	^{226}Ra	^{228}Ra	^{228}Th	^{40}K
HA 1	23.9± 5.5	17±3.2	19.4± 0.1	15.6±3.4	18.4± 3.1	275.3± 60.5
HA 2	26.1± 6.4	18.6± 3.8	21.2± 0.2	17.1± 3.9	20.1± 3.7	301.4± 71.1
HA 3	15± 0.1	15.4± 3.0	22.1± 0.1	12.3± 4.1	18.4± 2.0	322.9±82
HA 4	16.3±0.3	16.7± 3.4	24± 0.6	13.4± 4.6	20± 2.2	350.9± 95.4
HA 5	28.5± 8.7	21.5± 2.9	37.2± 4.2	29.9± 5.6	13.1± 0.2	375±111.1
HA 6	19.2± 4.3	14.5± 1.8	25.1± 1.8	20.2±3.2	8.8± 0.4	252.8± 54.3
HA 7	16.8± 0.1	17.2±3.6	24.7±0.4	13.8± 4.8	20.6± 2.3	361.8±101
HA 8	13± 2.3	13.2± 2.5	19±0.3	10.6± 3.3	15.9± 1.7	278.5±62.8
HA 9	23.9± 5.5	17± 3.2	19.4± 0.7	15.6± 3.4	18.4± 3.1	275.3± 60.5
HA 10	26.1± 6.4	18.6± 3.8	21.2± 0.1	17.1± 3.9	20.1± 3.7	301.4± 71.1
HA 11	25.2±5.0	18.0±3.4	19.0±0.1	16.0±3.0	18.0±3.0	276.4±59.0
HA 12	26.0±6.0	17.4±3.9	21.0±0.4	17.0±2.4	21.3±3.0	300.0±70.0
HA 13	16.0±0.6	17.4±3.2	21.1±0.1	14.3±3.7	19.4±2.4	324.0±84.0
HA 14	16.1±0.8	17.0±3.6	25.0±0.9	14.5±3.8	21.6±2.6	352.9±95.0
HA 15	27.0±9.0	23.0±3.2	36.2±3.6	31.0±4.8	13.0±0.8	376.6±12.3
HA 16	18.0±5.2	15.5±2.9	26.5±2.4	22.0±3.0	9.2±0.9	253.0±55.9
HA 17	14.8±0.1	18.6±5.6	23.4±0.8	15.3±4.9	21.6±1.9	363.8±101.9
HA 18	11.0±2.6	15.2±4.4	19.1±0.6	11.7±3.0	17.3±1.0	279.2±60.7
HA 19	24.5±6.0	18.7±3.0	19.0±0.9	17.2±3.6	19.9±2.8	275.0±59.0
HA 20	27.6±7.6	20.0±3.6	21.0±0.1	17.9±3.5	21.6±2.0	301.6±70.0
mean	20.75±4.13	17.53±3.4	23.23±0.92	17.13±3.8	17.84±2.14	309.89±71.88
max	28.5±8.7	23.0±3.2	37.2±4.2	31.0±4.8	21.6±1.9	376.6±12.3
min	11.0±2.6	13.2±2.5	19.0±0.3	10.6±3.3	8.8±0.4	252.8±54.3

Figure 4.4 shows the calculated activities of ^{40}K, ^{232}Th, ^{238}U, ^{226}Ra, ^{228}Ra, and ^{228}Th for coastal sand in Sekondi-Takoradi, Axim, Beyin and Half Asini. The calculated mean activity concentrations of ^{40}K, ^{232}Th, ^{238}U, ^{226}Ra, ^{228}Ra, and ^{228}Th for coastal sand in Sekondi-Takoradi, Axim, Beyin and Half Asini are represented in Fig. 4.5 which indicates the high levels of ^{40}K in all the sample locations. The overall averages of the activity concentration of each of the radionuclides found in beach sand from the sample area (western coast) is represented in Figure 4.6.

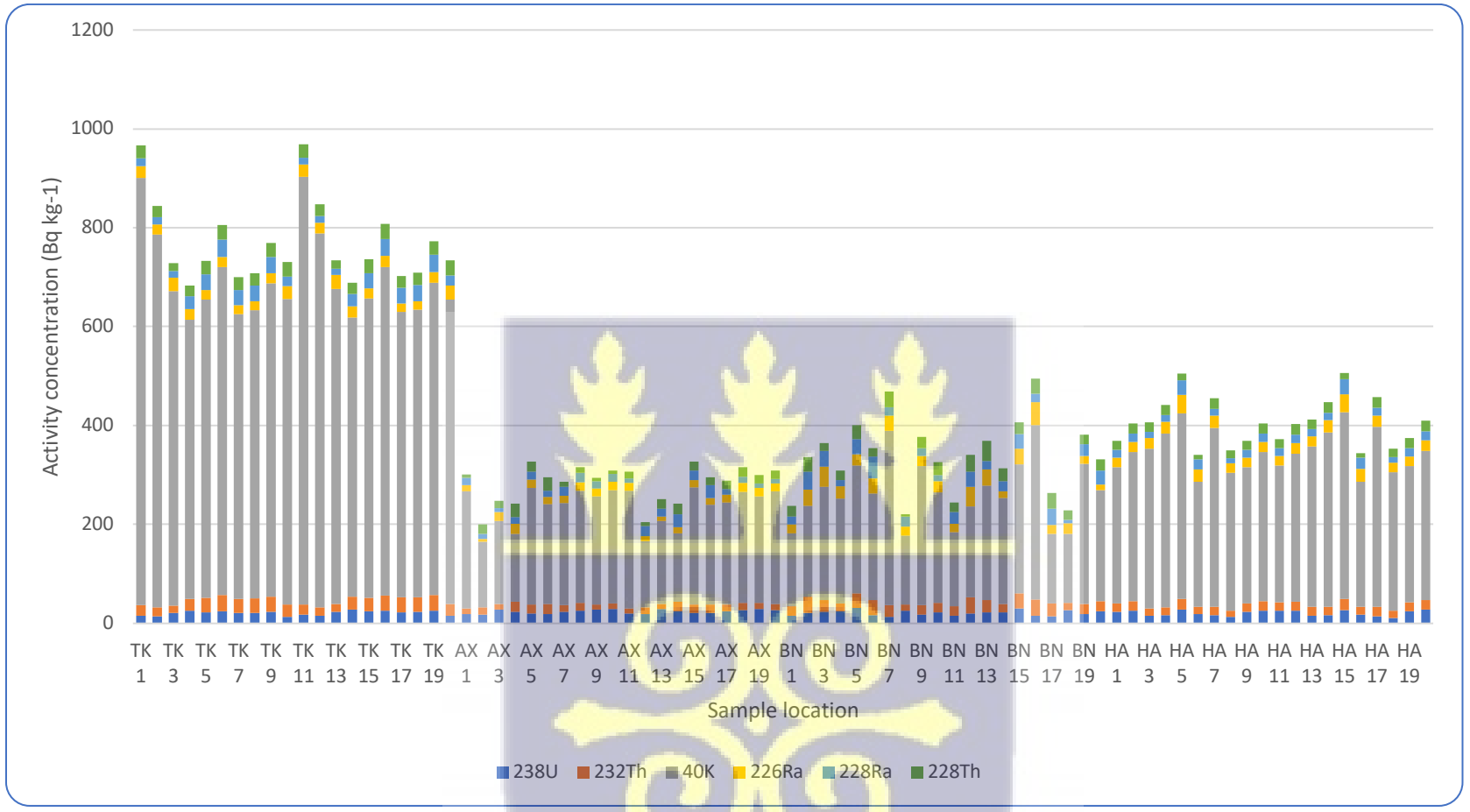

Figure 4.4: The ^{238}U, ^{232}Th, ^{226}Ra, ^{228}Ra, ^{228}Th and ^{40}K activity concentrations in each of the soil samples from the study area.

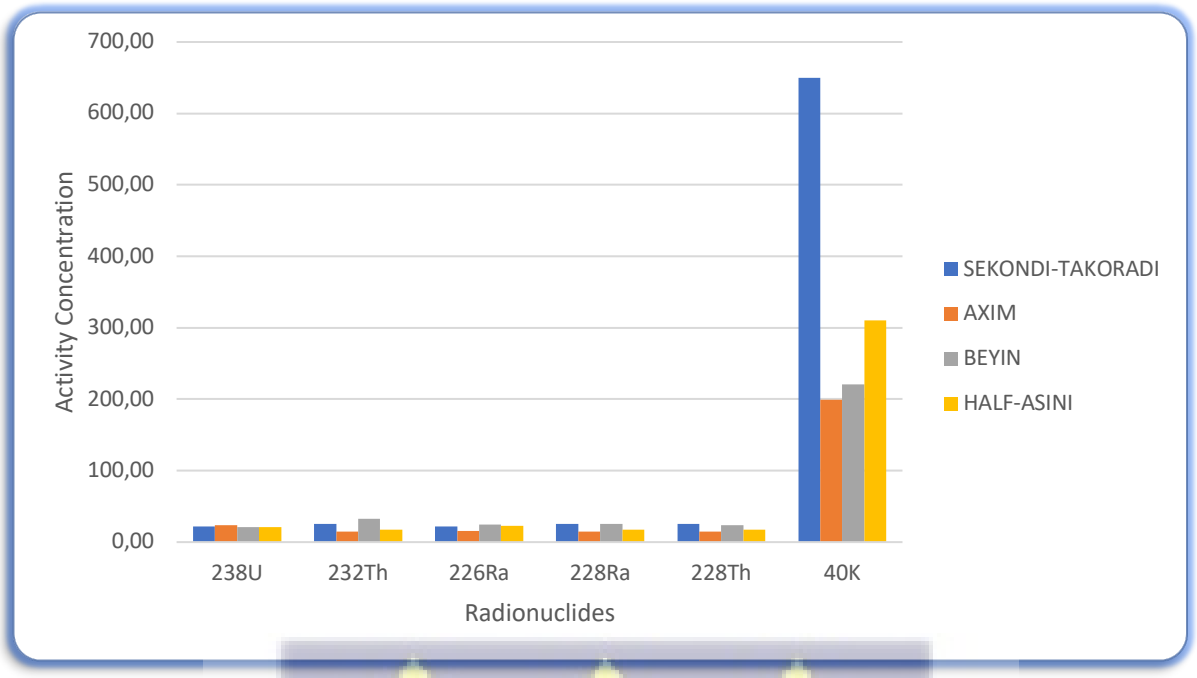

Figure 4.5: The ^{238}U, ^{232}Th, ^{226}Ra, ^{228}Ra, ^{228}Th and ^{40}K mean activity concentrations in all the soil samples from the individual study areas.

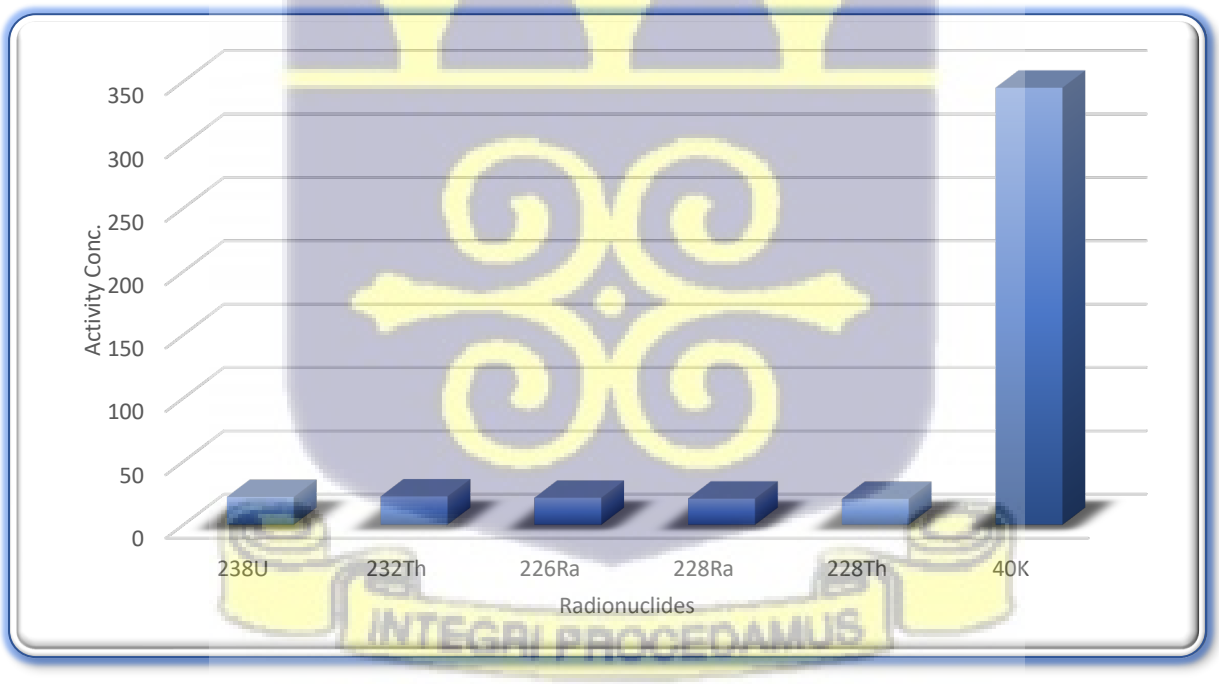

Figure 4.6: The mean activity concentrations of ^{238}U, ^{232}Th, ^{226}Ra, ^{228}Ra, ^{228}Th and ^{40}K in the soil samples of the western coast.

4.2.2 Activity Concentration Results of NORM in Sea Sediment

The calculated activities of ^{40}K, ^{232}Th, ^{238}U, ^{226}Ra, ^{228}Ra, and ^{228}Th for sea sediment from the coast of the same communities as the beach sand are shown in Figure 4.5 and Tables 4.6 – 4.9.

The average values of ^{40}K, ^{232}Th, ^{238}U, ^{226}Ra, ^{228}Ra, and ^{228}Th as shown in Table 4.6 were 540.32±96.9 $Bqkg^{-1}$ (in the range 577.6 – 489.1 $Bqkg^{-1}$), 19.8±2.1 $Bqkg^{-1}$ (in the range 27.9 – 11.8 $Bqkg^{-1}$), 19.64±2.6 $Bqkg^{-1}$ (in the range 25 – 13.4 $Bqkg^{-1}$), 10.67±1.4 $Bqkg^{-1}$ (in the range 24.3 – 1.9 $Bqkg^{-1}$), 15.13±2.8 $Bqkg^{-1}$ (in the range 24.1 – 8.6 $Bqkg^{-1}$), and 24.97±1.7 $Bqkg^{-1}$ (in the range 34.4 – 14.8 $Bqkg^{-1}$), respectively.

Comparatively, the results in the sea sediments are lower generally than that of the beach sand samples. However, the average activities of the radionuclides along the sample area were all within the recommended international standards except ^{40}K which exceeded the average recommended value of 400 $Bqkg^{-1}$ according to UNSCEAR (2000), from samples taken from Sekondi-Takoradi and Half-Asini.

Table 4.6: Activity concentration of radionuclides in coastal sediment from Sekondi-Takoradi determined by gamma spectrometry.

Sample ID	Activity Concentration ($Bqkg^{-1}$)					
	^{238}U	^{232}Th	^{40}K	^{226}Ra	^{228}Ra	^{228}Th
TK 1	21.1± 3.0	16.4± 2.3	545.3± 92.1	2.7±0.3	9.2± 3.3	23.7± 1.2
TK 2	19.5± 2.9	20.7± 2.1	559.6± 95.7	2.8± 0.5	10.5± 3.4	30.9± 0.7
TK 3	21.1± 3.1	27.3± 0.7	564.5±97.1	2.7± 0.1	22.9± 0.8	31.7± 2.1
TK 4	13.4± 2.5	23.6±2.9	576.5± 99.9	2.6± 0.3	18.3± 4.1	28.9± 1.7
TK 5	14.9± 0.5	19.4± 0.6	514.6± 98.6	22.5±2.5	13.7±1.0	25± 2.1
TK 6	23± 0.3	13.7± 0.1	489.1± 92.1	23.5± 1.8	11.4± 0.9	16.1± 1.1
TK 7	23.3± 0.3	13.9±0.1	495.8± 94.3	23.8± 1.9	11.5±1.0	16.3± 1.1
TK 8	15.8± 0.6	23.7± 0.4	568.6± 99.7	15.7±1.0	20.3± 0.8	27± 0.1
TK 9	22.8± 3.7	26.7±3.2	548.3± 100.6	2.5± 0.5	20.6± 4.3	32.8± 2.0
TK 10	14.3± 2.9	11.8± 1.7	534.3± 102.1	3.6± 0.4	8.6± 2.9	14.9± 0.5
TK 11	22.6± 4.0	15.2±3.7	546.5±91.2	3.7±1.0	10.7±4.2	24.8± 2.0
TK 12	20.8± 4.4	19.6±3.3	560.9±94.9	1.9±1.6	12.0±4.1	32.0±2.2
TK 13	22.9±4.2	25.7±2.2	565.8±96.4	4.2±1.0	24.1±2.0	33.2±2.8
TK 14	14.6±4.2	22.2±4.0	577.6±99.4	4.2±3.7	19.8±5.6	30.4±2.7
TK 15	16.0±1.7	18.1±1.6	515.4±97.6	23.3±3.0	14.9±2.0	23.0±2.5
TK 16	24.5±1.6	15.3±1.6	490.7±90.9	24.3±3.1	10.2±2.9	15.2±1.8
TK 17	25±1.5	15.5±0.1	497.1±92.9	23.0±1.8	9.6±1.6	14.8±1.8
TK 18	17.0±2.6	25.3±4.6	570.0±98.1	17.7±0.5	21.6±1.4	28.3±0.9
TK 19	21.2±4.9	27.9±3.6	549.5±101.8	4.5±0.9	22.2±5.5	34.4±4.0
TK 20	15.4 ±2.9	13.9±3.2	536.2±102.9	4.8±1.2	10.5±4.4	15.9±1.2
Mean	19.64±2.6	19.8±2.1	540.32±96.9	10.67±1.4	15.13±2.8	24.97±1.7
max	25±1.5	27.9±3.6	577.6±99.4	24.3±3.1	24.1±2.0	34.4±4.0
min	13.4±2.5	11.8±1.7	489.1±92.1	1.9±1.6	8.6±2.9	14.8±1.8

The calculated activities of ^{40}K, ^{232}Th, ^{238}U, ^{226}Ra, ^{228}Ra, and ^{228}Th for coastal sediment in Axim as shown in Table 4.7 were 162.94±37.2 $Bqkg^{-1}$ (in the range 286.6 –107.7 $Bqkg^{-1}$), 22.39±4.6 $Bqkg^{-1}$ (in the range 28.2 – 13 $Bqkg^{-1}$), 22.9±1.6 $Bqkg^{-1}$ (in the range 30.5 – 14.3 $Bqkg^{-1}$), 19.2±2.0 $Bqkg^{-1}$ (in the range 27.1 – 15.5 $Bqkg^{-1}$), 17.62±6.7 $Bqkg^{-1}$ (in the range 22.9 – 9.9 $Bqkg^{-1}$), and 26.92±2.6 $Bqkg^{-1}$ (in the range 34.9 – 15.5 $Bqkg^{-1}$), respectively.

Table 4.7: Activity concentration of radionuclides in sediment from Axim determined by gamma spectrometry analysis.

Sample ID	Activity Concentration (Bqkg^{-1})					
	^{238}U	^{232}Th	^{226}Ra	^{228}Ra	^{228}Th	^{40}K
AX 1	14.3±0.2	24.4±4.4	17.3± 2.2	18.6± 5.7	30.3± 3.1	148.9± 35.3
AX 2	21.7± 0.2	23.5± 6.1	19.6± 2.0	18.2± 0.7	28.7±1.5	152.5± 35.6
AX 3	20.8± 0.1	22.5± 5.6	18.8± 1.9	17.5±9.9	27.6± 1.3	146.3± 33.1
AX 4	21.9±0.2	23.6± 6.2	19.8± 1.9	18.3±10.8	28.9± 1.5	153.6±36.0
AX 5	22.1± 0.2	23.9± 6.3	20± 2.1	18.5± 11.1	29.3± 1.5	155.2± 36.7
AX 6	20.7± 0.1	22.4± 5.5	18.7± 1.9	17.3± 9.8	27.4± 1.3	145.3± 32.7
AX 7	21.4± 4.0	13±3.1	15.5± 0.6	9.9± 5.2	16.1± 1.0	107.7± 22.8
AX 8	29.1± 6.1	13.4± 2.3	19.6± 1.2	10.1± 3.7	16.6± 0.9	285.4± 57.4
AX 9	26.6± 0.2	273± 5.5	25.7±2.8	20.9±4.8	33.7± 6.3	168.1±41.5
AX 10	25.6± 0.1	24.6± 0.7	21.3± 2.2	20.1± 1.3	29.1± 2.7	162.3±38.4
AX 11	14.5±0.6	25.6± 5.6	18.2±2.2	19.6±5.7	30.5±3.0	150.1±36.0
AX 12	22.2±0.8	24.7±6.9	19.8±2.0	19.2±1.0	29.7±2.5	154.0±36.5
AX 13	21.4±0.5	23.7±6.6	20.4±1.5	19.0±11.4	28.8±1.6	146.9±35.1
AX 14	22.7±1.2	22.7±7.4	20.7±0.9	19.5±12.0	30.0±2.0	154.2±38.0
AX 15	23.0±1.4	25.3± 7.8	21.2±2.6	19.8±12.3	30.9±2.7	156.1±37.9
AX 16	21.9±1.1	23.9±6.0	20.1±2.2	18.5±10.6	26.5±2.7	146.2±31.5
AX 17	22.6±6.0	15.0±3.9	16.7±0.8	11.1±6.4	15.5±2.0	109.0±23.8
AX 18	30.5±6.9	14.6±3.5	21.0±1.6	11.2±3.8	17.2±2.1	286.6±58.6
AX 19	28.0±1.0	28.2±6.7	27.1±3.2	22.9±6.0	34.9±7.6	168.9±40.6
AX 20	26.9±1.1	25.5±1.9	22.5±3.8	22.1±1.5	27.5±4.7	161.5±36.6
mean	22.9±1.6	22.39±4.6	19.2±2.0	17.62±6.7	26.92±2.6	162.94±37.2
max	30.5±6.9	28.2±6.7	27.1±3.22	22.9±6.0	34.9±7.6	286.6±58.6
min	14.3±0.2	13±3.1	15.5±0.6	9.9±5.2	15.5±2.0	107.7±22.8

The calculated activities of ^{40}K, ^{232}Th, ^{238}U, ^{226}Ra, ^{228}Ra, and ^{228}Th for coastal sediment in Beyin are shown in Table 4.8. The calculated activities were 114.81±32.8 Bqkg^{-1} (in the range 127.9 – 102.1 Bqkg^{-1}), 19.21±4.1 Bqkg^{-1} (in the range 30.3– 15.1 Bqkg^{-1}), 20.1±5.2 Bqkg^{-1} (in the range 24.2 – 14 Bqkg^{-1}), 17.87±1.0 Bqkg^{-1} (in the range 24– 14.9 Bqkg^{-1}), 13.21±4.9 Bqkg^{-1} (in the range 15.8 – 10.7 Bqkg^{-1}), and 23.46±3.4 Bqkg^{-1} (in the range 41.7 – 16.5 Bqkg^{-1}), respectively.

Table 4.8: Activity concentration of radionuclides in coastal sediment from Beyin determined by gamma spectrometry analysis.

Sample ID	Activity Concentration ($Bqkg^{-1}$)					
	^{238}U	^{232}Th	^{226}Ra	^{228}Ra	^{228}Th	^{40}K
BN 1	14.5± 4.4	15.7±2.2	19±0.2	12.7± 3.4	18.6± 1.1	105.9± 31.6
BN 2	21.3± 6.4	18.9± 4.1	16.1± 0.2	14.1± 5.1	23.7± 3.1	121.7± 35.9
BN 3	22.2± 6.9	19.6±4.4	16.8± 0.1	14.7± 5.4	24.6± 3.3	126.5±38.6
BN 4	20.1± 5.8	17.8± 3.7	15.2± 0.3	13.3± 4.6	22.3± 2.8	114.7±32.2
BN 5	21.6± 6.6	19.2± 4.2	16.4± 0.2	14.3± 5.2	24± 3.2	123.5±36.9
BN 6	20.8± 6.2	18.4±3.9	15.8± 0.4	13.8± 4.9	23.1± 3.0	118.9± 34.4
BN 7	14± 4.1	15.1±2.1	18.3± 0.2	12.3± 3.2	17.9±1.0	102.1± 29.5
BN 8	19.8± 5.6	17.5±3.6	14.9±5.2	13.1± 4.5	21.9± 2.7	112.7± 31.2
BN 9	23.9± 0.2	16±3.1	22± 0.2	13.5± 4.2	18.5± 2.1	106.3± 26.8
BN 10	17.9± 4.5	29.3± 6.5	18.7±1.0	13.8± 3.8	41.7± 9.2	109.4± 26.6
BN 11	15.5±4.5	16.9±2.0	19.6±0.4	12.0±3.9	19.5±1.0	106.9±33.2
BN 12	21.6±6.6	20.3±4.0	17.1±0.4	12.7±5.4	24.9±3.0	123.1±36.9
BN 13	24.2±7.0	20.9±4.0	17.2±0.1	13.3±5.4	26.0±3.0	127.9±39.0
BN 14	22.1±6.2	19.5±3.9	17.2±0.3	13.0±5.8	23.6±2.6	116.0±34.2
BN 15	22.2±8.5	19.6±5.4	17.6±0.4	13.0 ±6.2	23.2±3.0	125.1±37.9
BN 16	22.0±7.4	19.7±5.2	17.8±0.8	12.0±6.2	19.2±4.2	120.0±36.0
BN 17	15.4±4.0	16.7±4.1	17.1±1.2	10.7±4.4	16.5±2.0	103.3±31.0
BN 18	21.0±4.4	18.7±4.2	16.5±6.4	13.0±5.7	20.0±3.5	114.0±32.4
BN 19	22.4±0.4	17.0±4.3	24.0±0.4	13.0±5.6	20.0±3.2	108.1±27.9
BN 20	19.5±4.0	30.3±7.5	20.0±1.8	15.8±5.2	40.0 ±10.6	110.0±25.0
mean	20.1±5.2	19.21±4.1	17.87±1.0	13.21±4.9	23.46±3.4	114.81±32.8
max	24.2±7.0	30.3±7.5	24±0.4	15.8±5.2	41.7±9.2	127.9±39
min	14±4.1	15.1±2.1	14.9±5.2	10.7±4.4	16.5±2.0	102.1±29.5

The calculated activities of ^{40}K, ^{232}Th, ^{238}U, ^{226}Ra, ^{228}Ra, and ^{228}Th for coastal sediment in Half-Asini are shown in Table 4.9. The calculated activities were 404.1±106.6 $Bqkg^{-1}$ (in the range 530.3–190 $Bqkg^{-1}$), 25.66±3.9 $Bqkg^{-1}$ (in the range 30.9– 20.8 $Bqkg^{-1}$), 22.32±5.7 $Bqkg^{-1}$ (in the range 31.3 – 13.3 $Bqkg^{-1}$), 28.28±1.0 $Bqkg^{-1}$ (in the range 39.1– 18 $Bqkg^{-1}$), 20.19±4.0 $Bqkg^{-1}$ (in the range 28.6 – 11.9 $Bqkg^{-1}$), and 32.15±4.0 $Bqkg^{-1}$ (in the range 44.2 – 18 $Bqkg^{-1}$), respectively.

Table 4.9: Activity concentration of radionuclides in coastal sediment from Half-Asini determined gamma spectrometry analysis.

Sample ID	Activity Concentration ($Bqkg^{-1}$)					
	^{238}U	^{232}Th	^{226}Ra	^{228}Ra	^{228}Th	^{40}K
HA 1	24.1± 6.3	22.8±3.8	20.6± 0.7	27.3± 7.2	18.2± 0.3	190.8± 48.1
HA 2	25.4± 6.6	24.3± 3.3	31.3± 0.8	20.7± 4.2	27.9± 2.4	427.8± 107.8
HA 3	25.9± 6.9	24.8± 3.4	31.9± 0.9	21.1±4.4	28.4±2.5	436.4± 111.8
HA 4	26± 6.9	24.9± 3.4	32.1± 0.9	21.2± 4.4	28.5± 2.5	438.2± 112.7
HA 5	31.3± 9.7	30± 4.7	38.7± 1.1	25.6± 6.0	34.4± 3.4	528.4± 159.5
HA 6	28.7± 8.2	27.5± 4.0	35.4± 1.0	23.4± 5.2	31.5±2.9	483.4± 135.1
HA 7	14.3± 4.3	21± 3.5	29.4± 0.9	17.9± 5.6	24.1±1.4	409.3± 119.5
HA 8	16.8± 1.7	26.8± 3.0	19± 0.2	12.6± 1.4	40.9± 7.5	372± 89.4
HA 9	15.8± 1.5	25.3± 2.7	18± 0.2	11.9±1.3	38.6± 6.6	351± 80.5
HA 10	18.1± 1.9	28.9± 3.6	20.6± 0.2	13.7± 1.5	44.2±8.7	402.1± 103
HA 11	23.6±6.6	20.8±4.0	22.0±0.9	28.6±6.4	18.0±0.7	190.0±46.6
HA 12	24.6±6.7	23.0±3.5	32.6±0.5	21.7±3.6	29.2±2.9	428.8±105.9
HA 13	24.5±5.0	23.3±4.8	33.0±0.6	22.2±3.7	30.0±2.8	435.0±110.1
HA 14	25.0±8.8	23.7±4.9	33.5±1.9	22.6±3.9	30.0±4.5	436.2±111.8
HA 15	30.3±9.0	30.9±5.9	39.1±1.4	27.2±8.0	36.0±3.0	530.3±157.5
HA 16	28.0±8.0	29.0±5.2	36.4±4.7	24.8±4.6	33.0±4.4	484.8±133.9
HA 17	13.3±5.6	22.0±5.0	30.8±1.1	19.8±3.8	23.2±3.2	410.6±120.8
HA 18	15.8±3.4	28.2±5.0	20.0±0.8	13.2±1.2	42.8±5.6	371.4±91.0
HA 19	17.8±3.0	25.8±1.9	19.0±0.9	13.0±1.5	40.6±8.2	352.6±82.3
HA 20	17.0±3.2	30.2±2.2	22.2±0.2	15.2±1.7	43.5±7.1	403.5±105.0
mean	22.32±5.7	25.66±3.9	28.28±1.0	20.19±4.0	32.15±4.0	404.1±106.6
max	31.3±9.7	30.9±5.9	39.1±1.4	28.6±6.4	44.2±8.7	530.3±157.5
min	13.3±5.6	20.8±4.0	18±0.2	11.9±1.3	18±0.7	190±46.6

Figure 4.7 displays the calculated activities of ^{40}K, ^{232}Th, ^{238}U, ^{226}Ra, ^{228}Ra, and ^{228}Th for coastal sediment from Sekondi-Takoradi, Axim, Beyin and Half Asini.

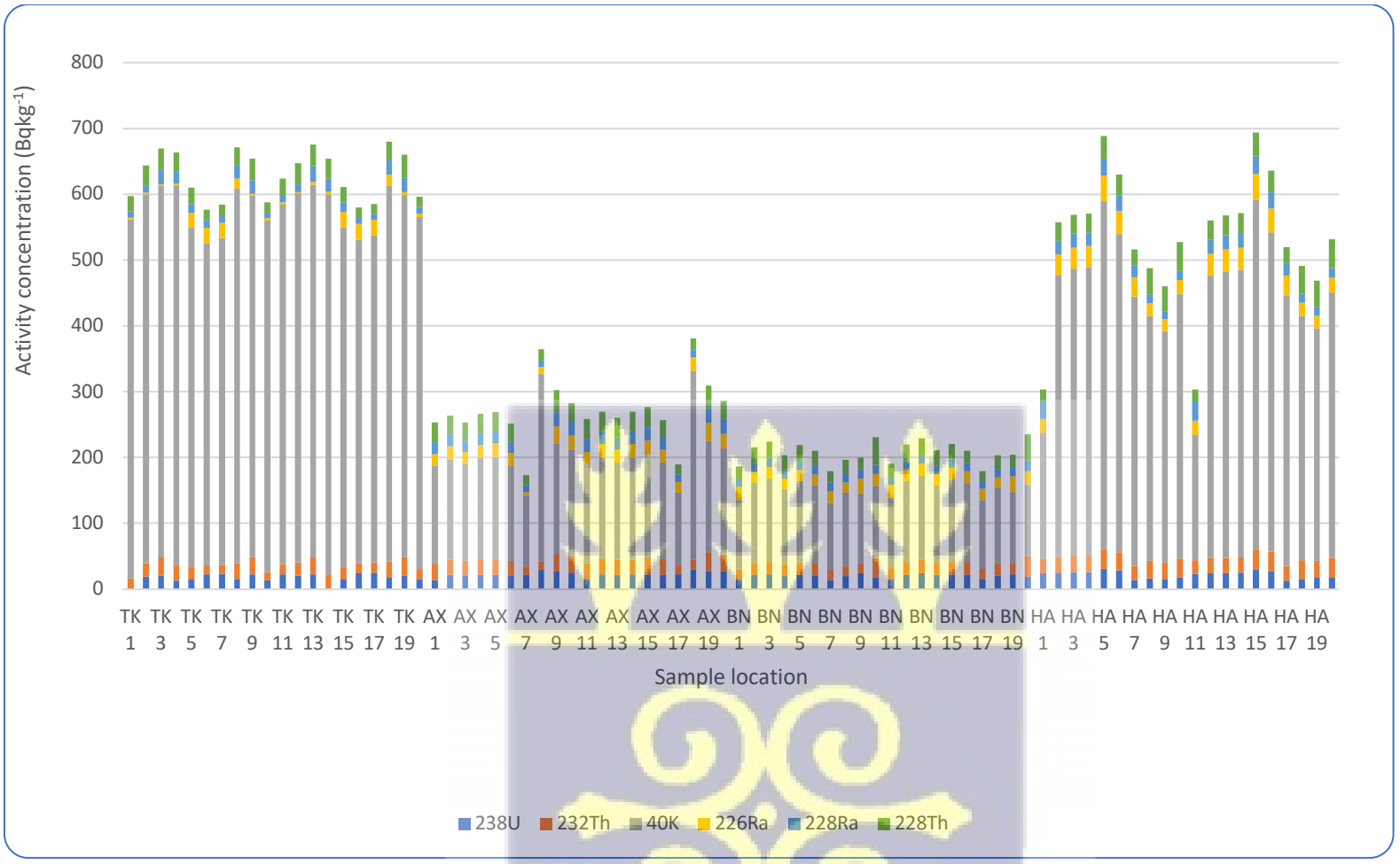

Figure 4.7: The ^{238}U, ^{232}Th, ^{226}Ra, ^{228}Ra, ^{228}Th and ^{40}K activity concentrations in each of the sediment samples from the study area.

The calculated mean activity concentrations of ^{40}K, ^{232}Th, ^{238}U, ^{226}Ra, ^{228}Ra, and ^{228}Th for coastal sediment from all four locations are represented in Fig. 4.8. While the overall average of the activity concentration of each of the radionuclides in sediment from the sample area (western coast) are represented in Figure 4.9.

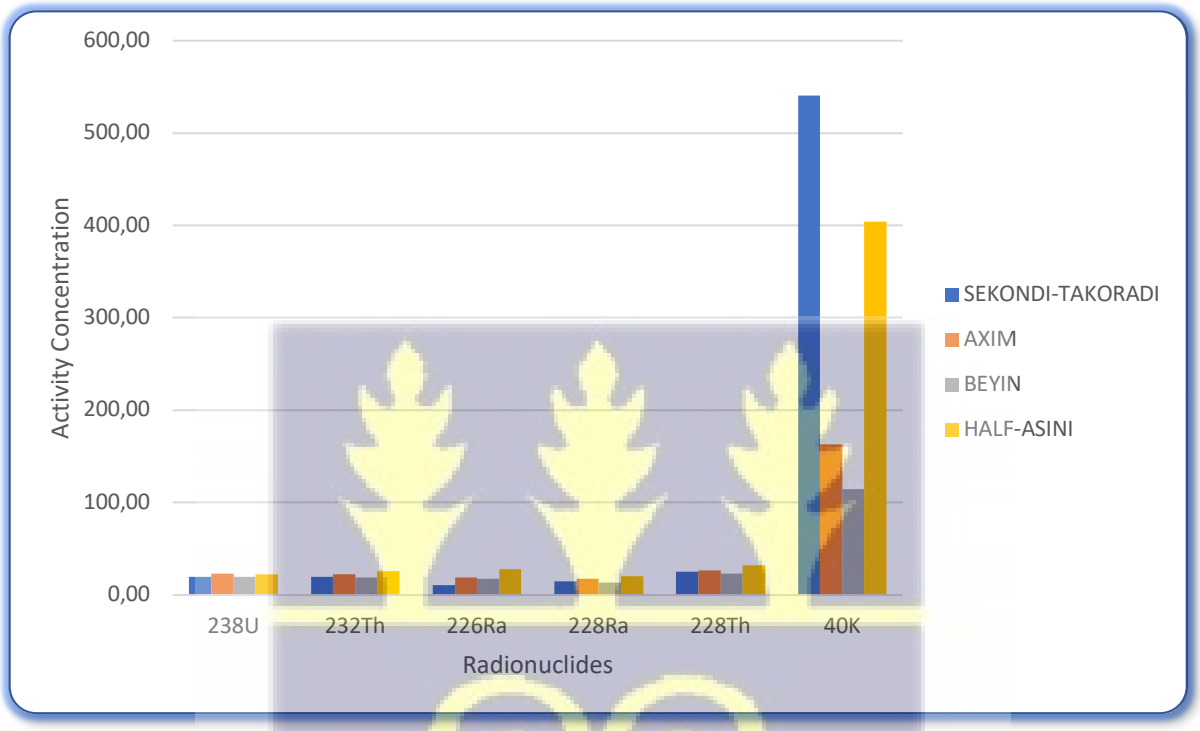

Figure 4.8: The ^{238}U, ^{232}Th, ^{226}Ra, ^{228}Ra, ^{228}Th and ^{40}K mean activity concentrations in all the sediment samples from the individual study areas.

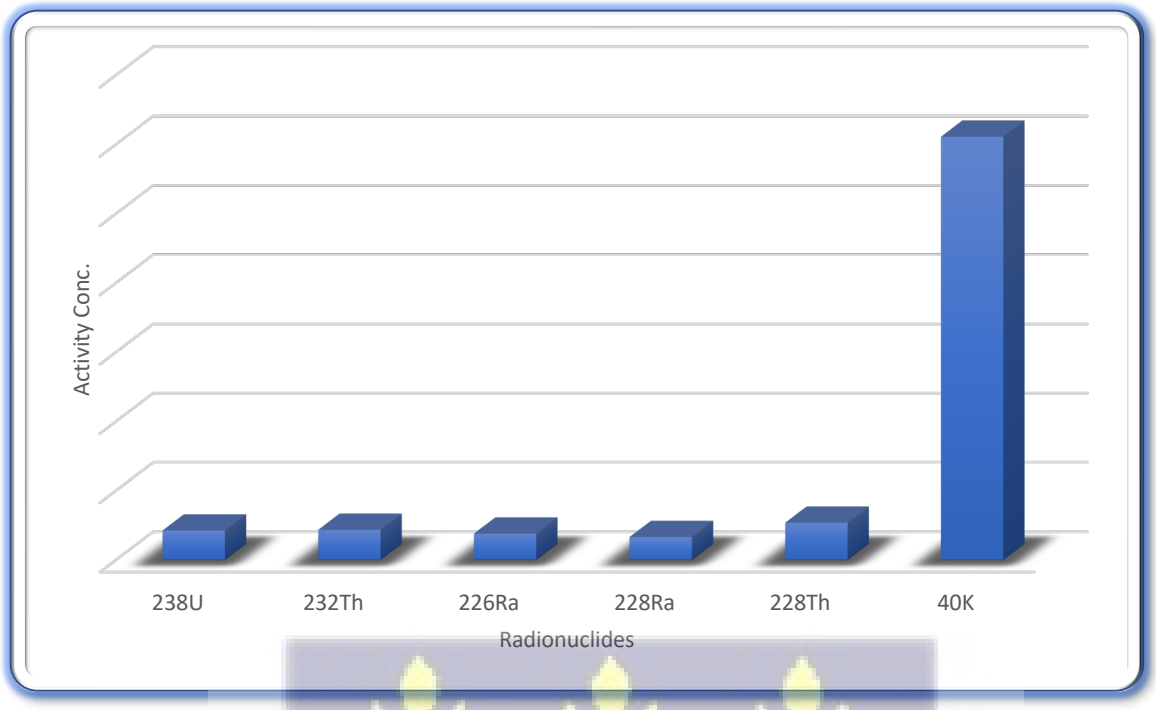

Figure 4.9: The mean activity concentrations of ^{238}U, ^{232}Th, ^{226}Ra, ^{228}Ra, ^{228}Th and ^{40}K in sediment samples of the western coast.

4.3 Results of Activity Concentrations Measured by Alpha Spectrometry Analysis.

The activity concentrations of the radionuclides in coastal soil and sediment for each of the four locations determined by alpha spectrometry are presented in Tables 4.10 to 4.11

4.3.1 Results of activity concentrations of NORM in beach sand.

The calculated activity concentrations of ^{232}Th, ^{238}U, ^{234}U and ^{230}Th for beach sand are shown in Table 4.10. The average values of ^{232}Th, ^{238}U, ^{234}U and ^{230}Th were 1.10 ±0.3 $Bqkg^{-1}$(in the range 0.2 – 1.9 $Bqkg^{-1}$), 2.02±0.6 $Bqkg^{-1}$ (in the range 0.6 – 3.9 $Bqkg^{-1}$), 1.34±0.7 $Bqkg^{-1}$ (in the range 0.5 – 2.6 $Bqkg^{-1}$), and 1.66±0.8 $Bqkg^{-1}$ (in the range 0.6 – 3.1 $Bqkg^{-1}$), respectively.

Table 4.10: Activity concentration of radionuclides in beach sand determined alpha spectrometry analysis.

Sample ID	Concentration Bqkg^{-1}			
	^{234}U	^{238}U	^{230}Th	^{232}Th
TK1	2.5 ± 1.0	0.9 ± 0.2	1.5 ± 0.3	0.2 ± 0.1
TK2	0.7 ± 1.2	0.7 ± 0.1	1.1 ± 0.1	0.7 ± 0.1
TK3	0.9 ± 1.4	1.2 ± 0.3	1.3 ± 0.1	1.2 ± 0.3
TK4	1.2 ± 0.5	1.1 ± 0.5	0.9 ± 0.4	0.8 ± 0.2
TK5	1.1 ± 0.1	2.1 ± 0.6	1.2 ± 0.7	1.3 ± 0.5
AX6	1.3 ± 0.5	2.5 ± 1.1	2.5 ± 1.2	0.5 ± 0.2
AX7	0.8 ± 0.3	1.9 ± 0.2	1.7 ± 0.6	0.3 ± 0.1
AX8	0.6 ± 0.2	1.3 ± 0.4	1.9 ± 0.7	1.5 ± 1.0
AX9	1.4 ± 0.4	1.7 ± 0.5	2.1 ± 1.4	0.4 ± 0.2
AX10	0.9 ± 0.1	0.8 ± 0.2	3.1 ± 1.7	0.9 ± 0.5
BN11	1.5 ± 1.1	2.9 ± 0.9	2.0 ± 1.3	1.3 ± 0.7
BN12	2.6 ± 1.2	3.1 ± 1.2	1.7 ± 1.1	1.7 ± 0.4
BN13	0.7 ± 0.2	1.9 ± 0.2	1.8 ± 1.0	0.9 ± 0.5
BN14	0.5 ± 0.1	2.9 ± 0.6	0.6 ± 0.3	1.5 ± 0.2
BN15	2.1 ± 1.3	0.6 ± 0.3	1.3 ± 0.4	1.7 ± 0.3
HA16	1.2 ± 0.1	1.8 ± 0.7	1.7 ± 0.2	1.8 ± 0.4
HA17	0.9 ± 1.1	3.5 ± 1.2	2.3 ± 1.8	1.9 ± 0.5
HA18	2.5 ± 1.6	2.9 ± 1.3	0.8 ± 0.3	0.5 ± 0.1
HA19	1.8± 0.5	2.7 ± 0.8	2.2 ± 0.9	1.6 ± 0.3
HA20	1.5± 0.3	3.9 ± 1.5	1.5 ± 0.7	1.2 ± 0.2
Mean	1.34±0.7	2.02±0.6	1.66±0.8	1.095±0.3
SD	0.66	0.99	0.61	0.54
Range	0.5 – 2.6	0.6 – 3.9	0.6 – 3.1	0.2 – 1.9

4.3.2 Results of activity concentrations of NORM in sea sediment

The calculated activity concentrations of ^{232}Th, ^{238}U, ^{234}U and ^{230}Th for sea sediment using alpha spectrometry are shown in Table 4.11.

The average values of ^{232}Th, ^{238}U, ^{234}U and ^{230}Th were 2.69±0.4 Bqkg^{-1} (in the range 1.3 – 4.5 Bqkg^{-1}), 3.11±0.8 Bqkg^{-1} (in the range 1.8 – 4.8 Bqkg^{-1}), 1.53±0.6 Bqkg^{-1} (in the range 0.7 – 2.9 Bqkg^{-1}), and 2.23±0.8 Bqkg^{-1} (in the range 0.9 – 3.6 Bq.kg^{-1}), respectively.

Table 4.11: Activity concentration of radionuclides in sea sediment determined alpha spectrometry analysis.

Sample ID	Concentration ($Bqkg^{-1}$)			
	^{234}U	^{238}U	^{230}Th	^{232}Th
TK1	2.3 ± 0.4	3.9 ± 0.5	1.8 ± 0.5	3.2 ± 0.1
TK2	2.9 ± 1.3	2.7 ± 0.2	1.5 ± 0.3	3.7 ± 0.4
TK3	0.7 ± 1.1	2.2 ± 0.4	1.8 ± 0.4	2.2 ± 0.3
TK4	1.5 ± 0.6	2.1 ± 0.5	2.9 ± 0.5	1.8 ± 0.2
TK5	1.4 ± 0.3	2.1 ± 0.4	1.9 ± 0.5	1.3 ± 0.3
AX6	1.1 ± 0.4	3.5 ± 1.5	2.9 ± 1.1	4.5 ± 0.2
AX7	0.7 ± 0.2	1.9 ± 0.2	2.7 ± 0.6	4.3 ± 0.6
AX8	0.8 ± 0.3	1.8 ± 0.5	1.9 ± 0.5	4.5 ± 1.1
AX9	1.9 ± 0.5	1.9 ± 0.4	3.1 ± 1.6	3.4 ± 0.6
AX10	0.8 ± 0.2	2.8 ± 0.7	3.6 ± 1.3	3.9 ± 0.5
BN11	1.7 ± 1.2	2.9 ± 0.7	2.9 ± 1.2	3.3 ± 0.8
BN12	2.3 ± 1.3	2.1 ± 1.4	1.8 ± 1.3	2.7 ± 0.4
BN13	0.9 ± 0.3	2.9 ± 0.6	1.9 ± 1.1	0.9 ± 0.2
BN14	0.7 ± 0.3	3.9 ± 0.8	0.9 ± 0.3	1.5 ± 0.6
BN15	2.6 ± 1.2	4.6 ± 0.9	1.6 ± 0.6	1.9 ± 0.4
HA16	1.8 ± 0.3	4.8 ± 0.8	2.7 ± 0.2	1.7 ± 0.3
HA17	0.9 ± 1.0	3.5 ± 1.3	2.5 ± 1.8	1.9 ± 0.3
HA18	2.6 ± 0.6	3.9 ± 1.5	1.8 ± 0.4	2.5 ± 0.1
HA19	1.4± 0.2	4.7 ± 0.9	2.6 ± 0.7	2.6 ± 0.3
HA20	1.6± 0.2	3.9 ± 1.2	1.7 ± 0.5	1.9 ± 0.4
Mean	1.53±0.6	3.11±0.8	2.23±0.8	2.69±0.4
SD	0.82	1.32	0.92	1.32
Range	0.7 – 2.9	1.8 – 4.8	0.9 – 3.6	1.3 – 4.5

4.4 Comparison of Activity Concentrations of ^{232}Th, ^{238}U and ^{40}K in Beach sand from the Study Area with Other Countries.

The research area's activity concentrations of ^{238}U, ^{232}Th, and ^{40}K were compared to published data from other nations and global average values. It was discovered that the activity concentrations in the beach sand from the research location were below the globally recognized standard values (UNSCEAR, 2017).

Table 4.12: Comparison of activity concentrations of ^{40}K ^{238}U and ^{232}Th in beach sand and sediment with countries worldwide.

S/N	Country	Activity (Bqkg^{-1})			Reference
		^{238}U	^{232}Th	^{40}K	
1.	Egypt	22.7	11.6	93.0	Harb (2008)
		9.57	8.64	13.77	Fares (2017)
		8.8	30.8	106.9	Awad et al., (2022)
2.	Namibia	63.46	54.88	416.99	Onjefu et al., (2022)
		18.91	15.58	79.17	Amwaalanga et al., (2019)
3.	Nigeria	26.1	55.6	499.3	Omeje et al., (2021)
4.	India	3.67	37.23	387.17	Ravisankar et al., (2014)
		BDL	14.29	360.23	Ravisankar et al., (2015)
		47.04	26.63	263	Thangam et al., (2022)
5.	Turkey	8.85	8.93	219.41	Korkulu & Özkan (2013)
6.	Arabian Gulf	22.7	14.8	392	Alshahri et al., (2017)
7.	Saudi Arabia (Red Sea)	19.5	9.38	403.31	Al-Mur & Gad (2022)
8.	Albania	8-27	13-40	266.675	Tsabaris et al., (2007)
9.	Iran (Caspian Sea)	34.4	11.4	310	Abbasi et al., (2022)
10.	Malaysia	3	3	70	Amin et al., (2013)
11.	Cyprus (East coast)	23	19	628.1	Abbasi et al., (2020)
12.	China	25.9	37.6	263	Lin et al., (2020)
13.	Kuwait	36	6	227	Saad & Al-Azmi (2002)
14.	South Carolina	21	45	609	Powell et al., (2007)
15.	Serbia	37	35	580	Radomirovic et al., (2021)
16.	Nigeria	12.07	13.02	60.55	Ugbede (2020)
17.	Northern Pakistan	51	70	532	Qureshi et al., (2014)
18.	Ghana	1.87-27	2.5-26.9	47.8-276	Lawluvi (2016)
		21.9	22.4	344.9	Present work
	Worldwide	35	30	400	UNSCEAR (2000)

4.5 Activity Concentration Results of NORM in Seawater Determined by Gamma Spectrometry.

Apart from the soil samples, multiple water samples originating from distinct locations were gathered along the same coastal communities in the area under investigation, where soil and beach sediments were extracted. Eighty (80) seawater samples in all, consisting of twenty (20) samples from each location were analyzed. The activity concentrations of the seawater samples were determined, and the outcomes are presented in Tables 4.13 – 4.16 for each of the four locations.

The calculated activities of ^{40}K, ^{232}Th, ^{238}U, ^{226}Ra, and ^{228}Th for seawater in Sekondi-Takoradi are shown in Table 4.13. The calculated activities were 12.62±2.13 BqL^{-1} (in the range 9.0 – 16.9 BqL^{-1}), 1.81±0.7 BqL^{-1} (in the range 1.0 – 3.5 BqL^{-1}), 2.47±0.8 BqL^{-1} (in the range 0.2 – 6.4 BqL^{-1}), 0.73±0.48 BqL^{-1} (in the range 0.1 – 2.3 BqL^{-1}), and 2.80±0.4 BqL^{-1} (in the range 1.0 – 4.5 BqL^{-1}), respectively.

Table 4.13: Activity concentration of radionuclides in seawater from Sekondi-Takoradi determined by gamma spectrometry analysis.

Sample ID	Activity Concentration (Bq L^{-1})				
	^{238}U	^{232}Th	^{40}K	^{226}Ra	^{228}Th
TK 1	5.5 ± 0.7	1.2 ± 0.1	10.6 ± 1.4	0.8 ± 0.5	2.4 ± 0.1
TK 2	0.4 ± 0.2	1.3 ± 0.1	11.8 ± 1.6	0.2 ± 0.1	2.6 ± 0.1
TK 3	3.0 ± 0.4	1.4 ± 0.2	16.1 ± 2.0	0.1 ± 0.1	2.8 ± 0.1
TK 4	2.5 ± 0.7	2.8 ± 0.7	9.5 ± 2.5	0.7 ± 0.3	3.6 ± 0.4
TK 5	0.6 ± 0.3	1.5 ± 0.2	16.9 ± 2.2	0.3 ± 0.2	2.9 ± 0.2
TK 6	4.8 ± 0.7	1.1 ± 0.1	11.9 ± 1.6	0.5 ± 0.3	2.3 ± 0.1
TK 7	0.2 ± 0.2	1.2 ± 0.1	14.3 ± 1.8	0.1 ± 0.1	2.4 ± 0.1
TK 8	4.2 ± 0.6	1.2 ± 0.1	13.8 ± 1.8	0.2 ± 0.4	2.4 ± 0.1
TK 9	0.3 ± 0.2	1.4 ± 0.2	11,5 ± 1.3	0.4 ± 0.1	2.7 ± 0.1
TK 10	0.3 ± 0.2	1.2 ± 0.2	13.7 ± 1.7	0.3 ± 0.1	2.4 ± 0.1
TK 11	5.0±0.8	1.0±0.9	9.0±3.0	0.9 ± 0.4	2.0±0.2
TK 12	0.3±0.4	1.5±0.8	10.0±3.2	0.4±0.8	1.6±0.3
TK 13	5.0±1.4	3.0±0.8	16.0±4.0	0.6±0.1	1.0±0.1
TK 14	2.5 ±1.2	2.3 ±1.1	15. 3 ± 2.1	1.2 ± 0.7	3.8 ± 1.2
TK 15	0.8±0.8	2.7±1.0	14.9±1.6	0.8±0.6	2.5±0.5
TK 16	6.4±0.9	2.2±0.9	10.5±1.4	1.1 ± 0.2	2.0±1.1
TK 17	0.8±0.6	3.5±0.6	12.3±1.4	0.6±0.6	4.2±0.5
TK 18	5.7±2.4	1.0±1.2	12.0±1.9	1.6 ± 0.5	4.0±0.6
TK 19	0.6±1.8	1.6±1.8	10.5±2.9	1.4±1.8	4.5±1.2
TK 20	0.5±1.9	3.0±2.1	11.8±3.1	2.3±1.6	3.9±0.7
Mean	2.47±0.8	1.81±0.7	12.62±2.13	0.73±0.48	2.80±0.4
STD	2.25	0.79	2.36	0.57	0.92
Range	0.2 – 6.4	1.0 – 3.5	9.0 – 16.9	0.1 – 2.3	1.0 – 4.5

The calculated activities of ^{40}K, ^{232}Th, ^{238}U, ^{226}Ra, ^{228}Ra, and ^{228}Th for coastal sediment in Axim is shown in Table 4.14. The calculated activities were 11.78±1.43 BqL^{-1} (in the range 9.6 – 13.3

BqL^{-1}), 2.66±0.43 BqL^{-1} (in the range 1.2 -3.6 BqL^{-1}), 0.58±0.5 BqL^{-1} (in the range 0.2 – 1 BqL^{-1}), 0.75±0.35 BqL^{-1} (in the range 0.1- 2.1 BqL^{-1}), 1.03±0.45 BqL^{-1} (in the range 0.4 – 1.8 BqL^{-1}), and 3.24±0.52 BqL^{-1} (in the range 1 – 5.1BqL^{-1}), respectively.

Table 4.14: Activity concentration of radionuclides in seawater from Axim determined by gamma spectrometry analysis.

Sample ID	Activity Concentration (BqL^{-1})					
	^{238}U	^{232}Th	^{226}Ra	^{228}Ra	^{228}Th	^{40}K
AX 1	0.3 ± 0.1	3.0 ± 0.1	0.4 ± 0.2	0.4 ± 0.2	3.1 ± 0.2	11.6 ± 1.6
AX 2	0.5 ± 0.2	2.5 ± 0.4	0.3 ± 0.1	0.7 ± 0.3	3.5 ± 0.6	13.1 ± 1.8
AX 3	0.9±0.1	2.9 ± 0.2	0.4 ± 0.1	0.6 ± 0.5	2.9 ± 0.7	12.5 ± 1.7
AX 4	0.4 ± 0.1	3.1 ± 0.5	0.2 ± 0.1	0.8 ± 0.2	3.1 ± 0.3	13.3 ± 1.3
AX 5	0.2 ± 0.1	3.3 ± 0.3	0.3 ± 0.2	0.5 ± 0.1	2.8 ± 0.4	11.7 ± 2.1
AX 6	0.6 ± 0.3	2.2 ± 0.1	0.5 ± 0.2	0.9 ± 0.5	2.9 ± 0.5	10. 5 ± 1.5
AX 7	0.5 ± 0.2	1.6 ± 0.3	0.4 ± 0.3	0.6 ± 0.3	3.8 ± 1.1	12.4 ± 0.9
AX 8	0.3 ± 0.1	2.4 ± 0.7	0.5 ± 0.3	1.2 ± 0.5	3.2 ± 0.8	12.6 ± 0.8
AX 9	0.8 ± 0.3	1.2 ± 0.2	0.2 ± 0.3	0.7 ± 0.3	2.5 ± 0.1	11.5 ± 1.5
AX 10	0.2 ± 0.2	1.4 ± 0.1	0.1 ± 0.1	0.5 ± 0.2	2.4 ± 0.1	12.2 ± 1.6
AX 11	0.7 ± 1.9	3.2 ± 1.0	0.8±0.1	1.4±0.4	4.7±0.2	11.0±2.5
AX 12	0.8 ± 0.3	2.8 ± 0.7	0.6±0.2	1.5±0.5	5.1±0.4	12.7±2.0
AX 13	0.6 ± 0.4	3,2 ± 0.4	0.4±0.2	1.4±0.2	5.1±1.5	11.6±2.4
AX 14	0.7 ± 1.0	2,4 ± 0.8	1.1±1.0	1.8±0.6	4.5±1.0	12.8±2.1
AX 15	0.4 ± 1.2	1.9 ± 0.5	1.2±1.1	1.1±1.1	4.8±1.1	10.7±0.8
AX 16	0.6 ± 1.0	2.6 ± 0.5	0.5±1.4	1.7±1.1	4.4±0.3	9.6±0.4
AX 17	1.0 ± 0.7	3.6 ± 0.5	1.0±0.5	1.4±1.0	1.9±0.3	12.0±1.1
AX 18	0.9 ± 0.4	2.9 ± 0.3	2.0±0.3	0.8±0.6	1.6±0.4	11.9±1.0
AX 19	0.4 ± 0.7	3.5 ± 0.6	2.1±0.1	1.5±0.2	1.5±0.2	10.8±0.8
AX 20	0.8 ± 0.7	3.4 ± 0.3	1.9±0.1	1.1±0.3	1.0±0.1	11.0±0.7
Mean	0.58±0.5	2.66±0.43	0.75±0.35	1.03±0.45	3.24±0.52	11.78±1.43
STD	0.24	0.70	0.62	0.44	1.24	0.96
Range	0.2 - 1	1.2 -3.6	0.1- 2.1	0.4 – 1.8	1 – 5.1	9.6 – 13.3

The calculated activities of ^{40}K, ^{232}Th, ^{238}U, ^{226}Ra, ^{228}Ra, and ^{228}Th for coastal sediment in Beyin are shown in Table 4.15. The calculated activities were 11.49±1.29 BqL^{-1} (in the range 9.4 – 13.4 BqL^{-1}), 2.51±0.4 BqL^{-1} (in the range 1.4 – 3.7 BqL^{-1}), 0.77±0.42 BqL^{-1} (in the range 0.3 – 1.3 BqL^{-1}

^{1}), 1.19±0.32 BqL^{-1} (in the range 0.5 – 2 BqL^{-1}), 1.16±0.34 BqL^{-1} (in the range 0.5 – 1.8 BqL^{-1}), and 2.63±0.43 BqL^{-1} (in the range 1.7 – 3.8 BqL^{-1}) respectively.

Table 4.15: Activity concentration of radionuclides in seawater from Beyin determined by gamma spectrometry analysis.

Sample ID	Activity Concentration (BqL^{-1})					
	^{238}U	^{232}Th	^{226}Ra	^{228}Ra	^{228}Th	^{40}K
BN 1	0.5 ± 0.3	3.7 ± 0.3	1.4 ± 0.2	1.4 ± 0.1	2.9 ± 0.2	12.5 ± 1.2
BN 2	0.3 ± 0.1	3.5 ± 0.2	0.8 ± 0.2	0.9 ± 0.2	2.5 ± 0.3	13.3 ± 1.5
BN 3	0.6 ± 0.2	2.8 ± 0.1	0.7 ± 0.3	0.7 ± 0.3	2.7 ± 0.4	11.5 ± 1.2
BN 4	0.8 ± 0.2	3.2 ± 0.3	0.5 ± 0.3	1.8 ± 0.2	3.1 ± 0.2	12.3 ± 1.1
BN 5	0.7 ± 0.3	3.4 ± 0.2	0.6 ± 0.1	1.5 ± 0.1	2.6 ± 0.3	10.7 ± 1.2
BN 6	0.5 ± 0.2	2.5 ± 0.3	1.5 ± 0.2	0.9 ± 0.2	1.9 ± 0.4	10.9 ± 1.7
BN 7	0.4 ± 0.3	2.6 ± 0.2	1.4 ± 0.4	1.6 ± 0.4	2.8 ± 0.3	13.4 ± 1.7
BN 8	0.5 ± 0.4	2.9 ± 0.6	0.5 ± 0.2	1.3 ± 0.2	3.2 ± 0.6	11.6 ± 1.8
BN 9	0.9 ± 0.3	2.5 ± 0.2	0.8 ± 0.2	0.9 ± 0.4	3.5 ± 0.2	10.5 ± 1.2
BN 10	0.8 ± 0.1	1.9 ± 0.1	0.9 ± 0.3	0.6 ± 0.3	2.5 ± 0.3	11.2 ± 1.3
BN 11	0.6 ± 1.1	2.1 ± 1.1	1.8±0.2	0.7±0.3	1.7±0.1	12.5 ±1.5
BN 12	1.1 ± 0.2	1.8 ± 0.6	1.6±0.3	1.1 ±0.3	2.1±0.3	10.7±1.3
BN 13	1.3 ± 0.3	3.3 ± 0.5	1.4±0.1	1.2 ±0.2	3.1±1.2	12.4 ± 1.4
BN 14	0.9 ± 1.0	2,1 ± 0.6	1.1±0.6	1.6 ±0.4	2.5±1.2	12.5 ±2.2
BN 15	1.2 ± 1.1	1.9 ± 0.3	1.2±0.4	1.4 ±1.0	3.8±1.1	11.7±0.6
BN 16	0.8 ± 1.0	1.6 ± 0.3	0.6±1.1	0.7±1.2	3.4±0.2	10.6±0.8
BN 17	1.0 ± 0.2	2.6 ± 0.7	1.2±0.4	1.7 ±1.3	2.9±0.4	9.9 ±1.3
BN 18	0.7 ± 0.3	1.8 ± 0.4	2.0±0.2	0.5 ±0.2	1.9±0.3	11.7±1.6
BN 19	0.6 ± 0.2	2.5 ± 0.5	1.8 ±0.4	1.3 ±0.2	1.7±0.4	10.4±0.7
BN 20	1.2 ± 0.5	1.4 ± 0.4	1.9±0.3	1.4 ±0.3	1.8±0.2	9.4 ±0.5
Mean	0.77±0.42	2.51±0.4	1.19±0.32	1.16±0.34	2.63±0.43	11.49±1.29
STD	0.28	0.68	0.49	0.40	0.63	1.10
Range	0.3 – 1.3	1.4 – 3.7	0.5 – 2	0.5 – 1.8	1.7 – 3.8	9.4 – 13.4

The calculated activities of ^{40}K, ^{232}Th, ^{238}U, ^{226}Ra, and ^{228}Th for coastal sediment in Half-Asini are shown in Table 4.16. The calculated activities were 11.42±1.48 BqL^{-1} (in the range 8.5 – 14.3 BqL^{-1}), 1.24±0.4 BqL^{-1} (in the range 0.7 – 1.8 BqL^{-1}), 2.38±0.6 BqL^{-1} (in the range 1.4 – 3.3BqL^{-}

^{1}), 0.77±0.4 BqL^{-1} (in the range 0.2 – 1.3 BqL^{-1}), and 1.92±0.4 BqL^{-1} (in the range 1.3 – 2.6 BqL^{-1}), respectively.

Table 4.16: Activity concentration of radionuclides in seawater from Half-Asini determined by gamma spectrometry analysis.

Sample ID	Activity Concentration (BqL^{-1})				
	^{238}U	^{232}Th	^{226}Ra	^{228}Th	^{40}K
HA 1	2.5 ± 0.3	1.5 ± 0.2	0.6 ± 0.2	1.4 ± 0.1	11.4 ± 1.2
HA 2	2.4 ± 0.4	1.7 ± 0.3	0.4 ± 0.3	1.6 ± 0.2	10.8 ± 1.1
HA 3	3.1 ± 0.2	1.2 ± 0.2	0.2 ± 0.2	1.8 ± 0.3	12.1 ± 1.5
HA 4	2.5 ± 0.7	1.8 ± 0.4	0.5 ± 0.1	1.6 ± 0.4	10.5 ± 1.6
HA 5	2.6 ± 0.1	1.6 ± 0.3	0.4 ± 0.2	1.9 ± 0.2	13.9 ± 2.1
HA 6	1.8 ± 0.6	1.3 ± 0.4	0.7 ± 0.3	1.3 ± 0.1	10.9 ± 1.2
HA 7	2.2 ± 0.3	1.4 ± 0.1	0.6 ± 0.1	2.1 ± 0.2	12.3 ± 0.8
HA 8	3.2 ± 0.5	1.5 ± 0.3	0.5 ± 0.3	1.4 ± 0.3	10.8 ± 1.7
HA 9	2.3 ± 0.3	0.9 ± 0.2	0.3 ± 0.1	1.7 ± 0.2	11.5 ± 1.2
HA 10	3.3 ± 0.1	1.2 ± 0.1	0.8 ± 0.1	2.4 ± 0.3	9.7 ± 1.5
HA 11	2.0 ± 0.4	1.1 ± 0.9	0.7 ± 0.4	2.0±0.1	9.9 ± 1.6
HA 12	2.3 ± 0.3	1.5 ± 0.2	0.9 ±0.8	2.6±0.3	11.0±1.2
HA 13	1.9 ± 1.1	0.8 ±0.3	1.1 ±0.1	2.0±0.1	13.0 ± 2.0
HA 14	2.4 ± 1.3	1.3 ± 1.1	1.2 ± 0.5	1.8 ± 1.2	14.3 ± 1.1
HA 15	1.8 ± 0.6	0.7 ± 1.0	0.9±0.4	2.5±0.2	12.9±1.3
HA 16	1.4 ±0.7	0.9 ±0.2	1.2 ± 0.4	2.2±1.3	8.5±1.2
HA 17	2.8±0.4	1.5±0.3	0.7 ± 0.6	2.4±0.2	10.3±1.3
HA 18	2.7±1.4	1.0 ± 0.4	1.2 ± 0.2	2.3±0.5	12.3±1.9
HA 19	2.6 ± 1.5	0.7 ±1.1	1.1±1.2	1.5±1.3	11.5±1.9
HA 20	1.8 ± 0.9	1.1 ± 0.1	1.3±1.2	1.9±0.6	10.8±2.1
Mean	2.38±0.6	1.24±0.4	0.77±0.4	1.92±0.4	11.42±1.48
STD	0.50	0.33	0.33	0.39	1.43
Range	1.4 – 3.3	0.7 – 1.8	0.2 – 1.3	1.3 – 2.6	8.5 – 14.3

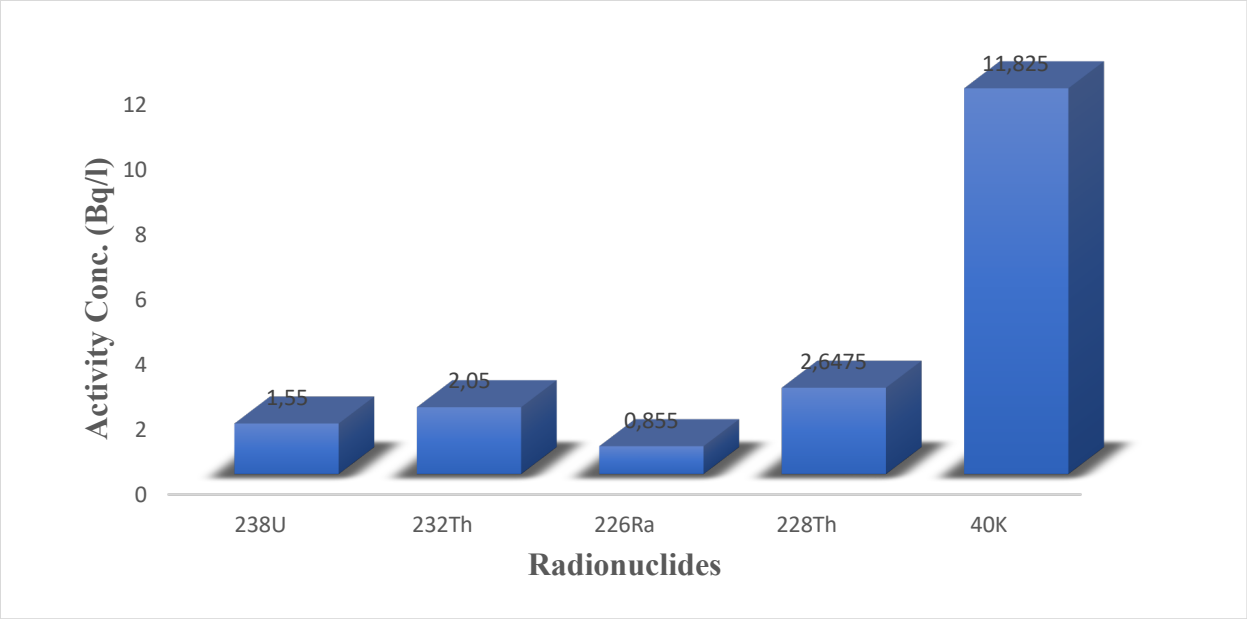

Fig. 4.10: The mean activity concentrations of ^{238}U, ^{232}Th, ^{226}Ra, ^{228}Th and ^{40}K in seawater samples of the western coast.

4.6 Results of Hazard Assessment

The key goal for studies of environmental radioactivity from beach sand or sea sediment samples is the estimation of radiation dose and biological impacts on people exposed to ionizing radiation. The actual indication of the radiation hazard linked to natural radioactivity in relation to coastal sand is not depicted by the activities of the various radionuclides. Therefore, radiation hazard parameters are assessed to determine the level of risks, and the outcomes are then contrasted with standards that are accepted globally.

Radiological hazard assessment of sand and sediment for each of the locations requires the estimation of parameters such as the annual effective dose (AED), radium equivalent activity (Ra_{eq}), internal and external hazard index (H_{in} and H_{ex}), the annual gonadal dose (AGD), the

representative level index ($I\gamma r$), the activity utilization index (AUI), the excess lifetime cancer risk (ELCR) and the absorbed dose rate (D_R).

The absorbed dose rate in air due to terrestrial gamma rays at 1 meter above the ground can be evaluated from the activity concentration. In calculating the annual dose, it is important to take into consideration the time people spend at a location, that is the occupancy factor. According to UNSCEAR (2000), the outdoor occupancy factor is 0.2, thus 20 % of the day is spent outdoors, indicating that 80 % of the day is spent indoors averagely worldwide.

The annual effective dose obtained from all the sampling locations is lower compared to the average worldwide background doses. The average values of the annual effective dose were lower than the international level of 0.07 $mSvy^{-1}$ (UNSCEAR, 2000). Due to the low values of gamma rays recorded for each of the locations, the western coast of Ghana can be considered not radiologically hazardous.

Parameters such as radium equivalent activity (Ra_{eq}), internal hazard index (H_{in}) and external hazard index (H_{ex}) aid in calculating the potential hazards of gamma radiation to humans associated with using soil samples as construction materials. The worldwide accepted reference value of 370 Bq kg^{-1} on average was not exceeded, as well as the internal and external hazard indices which must be less than one.

The AGD evaluates the possible results of the concentrations of ^{40}K, ^{226}Ra and ^{232}Th on some important organs. In other words, it measures the biological relevance of the dose received by the genital system of the community annually. UNSCEAR regards the activity of bone surface cells and bone marrow as being relevant organs, in the same context.

The degree of gamma radiation hazard related to natural gamma emitters in sand can be evaluated using the *Iγr* of the sand. This index can be used to identify substances that, when used as building materials, could pose risks to human health. It can also be utilized in calculating the dose rate annually brought on by the additional external gamma radiation that surface materials produce.

For the usage of building materials, an Activity Utilization Index (AUI) is estimated. This is to simplify the evaluation of dose rates in air using the necessary conversion factors from the combination of the three distinct radionuclides in soil.

The estimated hazard parameters associated with exposure to radioactivity from beach sand and sediment recorded for each of the four sampling areas are shown in appendices A to H. However, the average hazard parameters estimated are presented in Tables 4.17 and 4.18

Table 4.17: Average hazard parameters associated with coastal sand from the sampling locations.

Location	Dr (nGy^{-1})	Raeq	Hin	Hex	AED ($mSvy^{-1}$)	AGD ($uSvy^{-1}$)	RLI	AUI	ELCR ($\times10^{-3}$)
Sekondi-Takoradi	52.42	108.0	0.35	0.29	0.06	377.14	0.09	0.56	0.23
Axim	24.23	51.57	0.18	0.14	0.03	171.06	0.15	0.33	0.15
Beyin	35.49	76.76	0.28	0.21	0.04	248.84	0.09	0.54	0.15
Half Asini	34.34	72.15	0.26	0.20	0.04	242.35	0.11	0.45	0.15

Table 4.18: Average hazard parameters associated with coastal sediment from the sampling locations.

Location	Dr (nGy^{-1})	Raeq	Hin	Hex	AED ($mSvy^{-1}$)	AGD ($uSvy^{-1}$)	RLI	AUI	ELCR ($\times10^{-3}$)
Sekondi-Takoradi	42.04	86.22	0.28	0.23	0.05	302.87	0.17	0.43	0.18
Axim	29.65	64.75	0.23	0.17	0.04	207.13	0.10	0.47	0.13
Beyin	24.73	54.38	0.20	0.15	0.03	172.16	0.12	0.41	0.11
Half Asini	45.41	96.09	0.34	0.26	0.06	321.56	0.08	0.60	0.20

4.7 Descriptive Statistics of the Natural Radionuclides

The fundamental descriptive statistical characteristics of the natural radionuclides in coastal sand and sediment are shown in Tables 4.19 and 4.20. They include the maximum, minimum, skewness, mean, kurtosis, and standard deviation for the radionuclides under investigation. The averages of ^{40}K, ^{232}Th, ^{238}U, ^{226}Ra, ^{228}Ra, and ^{228}Th in the study are higher compared to their standard deviation values. This indicates that the activity concentrations of all the radionuclides in the beach sand and sediment have an elevated level of homogeneity. A lower standard deviation than the average value shows a high degree of homogeneity and the other way around (Bland, 2006). Skewness measures and characterizes the strength of lopsidedness of a distribution about its mean. A skewed distribution means an asymmetrical distribution or a frequency distribution's shape that is not symmetrical (Bland, 2006). The skewness of the activity concentrations of ^{40}K, ^{232}Th, ^{226}Ra, ^{228}Ra, and ^{228}Th of sand are positive except ^{238}U. This indicates that their distributions are asymmetric, while that of ^{238}U is symmetric as shown in the frequency distribution in Figure 4.11. The skewness of the activity concentrations of ^{238}U, ^{40}K, ^{228}Ra, and ^{228}Th of sediment, on the other hand, are positive except ^{232}Th and ^{226}Ra. The frequency distributions are shown in Figure 4.12.

Kurtosis is a statistical indicator of how peaked a probability distribution of a random variable with a real value is. It is referred to as leptokurtic, mesokurtic, or platykurtic, with respect to how pronounced the peak is. The term "normal curve" or "mesokurtic" is used to describe the kurtosis of zero. The curve is leptokurtic if the value of kurtosis is positive, or more pronounced than the typical curve. The activity concentration of ^{40}K, ^{232}Th, ^{238}U, and ^{228}Ra in this research work had negative kurtosis values, which imply a platykurtic distribution with a relatively high peak. ^{226}Ra and ^{228}Th, however, had positive kurtosis values, which imply a leptokurtic distribution (Bland,

2006; Lawluvi, 2016). This finding could be explained by a disparity in the spread of natural radionuclides in the samples.

Table 4.19: Fundamental statistics of natural radionuclides in sea sand.

Variables	^{238}U	^{232}Th	^{40}K	^{226}Ra	^{228}Ra	^{228}Th
Mean	21.71	22.41	344.97	21.34	20.22	20.82
Standard Deviation	4.85	6.45	191.95	7.00	8.48	6.94
Minimum	11.00	10.40	132.50	6.40	6.20	5.10
Maximum	30.90	33.30	865.60	46.30	44.90	41.00
Skewness	-0.22	0.54	1.04	1.09	0.67	0.00
Kurtosis	-1.01	-0.83	-0.11	1.70	-0.52	0.08

Table 4.20: Fundamental statistics of natural radionuclides in sea sediment.

Variables	^{238}U	^{232}Th	^{40}K	^{226}Ra	^{228}Ra	^{228}Th
Mean	21.19	21.76	305.55	19.00	16.35	26.87
Standard Deviation	4.43	4.94	182.67	8.97	4.98	7.50
Minimum	13.30	11.80	102.10	1.90	8.60	14.80
Maximum	31.30	30.90	577.60	39.10	28.60	44.20
Skewness	0.03	-0.13	0.22	-0.11	0.40	0.30
Kurtosis	-0.62	-1.01	-1.72	-0.10	-0.90	-0.51

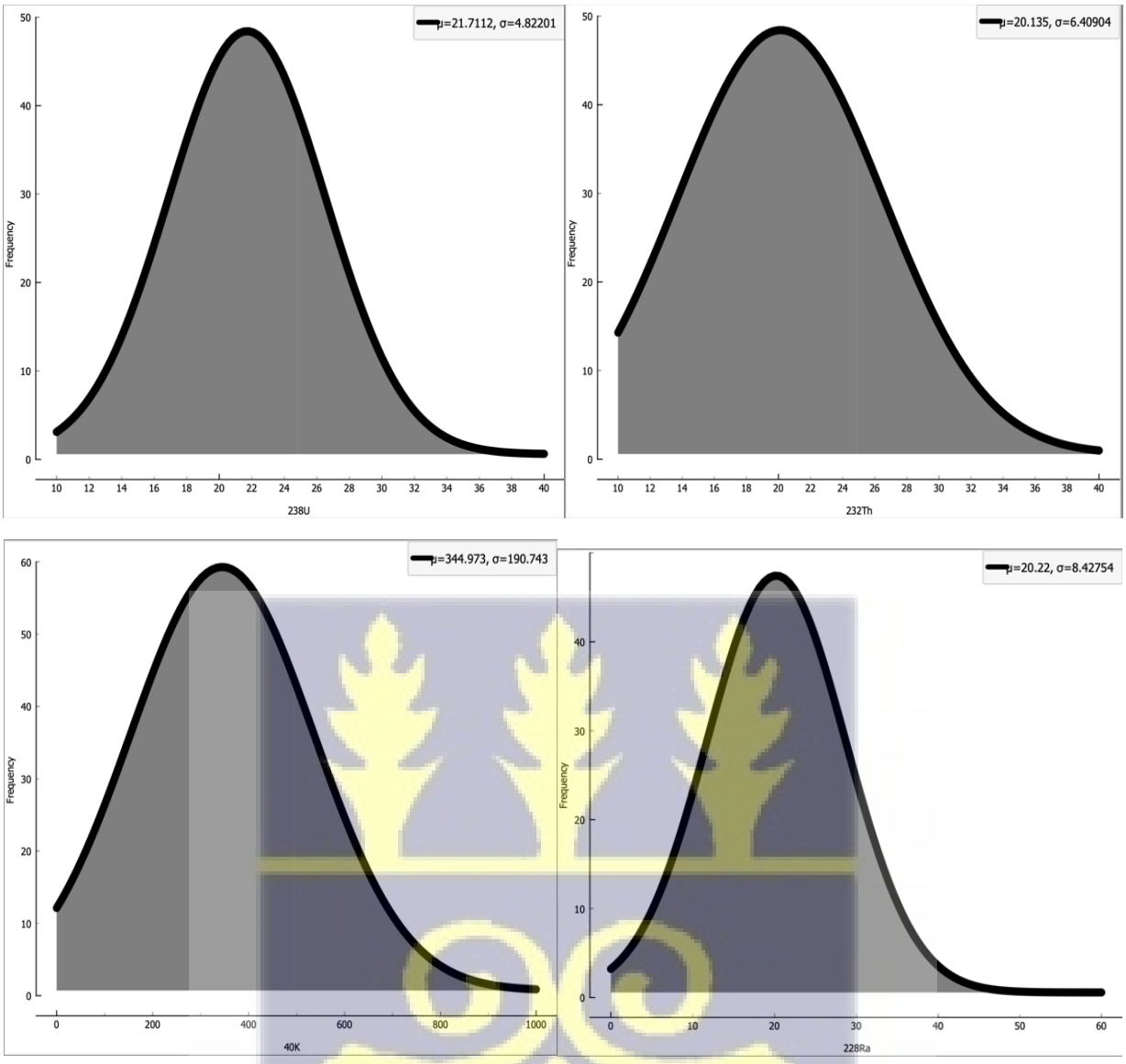

Figure 4.11: Frequency distribution curve of ^{40}K, ^{232}Th, ^{238}U, and ^{228}Ra in beach sand.

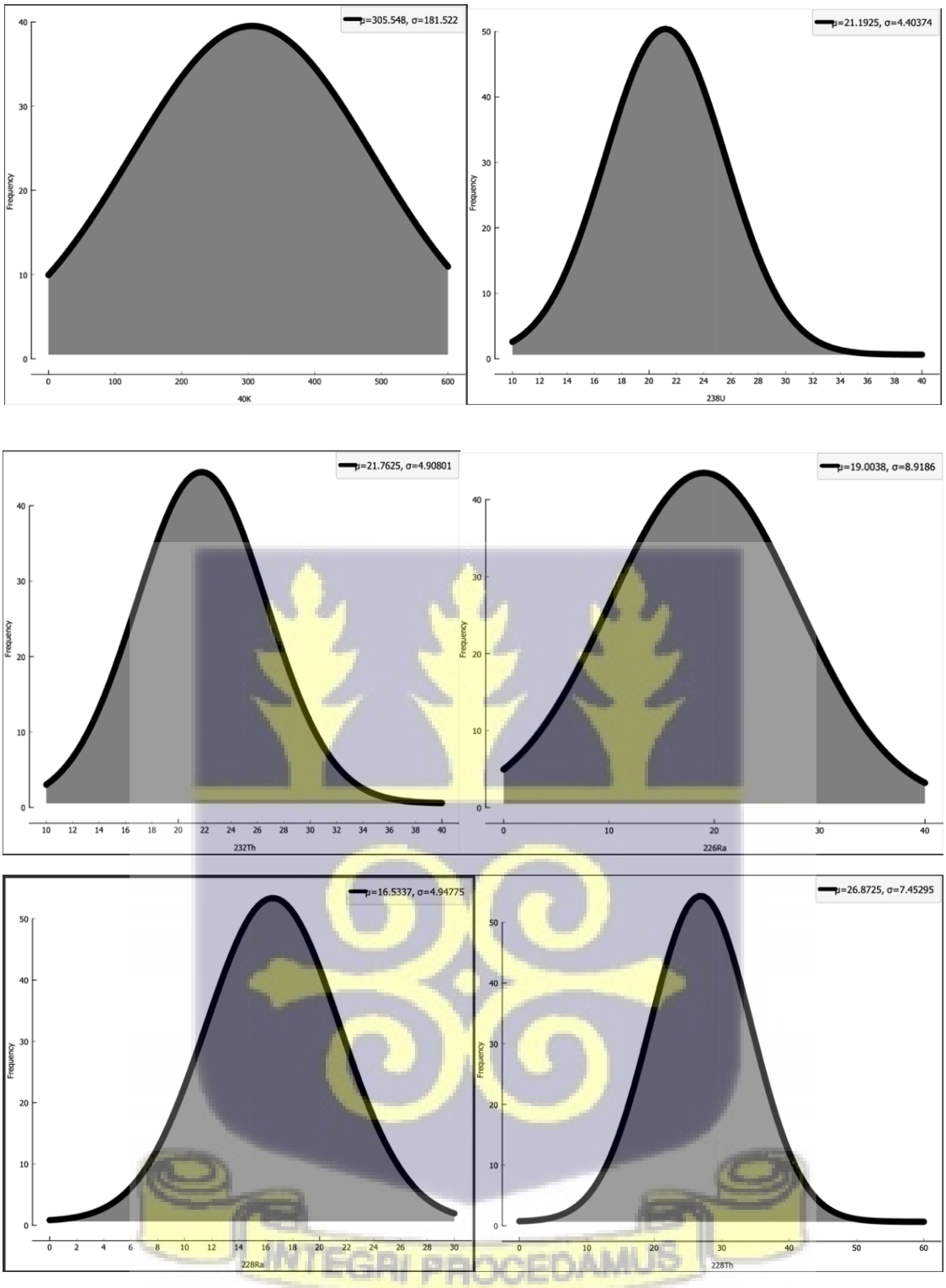

Figure 4.12: Frequency distribution curve of ^{40}K, ^{232}Th, ^{238}U, ^{226}Ra, ^{228}Ra, and ^{228}Th in coastal sediment.

A linear modeling procedure from the data was used to develop an empirical model using R programming software. The model was based on correlations obtained from analysis of the experimental data for assessment of the risk of exposure to naturally occurring radioactive materials. The model fits the data using regression analysis to reflect all data points.

The simple linear regression equations were represented generally as:

$$Y = \beta_0 + \beta_1 X \qquad (4.1)$$

where:

Y is the predicted value of the dependent variable,

β_0 is the intercept,

β_1 is the coefficient of the independent variable, and

X is the value of the independent variable.

While the multiple linear regression equations were represented generally as:

$$Y = \beta_0 + \beta_1 X_1 + \beta_2 X_2 + \cdots + \beta_n X_n \qquad (4.2)$$

where:

Y is the dependent variable (the outcome),

$X_1, X_2, \ldots, X_n$ are the independent variables (the predictors),

β_0 is the intercept (the predicted value of Y when all X's are 0), and

$\beta_1, \beta_2, \ldots, \beta_n$ are the coefficients (the contribution of each independent variable).

A multiple regression analysis and diagnostics were done to check if the model is a good fit for the data from the beach sand as shown in Figures 4.13 and 4.14.

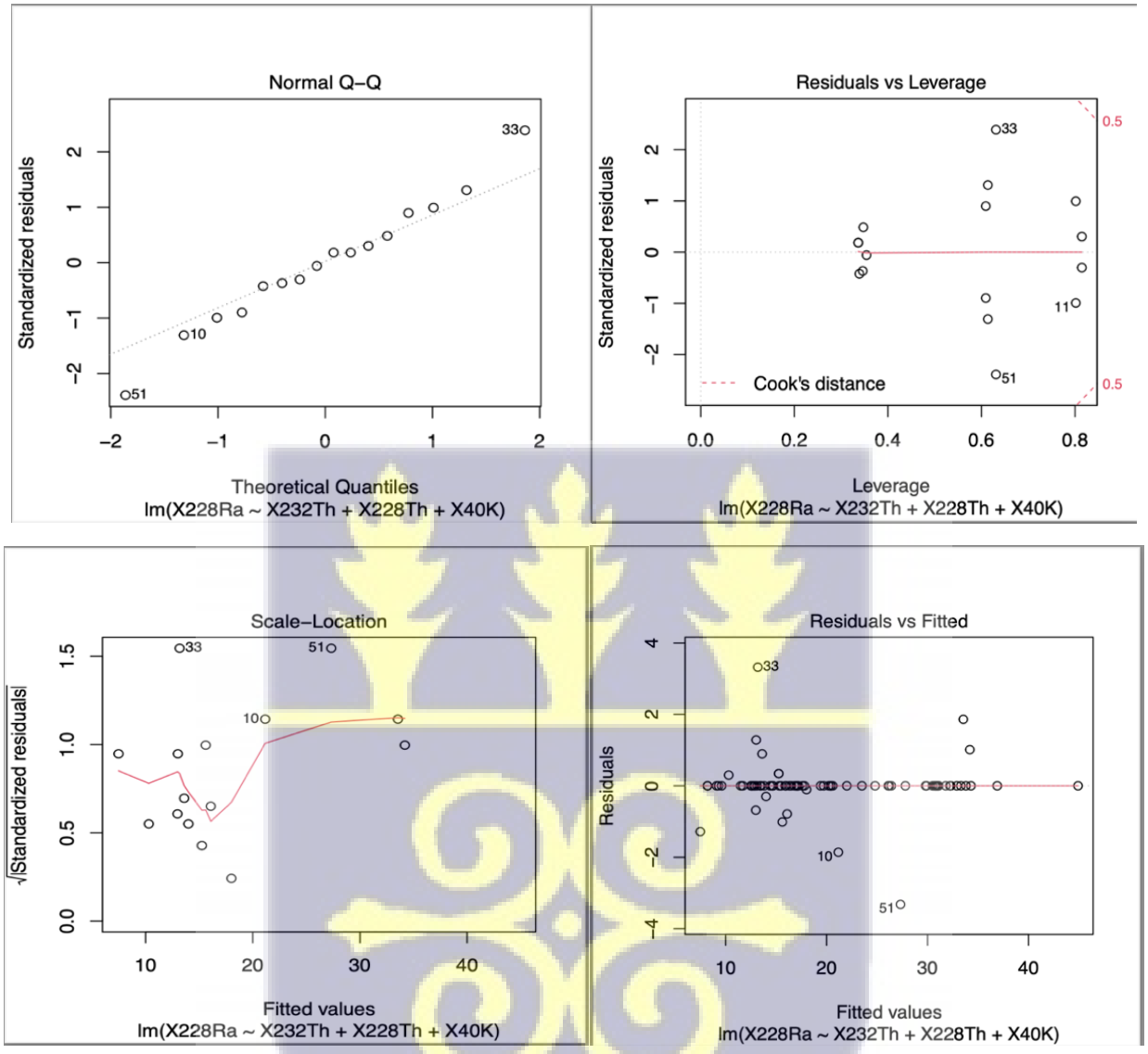

Figure 4.13: Residual plots produced by ^{228}Ra and ^{232}Th+^{228}Th+^{40}K in beach sand.

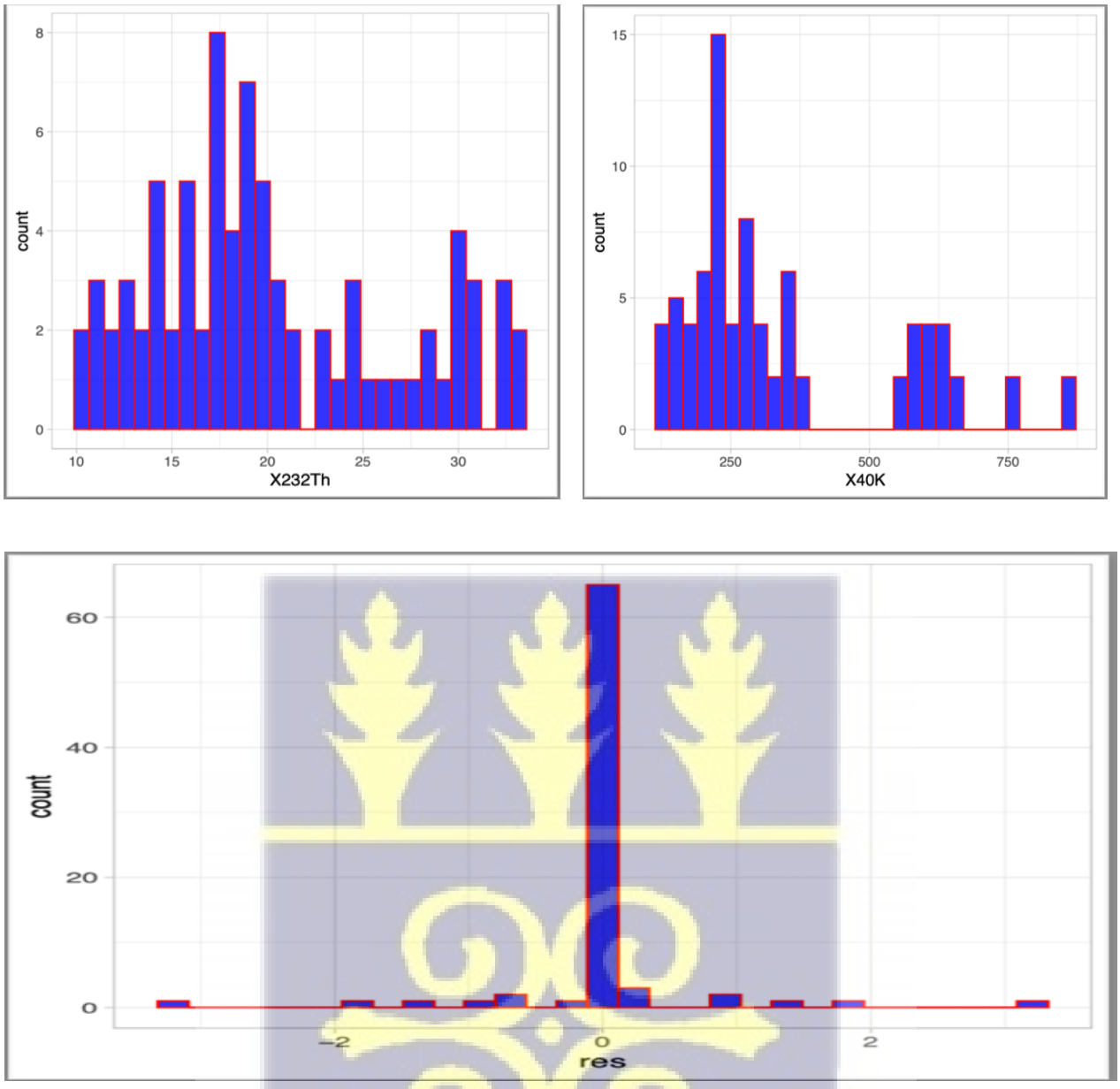

Figure 4.14: Histogram of residual plots of radionuclides in beach sand.

Figures 4.13 and 4.14 show a multiple linear regression model from the data, with ^{228}Ra as the response variable and ^{232}Th, ^{228}Th, and ^{40}K as the predictor variables (Appendix I). The regression equation from the model is given as:

$$^{228}Ra = 1.5273\,^{232}Th + 0.003505\,^{40}K - 4.3024 \qquad (4.3)$$

The estimated intercept from the model is -4.302428. This is the expected value of ^{228}Ra when all the three predictor variables (^{232}Th and ^{40}K) are zero. The coefficient for ^{232}Th is 1.527277.

An increase of ^{228}Ra of about 1.53 units is correlated with a one-unit increase in ^{232}Th. For ^{40}K, the coefficient is 0.003505.

A one-unit increase in ^{40}K corresponds to an increase of roughly 0.0035 units in ^{228}Ra, holding all other variables constant. If the estimated coefficients differ significantly from zero, it is indicated by the p-values assigned to the coefficients. The p-value of ^{232}Th is 6.34e-05, which is statistically significant. ^{40}K, however, is not statistically significant with a p-value of 0.62995. The model describes the data correctly since all the residuals are close to zero. The model explains 99.36% of the variability in ^{228}Ra with a Multiple R-squared value of 0.9936. The Adjusted R-squared value is 0.9272 which accounts for the number of predictors. The large value increases the risk of overfitting even though the adjusted R-squared is significantly lower than the Multiple R-squared. The significance of the model is evaluated using the F-statistic. The model is statistically significant with a low p-value of 0.0004895. The residual standard error of 2.288 shows the variability of the residuals around the regression line. The high percentage of variability in ^{228}Ra indicates that the model fits the data very well.

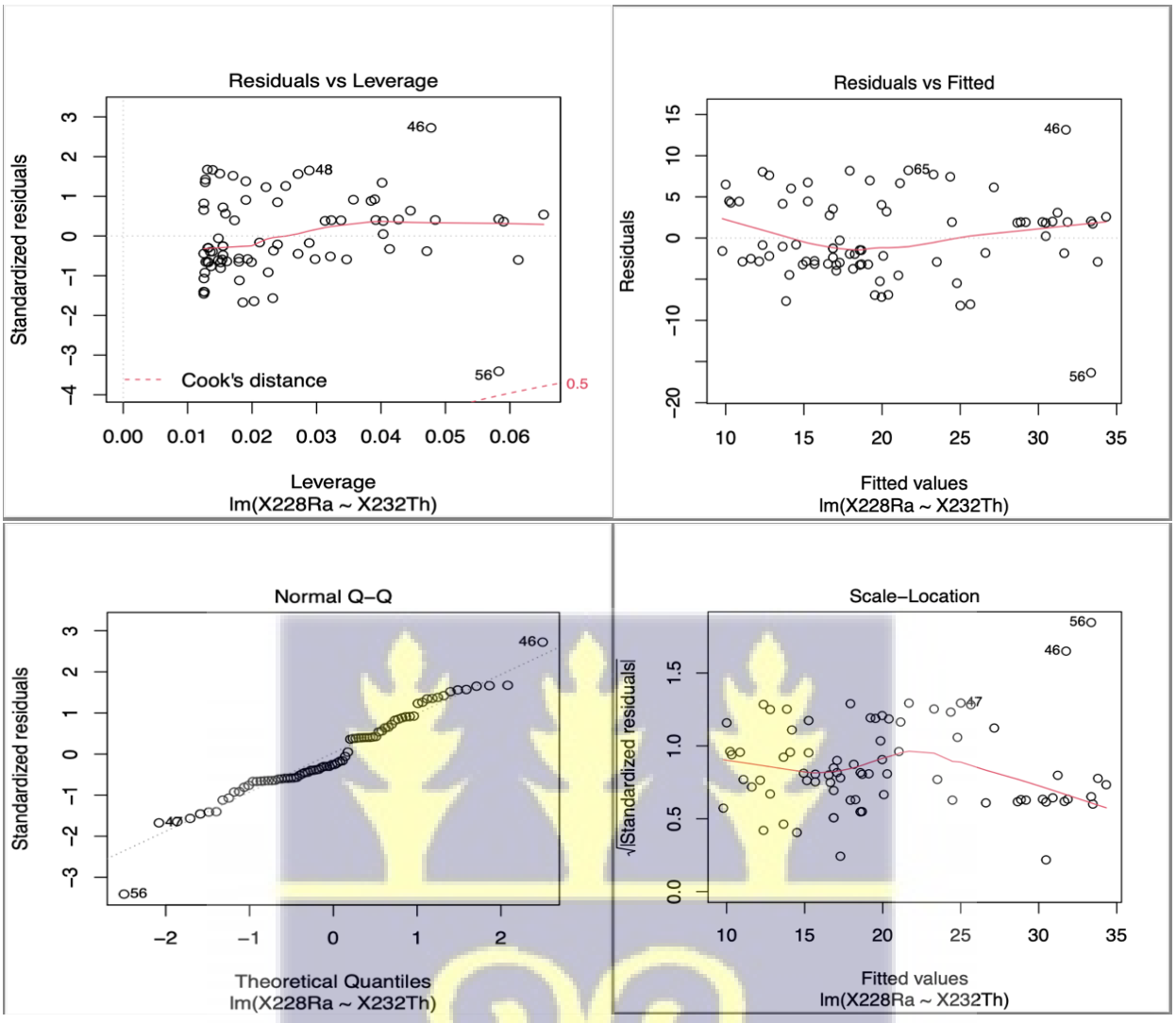

Figure 4.15: Residual plots produced by ^{228}Ra and ^{232}Th in beach sand.

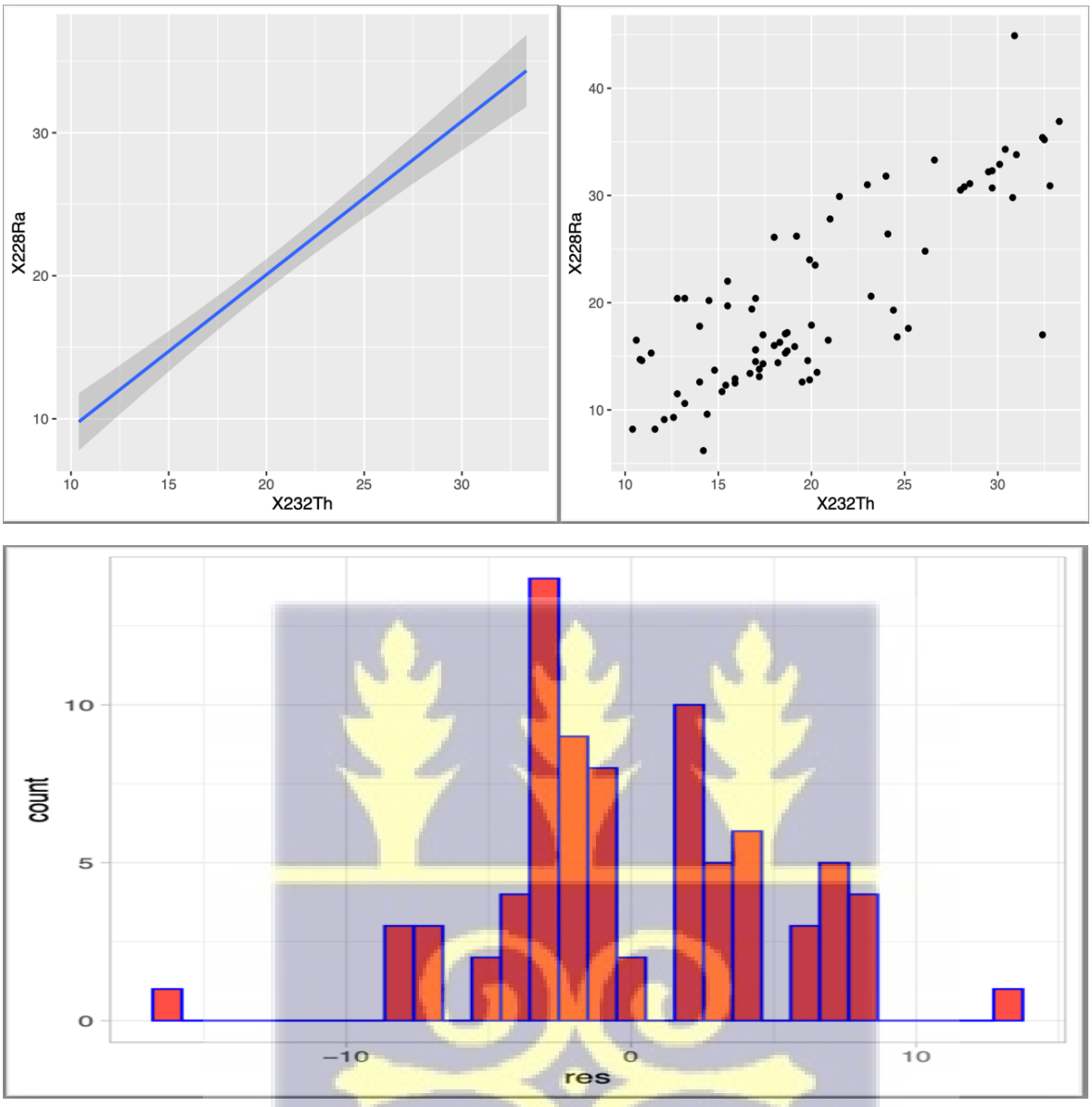

Figure 4.16: Histogram of the residual and a linear distribution graph of ^{228}Ra and ^{232}Th.

The summary statistics of the residuals show the spread and distribution of the model's errors as represented in Figures 4.15 and 4.16.

The predictor variable ^{232}Th, is fundamental for the prediction of the variable ^{228}Ra. The residuals are between -16.363 and 13.144 (Appendix J). With a coefficient of 1.07161 for ^{232}Th and an intercept of -1.35679, as given in the equation below:

$$^{228}Ra = 1.0716\,^{232}Th - 1.3568 \qquad (4.4)$$

The p-value of less than 2e-16 indicates high significance for the coefficient of ^{232}Th. The response variable ^{228}Ra should rise by about 1.07161 units for every unit increase in ^{232}Th according to its coefficient. The standard magnitude of the errors is shown by the residual standard error, which is 4.946. According to a multiple R-squared value of 0.6641, the model explains 66.41% of the variance in the dependent variable (^{228}Ra). The complexity of the model is considered by the adjusted R-squared value of 0.6598. This accounts for the number of predictors and depicts that roughly 65.98% of the variance is explained. With an F-statistic of 154.2 and a corresponding p-value of less than 2.2e-16, the model is statistically significant.

To find the extent of the presence and distribution of the radionuclides in the coastal sand, correlation studies were performed between the combinations of radionuclides such as ^{228}Ra and ^{232}Th, and ^{40}K and ^{232}Th.

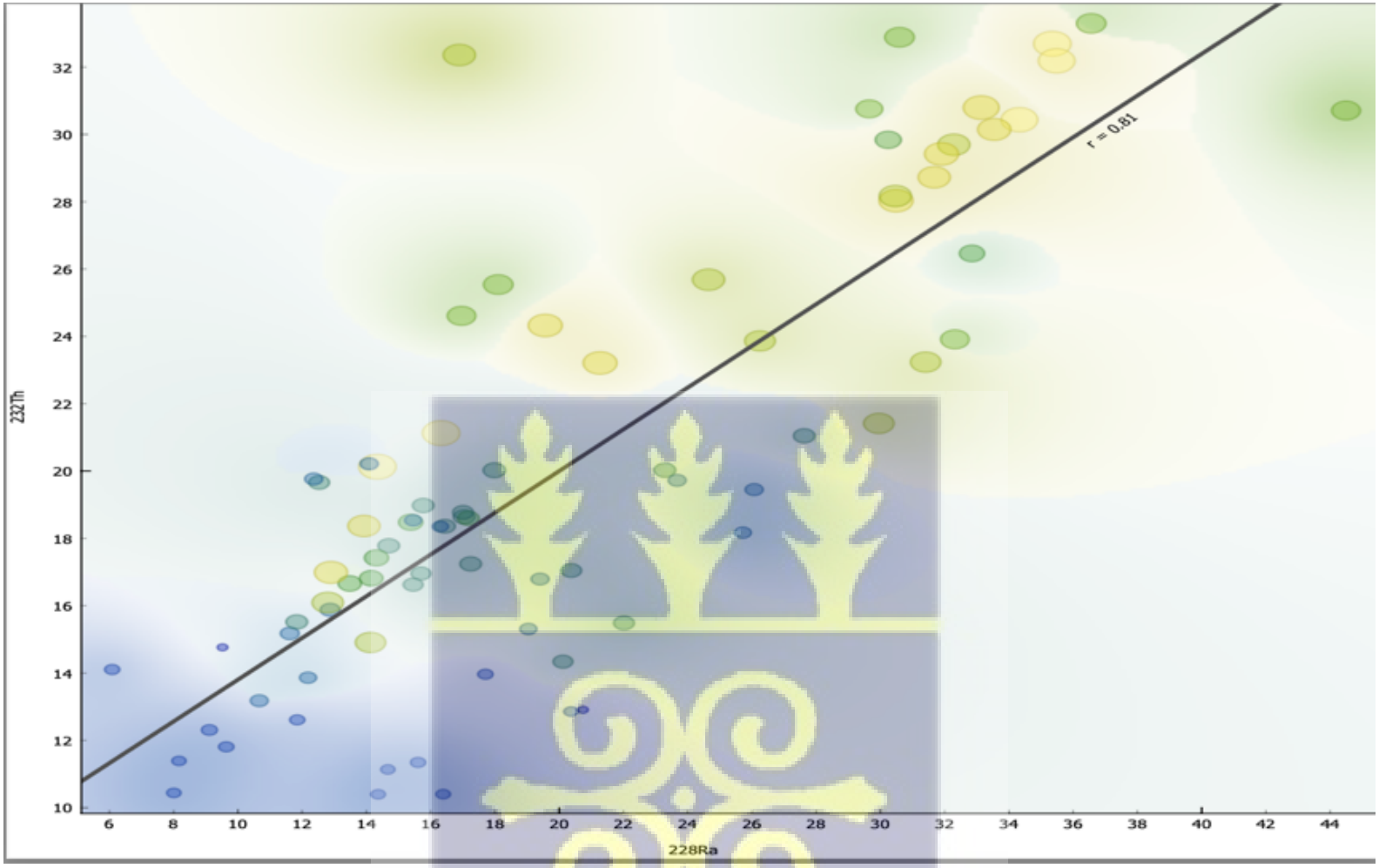

Figure 4.17: Correlation between ^{228}Ra and ^{232}Th

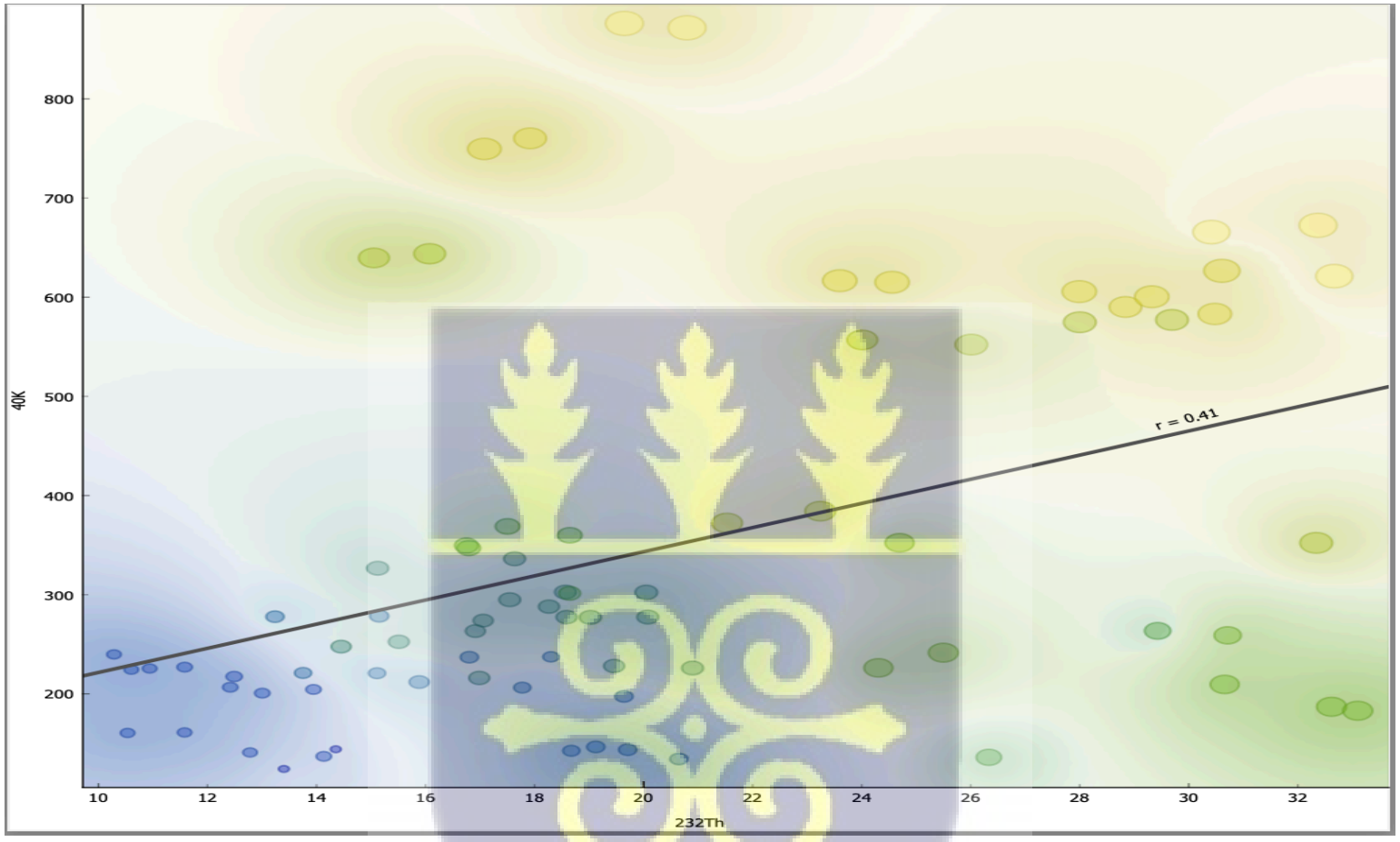

Figure 4.18: Correlation between ^{40}K and ^{232}Th

Figures 4.17 and 4.18 show a linear regression of their activity concentrations in beach sand samples. The correlation shows a strong positive relationship with a coefficient of correlation of 0.81 for ^{228}Ra and ^{232}Th (Figure 4.17). This means that as the concentration of ^{232}Th increases, the concentration of ^{228}Ra tends to increase as well. The data points are closely clustered around the regression line, which indicates that there is a strong and consistent relationship between ^{228}Ra and ^{232}Th concentrations in the samples. Some of the data points scatter around the regression line. Points that are far from the line suggest variations in the relationship, which could be due to measurement errors or sample variability. Given the significant association, it is probable that a process or shared source is affecting both radionuclides in the beach sand. For instance, since ^{228}Ra and ^{232}Th are both naturally occurring, they might be impacted by comparable environmental or geological processes. ^{40}K and ^{232}Th, however, show a moderately weak relationship with a coefficient of correlation of 0.41 (Figure 4.18). The data points are dispersed around the line of best fit. Because the correlation is only moderately weak, there is noticeable variability, with some points deviating quite a bit from the regression line. Despite the weak correlation, there is still a general upward trend. There is a slight tendency for the concentration of ^{40}K to increase as the concentration of ^{232}Th increases, though this trend is not strong. The spread of data points shows that while there is some relationship between the two variables, it is not very strong. While some beach sand might have high concentrations of ^{40}K and not ^{232}Th, other beach sand samples will show high concentrations of both ^{40}K and ^{232}Th. The coefficient of correlation of 0.41 suggests a significant amount of variability that is not explained by the linear relationship. This means that other factors may be influencing the concentrations of ^{40}K and ^{232}Th in the samples.

Figures 4.19 and 4.20 show the residual plots produced between ^{228}Th and ^{232}Th (Appendix L). The model forecasts the variable ^{232}Th by using the predictor variable ^{228}Th as a basis.

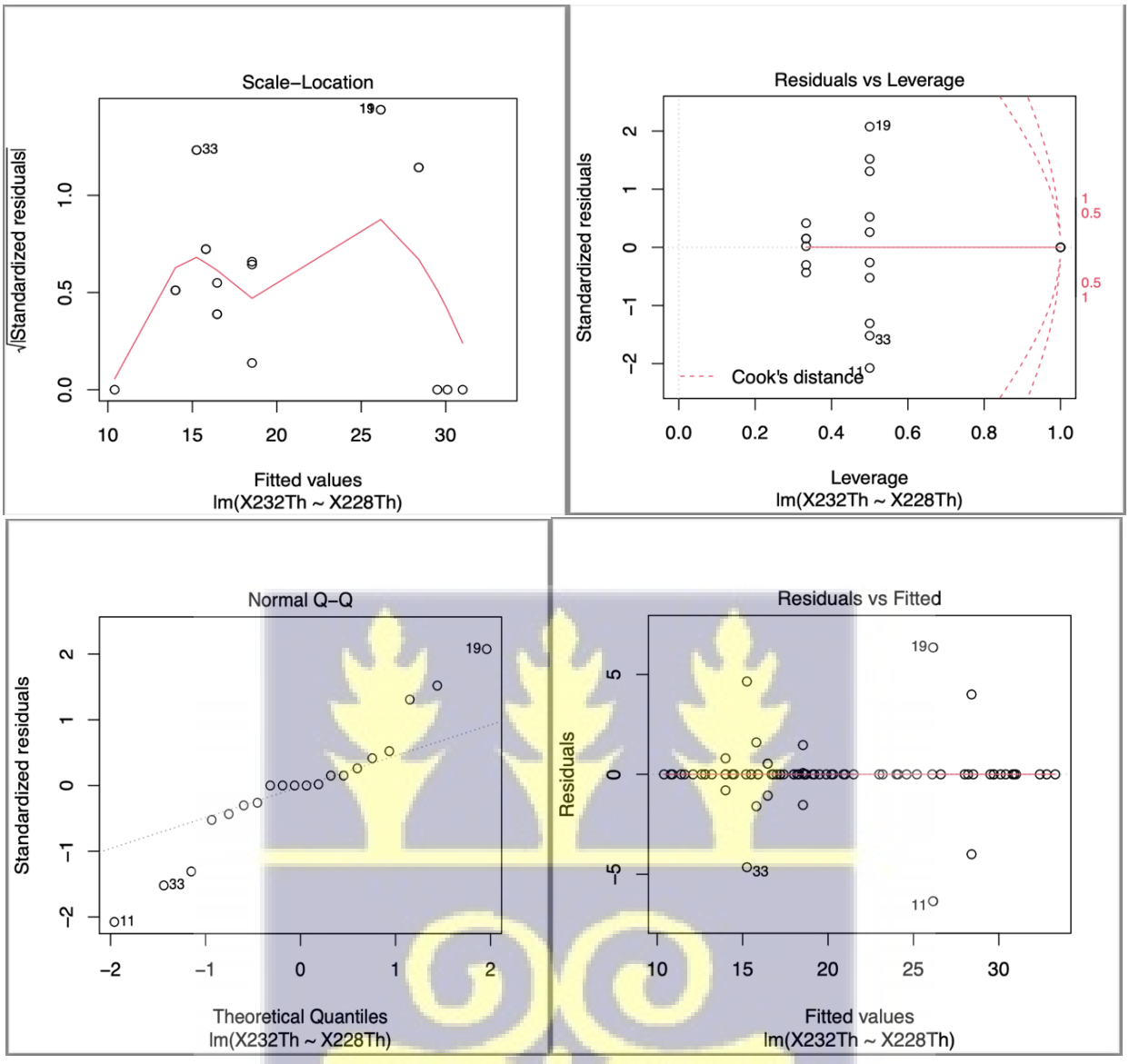

Figure 4.19: Residual plots produced by ^{228}Th and ^{232}Th in beach sand.

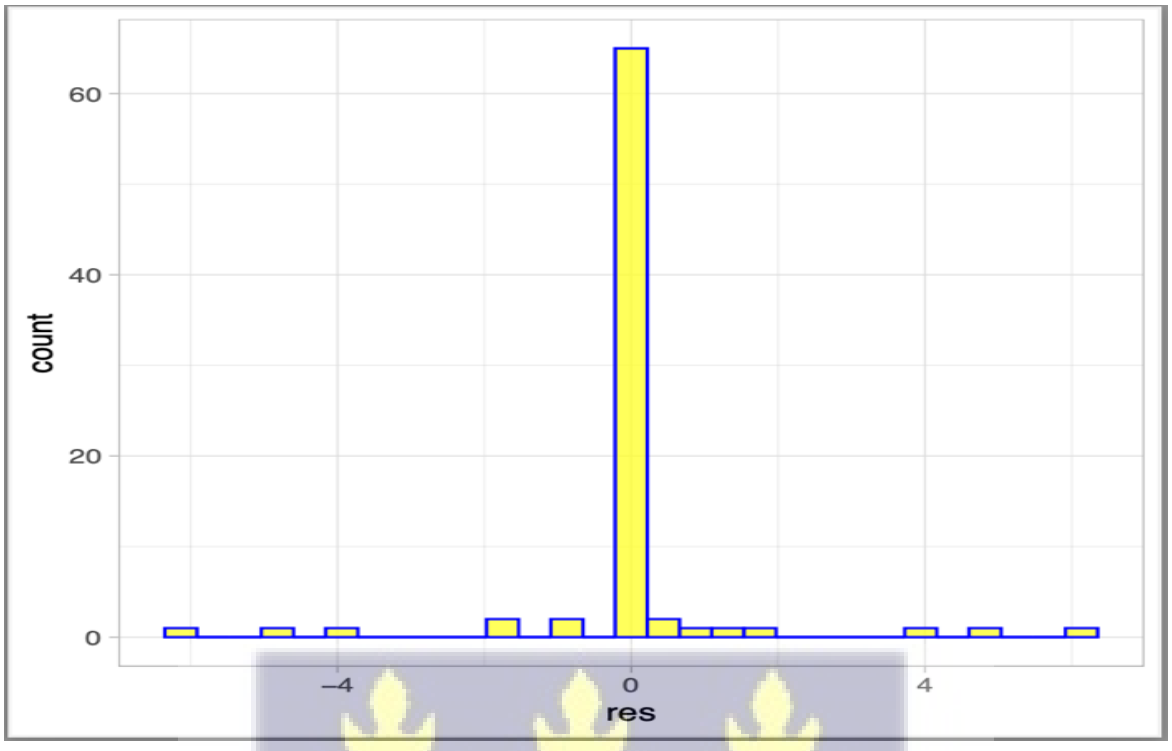

Figure 4.20: Histogram of residual plot produced by ^{228}Th and ^{232}Th in beach sand.

The discrepancies between the actual observed values and the values the model predicted are represented by residuals plots (Figures 4.19 and 4.20). The residuals' summary statistics (Min, 1Q, Median, 3Q, Max) shed light on the model's error distribution.

The p-value denotes the likelihood of observing an F-statistic as extreme as the one computed, assuming the null hypothesis that the true coefficient is zero. This represents an estimate of the standard deviation of the residuals, which in this case is 4.327 and indicates the typical magnitude of the errors. The model explains approximately 94.87% of the variance in the dependent variable, according to multiple R-squared (0.9487). The adjusted R-squared (0.5499), which takes the number of predictors into account and shows that about 54.99% of the variation is explained, represents the model's complexity. The significance of the model is determined using the F-statistic which is 2.379 with an associated p-value of 0.07999. The model is not statistically significant as

indicated by the p-value of 0.07999, which is near to the traditional significance level of 0.05 at the 95% confidence level.

Figures 4.21 and 4.22 show the residual plots produced by the code between ^{40}K and ^{232}Th in beach sand.

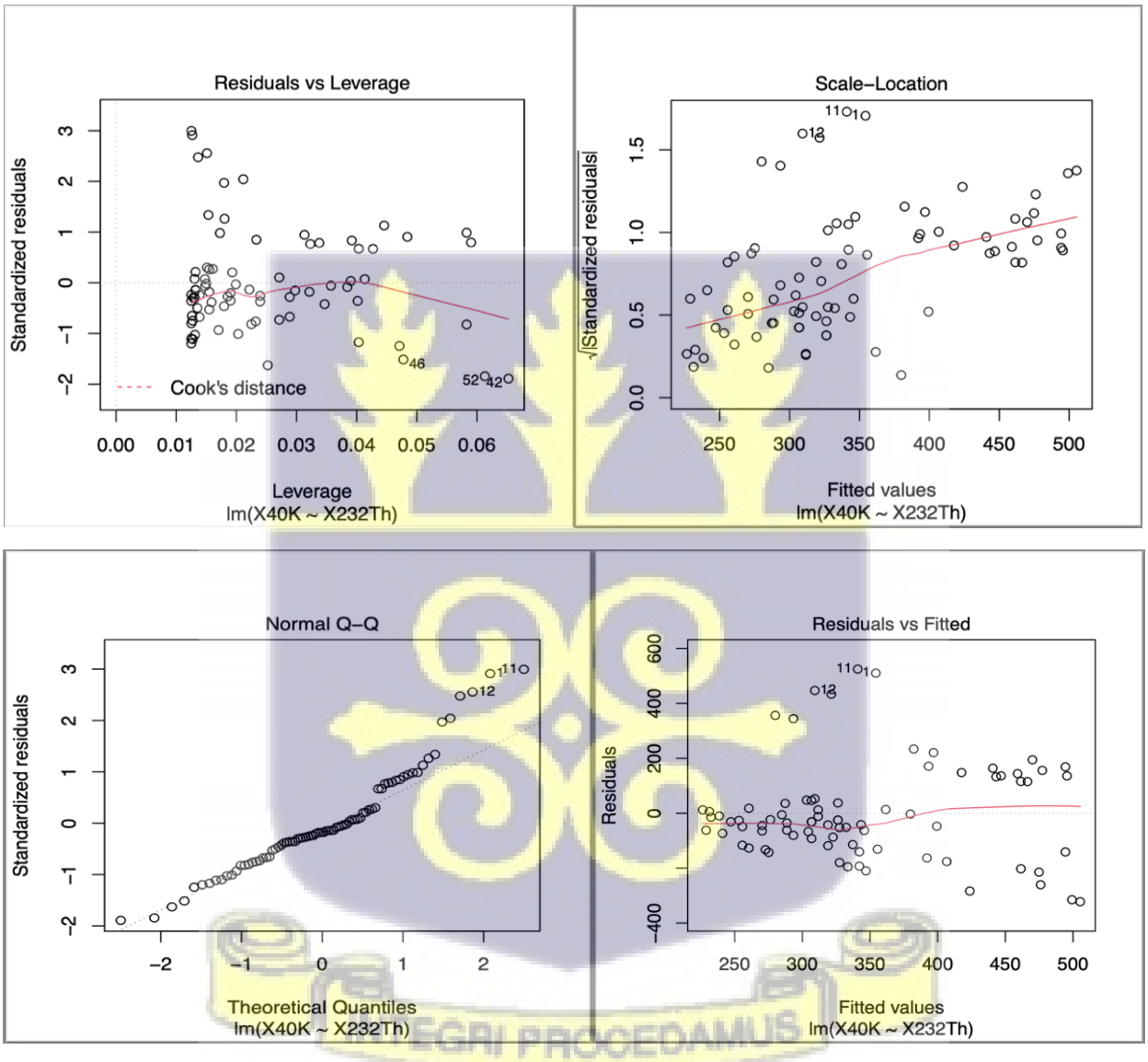

Figure 4.21: Residual plots produced by ^{40}K and ^{232}Th in beach sand.

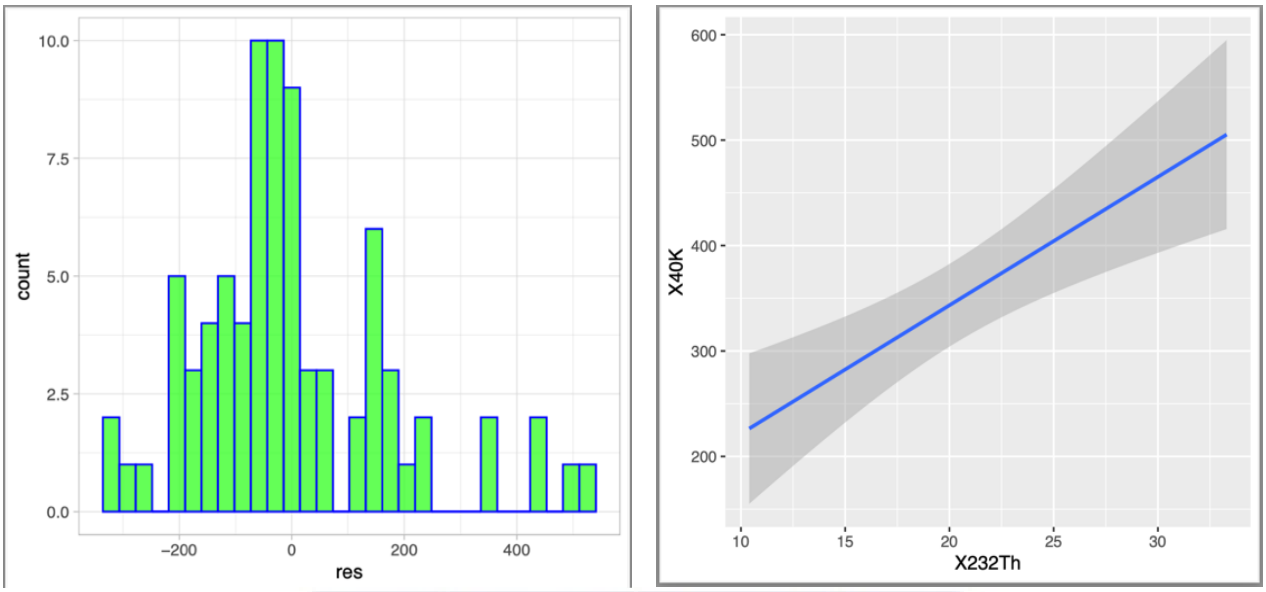

Figure 4.22: Graph showing the linear distribution and histogram of the residual.

The estimated intercept of the model for ^{40}K and ^{232}Th is 99.764. When ^{232}Th is zero, this is the predicted value of ^{40}K. The coefficient for ^{232}Th is 12.178. The regression equation is given as;

$$^{40}K = 12.1780\,^{232}Th + 99.7640 \qquad (4.5)$$

There is a correlation between an increase in ^{40}K of approximately 12.178 and a one-unit rise in ^{232}Th (Appendix K). The intercept's p-value is more than 0.05 at 0.128708. Therefore, the intercept is not statistically significant. The low p-value of 0.000164 for ^{232}Th suggests that there is a statistically significant association between ^{232}Th and ^{40}K.

The residuals' summary statistics display central tendency and spread metrics as shown in Fig. 4.21. With a Multiple R-squared of 0.1674, the model can only account for 16.74% of the variability in ^{40}K. The Adjusted R-squared is 0.1568 after accounting for the number of predictors. When there is just one predictor, the Multiple R-squared is typically slightly higher. The residual standard error of 176.3 shows how variable the residuals are around the regression line. The low

p-value for the coefficient of ^{232}Th in the model suggests a statistically significant positive association between ^{232}Th and ^{40}K. However, the R-squared values are conversely moderate, depicting the variability in ^{40}K can be explained by ^{232}Th relatively. In conclusion, notwithstanding the statistical significance of the model, the low R-squared values indicate that ^{232}Th may not be a very good predictor of ^{40}K.

Figures 4.23 and 4.24 show the linear regression plots of all the radionuclides of interest in sea sediment, and the histogram of residual plots of all the radionuclides including ^{228}Ra, ^{232}Th, ^{228}Th, ^{40}K and ^{226}Ra.

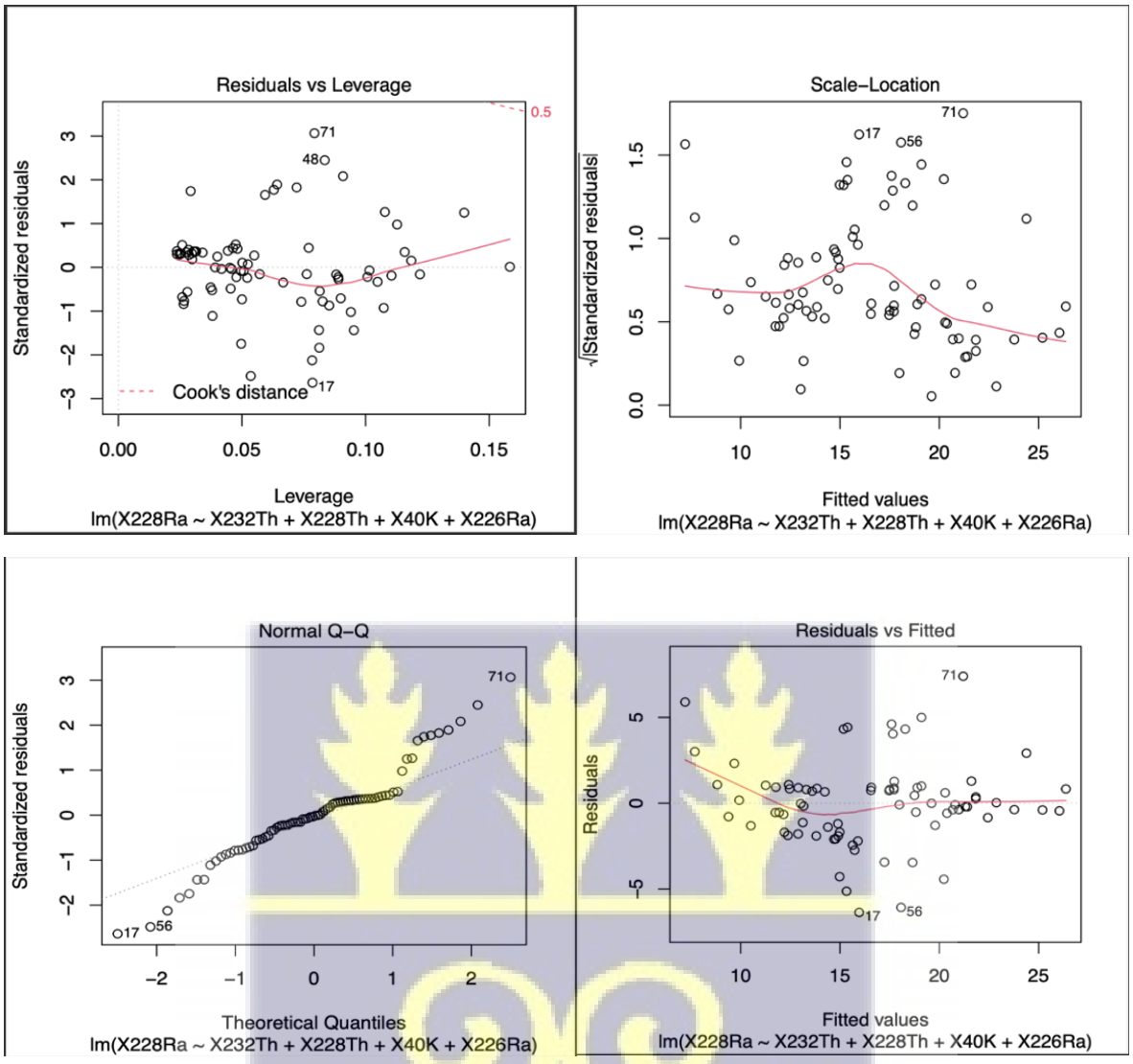

Figure 4.23: Residual plots produced by ^{228}Ra and ^{232}Th+^{228}Th+^{40}K+ ^{226}Ra in sea sediment.

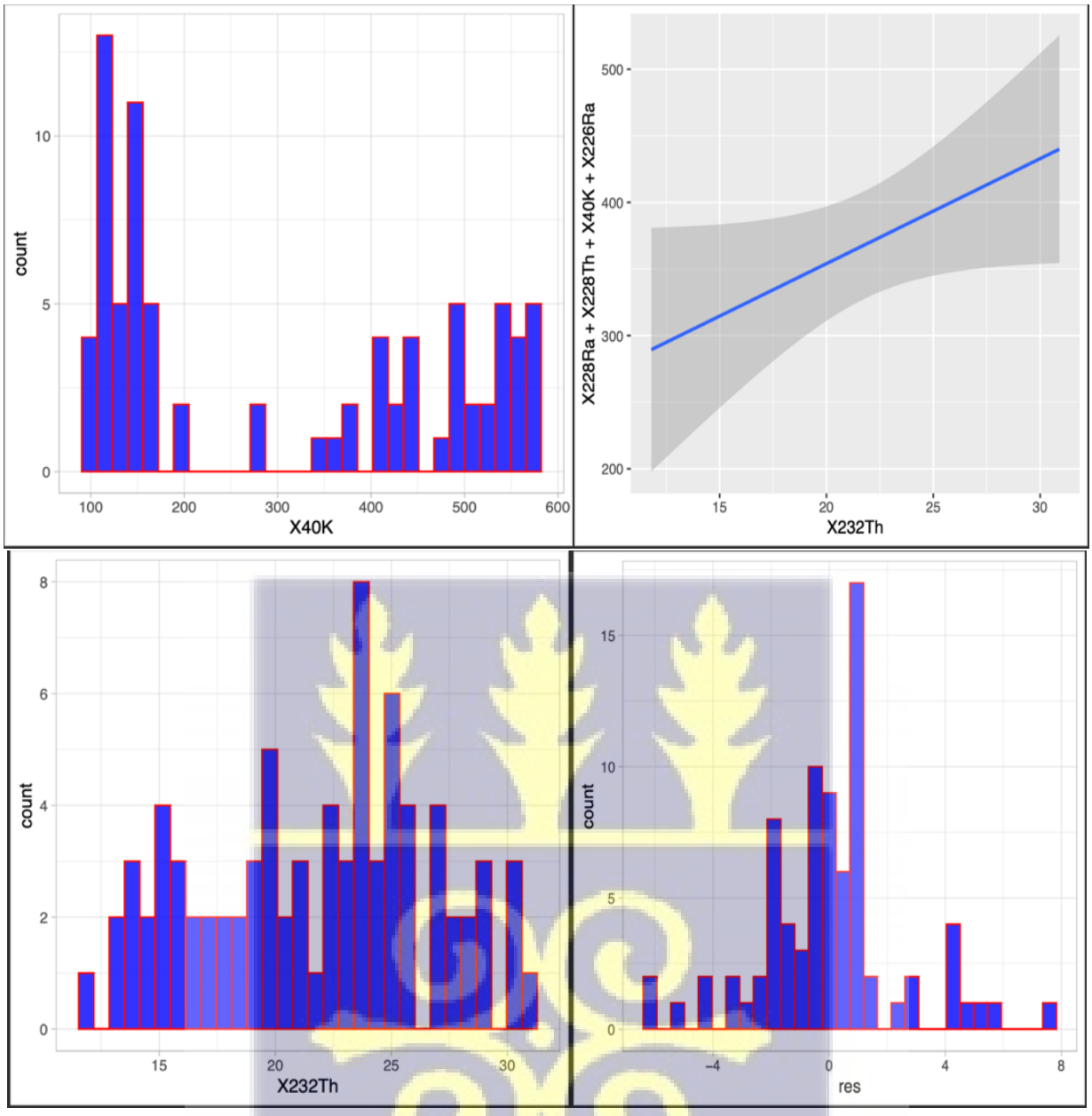

Figure 4.24: Histogram of residual plots of radionuclides in sea sediment.

The linear regression model obtained, with ^{228}Ra as the response variable and ^{232}Th, ^{228}Th, ^{40}K, and ^{226}Ra as the predictor variables is shown in Appendix M. The estimated intercept between the variables is -1.456544, which shows the expected value of ^{228}Ra when all predictor variables are zero. The coefficient for ^{232}Th is 1.680992. An increase of one unit in ^{232}Th is associated with an

increase of roughly 1.68 units in ^{228}Ra, holding other variables constant. The coefficient for ^{228}Th is -0.753465. A one-unit increase in ^{228}Th is associated with a decrease of roughly 0.75 units in ^{228}Ra, holding other variables constant. The coefficient for ^{40}K is 0.004029. A one-unit increase in ^{40}K is associated with an increase of roughly 0.004 units in ^{228}Ra, holding other variables constant. Holding all other variables fixed, a one-unit rise in ^{226}Ra corresponds to an increase of roughly 0.022 units in ^{228}Ra. The statistical significance of the association between ^{228}Ra and ^{232}Th is indicated by their extremely low p-values (<0.001). At the 0.05 level of significance, ^{40}K's p-value of 0.0134 indicates a significant association. In this model, ^{226}Ra may not be a statistically significant predictor, as indicated by its p-value of 0.5404 as shown in Appendix M. the equation from the multiple linear regression is given as:

$$^{228}Ra = 1.6810^{232}Th - 0.7835^{228}Th + 0.004029^{40}K + 0.02232^{226}Ra - 1.4565 \quad (4.6)$$

The discrepancies between observed and expected values are represented by residuals. Measures of central tendency and dispersion are shown in the summary statistics for the residuals, which indicates how well the model fits the data. The residual plots produced by the code are shown in Figures 4.23 and 4.24.

The regression model may account for 75.78% of the variability in ^{228}Ra with the Multiple R-squared value of 0.7578. The number of predictors is considered by the Adjusted R-squared, which modifies the R-squared value respectively, which is 0.7449 in this case. The statistical significance of the model is indicated by the low p-value (< 2.2e-16). The residual standard error of 2.515 suggests how reliable the residuals are around the regression line.

The large F-statistic and strong R-squared value indicates how well the model fits the data. Each of the individual predictor factors (^{232}Th, ^{228}Th, and ^{40}K) is statistically significant in terms of forecasting ^{228}Ra. Although ^{226}Ra's lack of significance indicates that it might not be a significant predictor in the model. The model's prediction accuracy is indicated by the residuals and the residual standard error. In conclusion, a sizable amount of the variability in ^{228}Ra appears to be explained by this linear regression model, which appears to offer a statistically significant and generally decent fit to the data.

Figures 4.25 and 4.26 show the residual plots produced by the sea sediment (Appendix N).

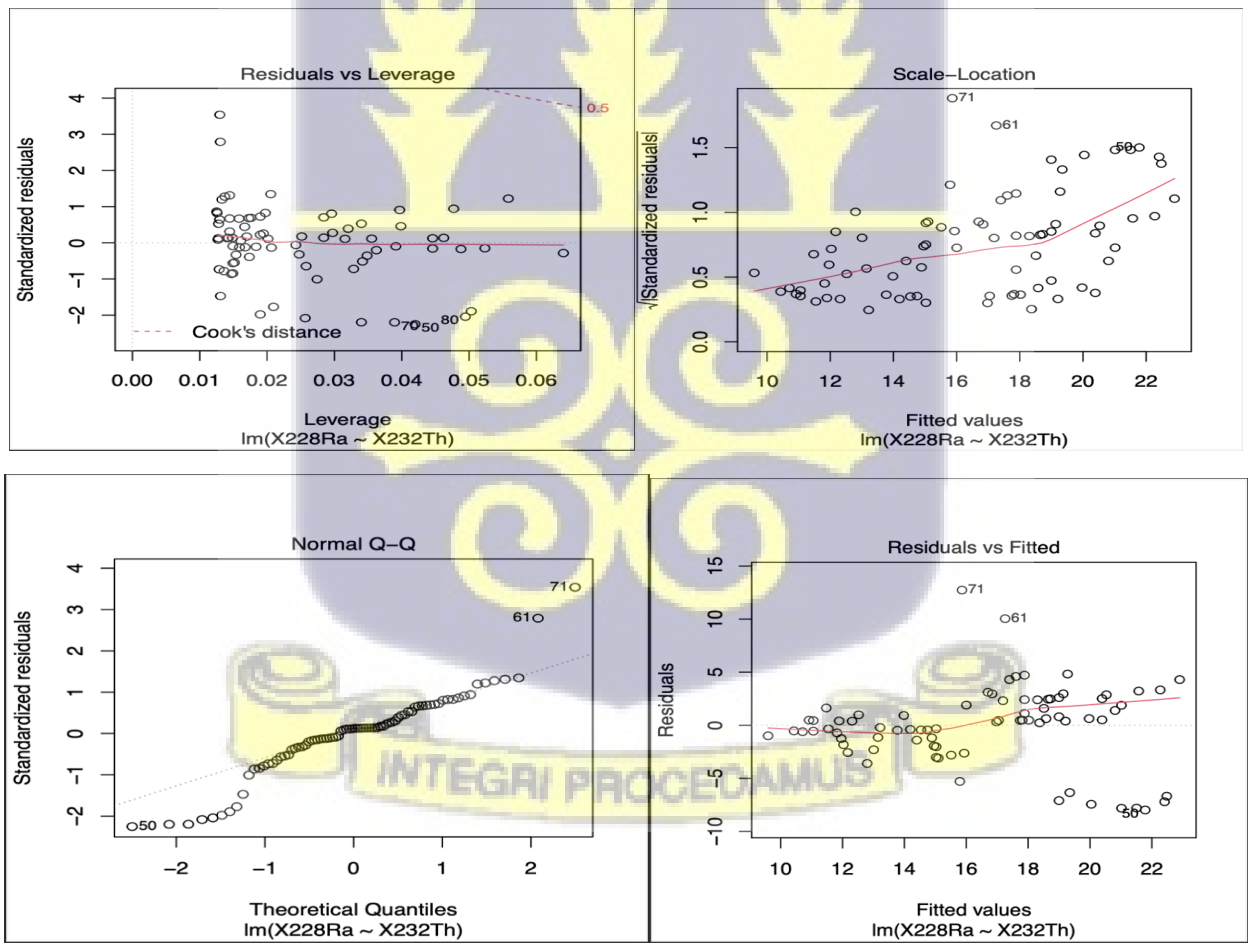

Figure 4.25: Residual plots produced by ^{228}Ra and ^{232}Th in sea sediment.

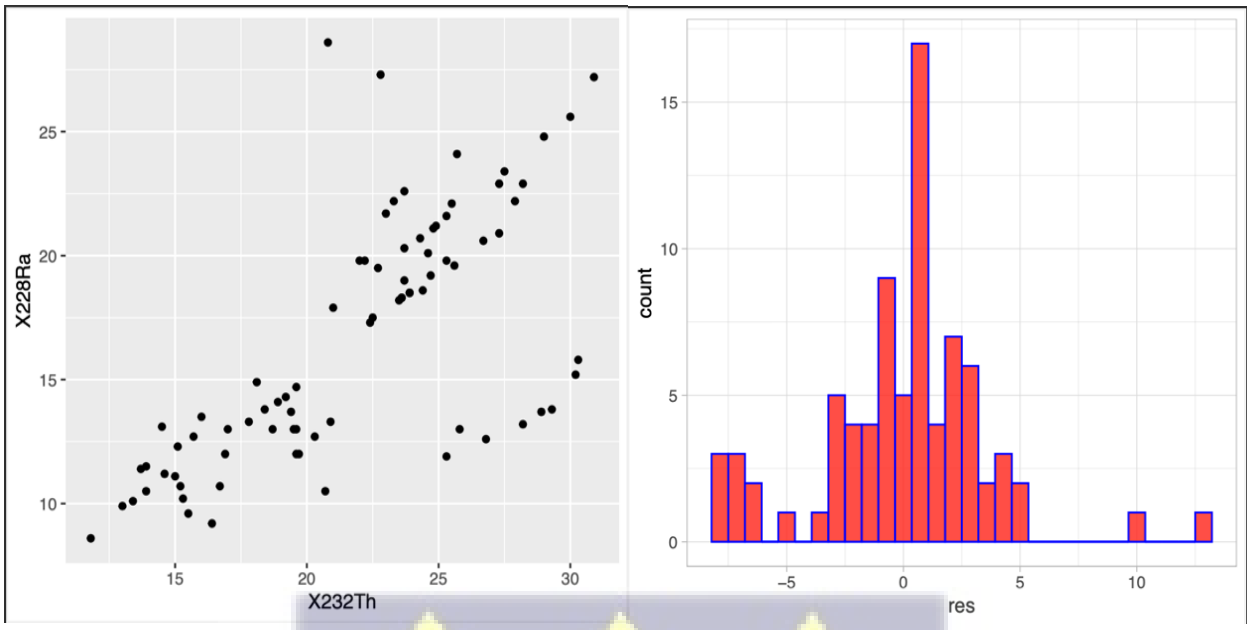

Figure 4.26: Graph showing the linear distribution and histogram of the residual.

The linear regression model between ^{228}Ra and ^{232}Th has an intercept estimated to be 1.37374. This is ^{228}Ra's expected value when ^{232}Th is equal to zero. The coefficient for ^{232}Th is 0.69661. When all other factors are held constant, an increase of one unit in ^{232}Th corresponds to an increase of roughly 0.70 units in ^{228}Ra. The intercept has a p-value of 0.458, while the p-value for ^{232}Th is extremely low (< 0.001), indicating a statistically significant correlation between ^{232}Th and ^{228}Ra. The regression equation is given as:

$$^{228}Ra = 0.6966\,^{232}Th + 1.3737 \qquad (4.7)$$

The discrepancies between the observed and anticipated values are represented by the residuals (Figure 4.25). The model accounts for 47.75 % of the variability in ^{228}Ra with a Multiple R-squared value of 0.4775. The Adjusted R-squared value of 0.4708 accounts for the number of predictors. The low p-value of 1.302e-12 indicates a statistically significant model. The residual standard error which shows the residuals' variability has a value of 3.622. ^{232}Th and ^{228}Ra have a positive

statistically significant relationship according to the model. The model explains roughly 47.75 % of the variability in ^{228}Ra, according to the R-squared value.

Figures 4.27 and 4.28 show the residual plots produced by the code between ^{40}K and ^{232}Th in sea sediment.

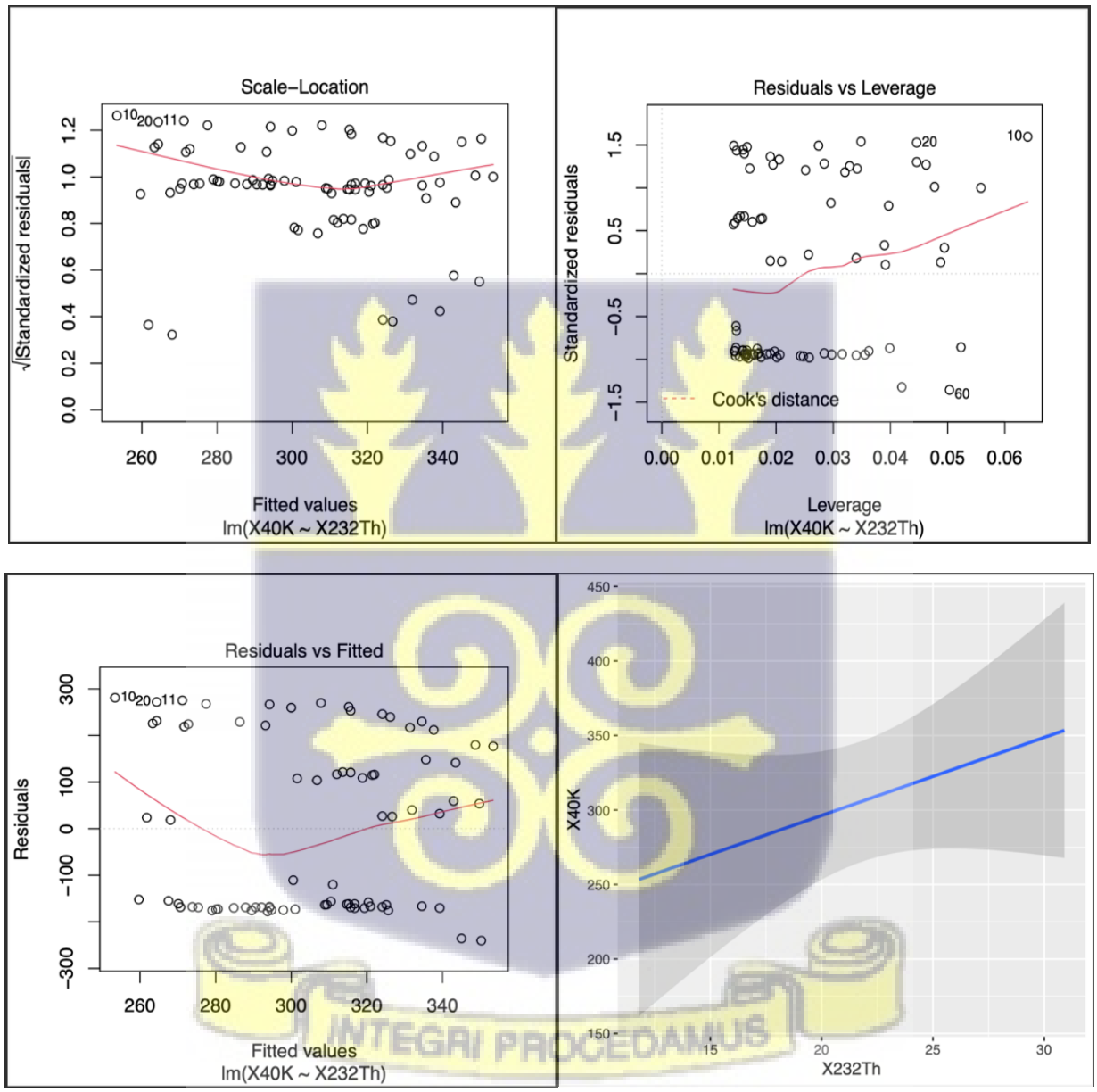

Figure 4.27: Residual plots produced by ^{40}K and ^{232}Th in sea sediment.

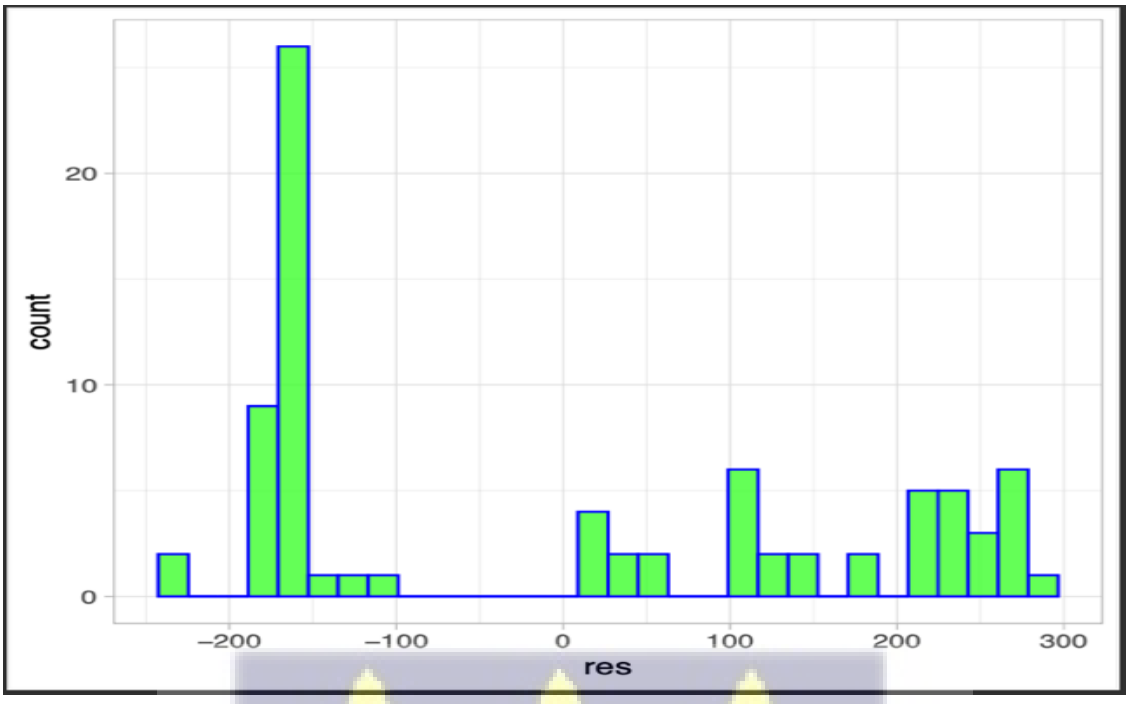

Figure 4.28: Histogram of the residual plot of ^{40}K and ^{232}Th in sea sediment.

These residual plots come from a basic linear regression model derived from the code lm(formula = X^{40}K ~ X^{232}Th, data = df) with ^{40}K as the response variable and ^{232}Th as the predictor variable as shown in Appendix O. The regression equation is given as:

$$^{40}K = 5.2360^{232}Th + 191.5970 \qquad (4.8)$$

191.597 is the estimated intercept. This is ^{40}K's expected value when ^{232}Th is equal to zero. The coefficient for ^{232}Th is 5.236. An increase of 5.236 units in ^{40}K is correlated with a one-unit increase in ^{232}Th. The intercept's p-value is 0.0416, which is below the significance level of 0.05. The intercept is therefore regarded as statistically significant. ^{232}Th has a p-value of 0.2103, which is higher than 0.05. For this reason, at the 0.05 significance level, ^{232}Th is not regarded as statistically significant. The model can only account for roughly 2% of the variability in ^{40}K, according to the Multiple R-squared value of 0.02004. Regarding the number of predictors, the

adjusted R-squared is 0.00748, which is accurate. The extremely low value indicates that the addition of ^{232}Th does not considerably improve the model. The overall significance of the model is tested using the F-statistic. Because it is higher than 0.05, the p-value in this instance is 0.2103 which indicates the statistical non-significance of the model. The value of the residual standard error is 182. This measures the residual variability around the regression line. The model has limited explanatory power based on the low R-squared values. Regarding the prediction of ^{40}K at the 0.05 significance level, the p-value for ^{232}Th shows that it is not statistically significant. To summarize, the information presented suggests that the simple linear regression model, which predicts ^{40}K from ^{232}Th, is not very significant or robust.

Figures 4.29 and 4.30 show the residual plots produced by the code between ^{228}Th and ^{232}Th in sea sediment.

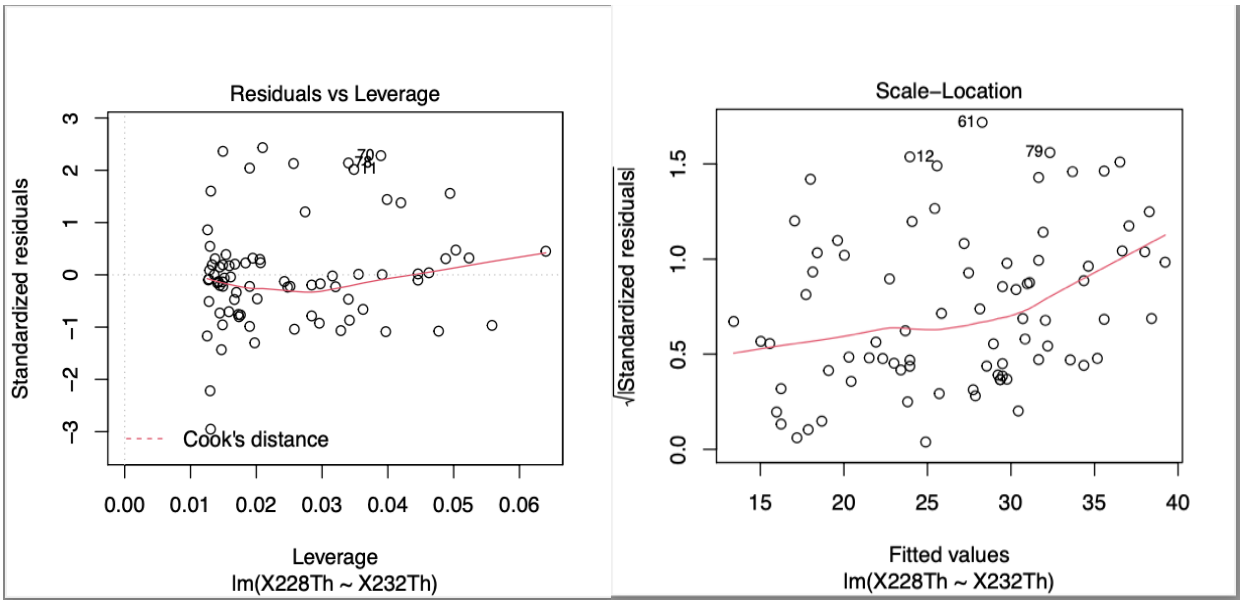

Figure 4.29: Residual plots produced by ^{228}Th and ^{232}Th in sea sediment.

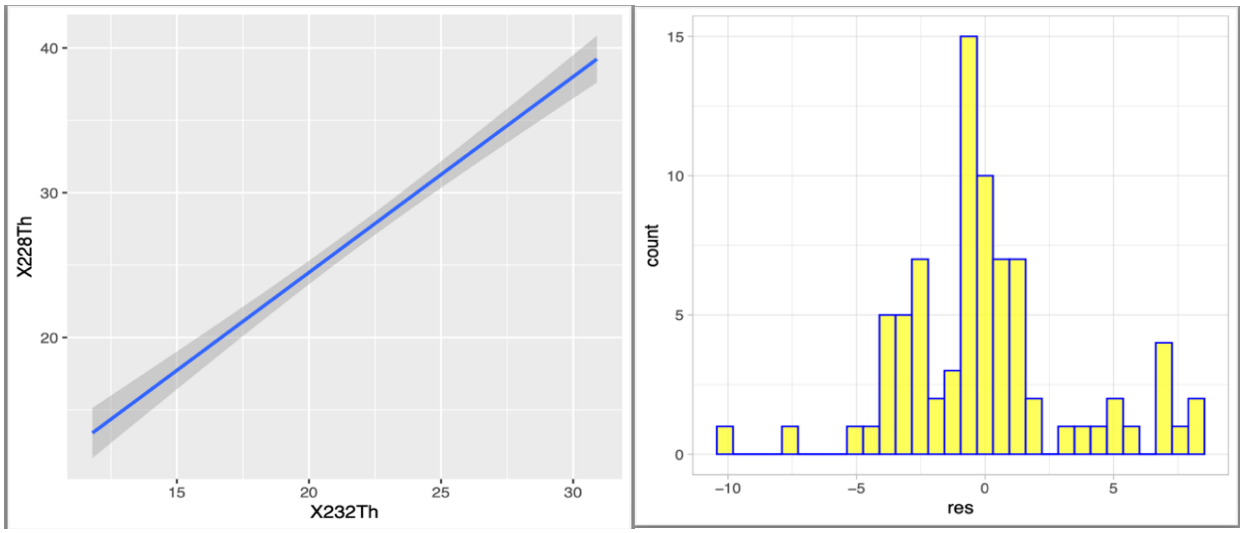

Figure 4.30: Histogram of residual plots of ^{228}Th and ^{232}Th in sea sediment.

In this linear regression model, which was derived ^{228Th} and ^{232}Th, ^{228}Th is the response variable while ^{232}Th is the predictor variable. The estimated intercept from the model is -2.55452 which is ^{228}Th's expected value if ^{232}Th is zero. ^{232}Th has a coefficient of 1.35219 as shown in the equation:

$$^{228}Th = 1.3522\,^{232}Th - 2.5545 \qquad (4.9)$$

An increase of one unit in ^{232}Th corresponds to an increase of roughly 1.35 units in ^{228}Th if all other factors do not change. The intercept's p-value is 0.147, and ^{232}Th's is extremely low (< 0.001), indicating a statistically significant correlation between the two variables. The measures of central tendency and spread are displayed in the summary statistics for the residuals (Appendix P). The residual plots from the code are shown in Figure 4.29. The model accounts for 79.29% of the variability in ^{228}Th with a Multiple R-squared value of 0.7929. The number of predictors is factored by the Adjusted R-squared value of 0.7903. The statistical significance of the model is indicated by the low p-value of less than 2.2e-16. The residuals' variability is measured by the residual

standard error which is 3.435 in this case. According to the model, ^{232}Th and ^{228}Th have a positive statistically significant relationship. Given the high R-squared value, it can be concluded that the model accounts for a significant amount (79.29 %) of the variability observed in ^{228}Th.

In a regression analysis to establish the distribution of the radionuclides in the coastal sediment, correlation studies were performed between radionuclides such as ^{226}Ra and ^{238}U, ^{226}Ra and ^{228}Ra, ^{226}Ra and ^{228Th}, and ^{228}Ra and ^{228}Th.

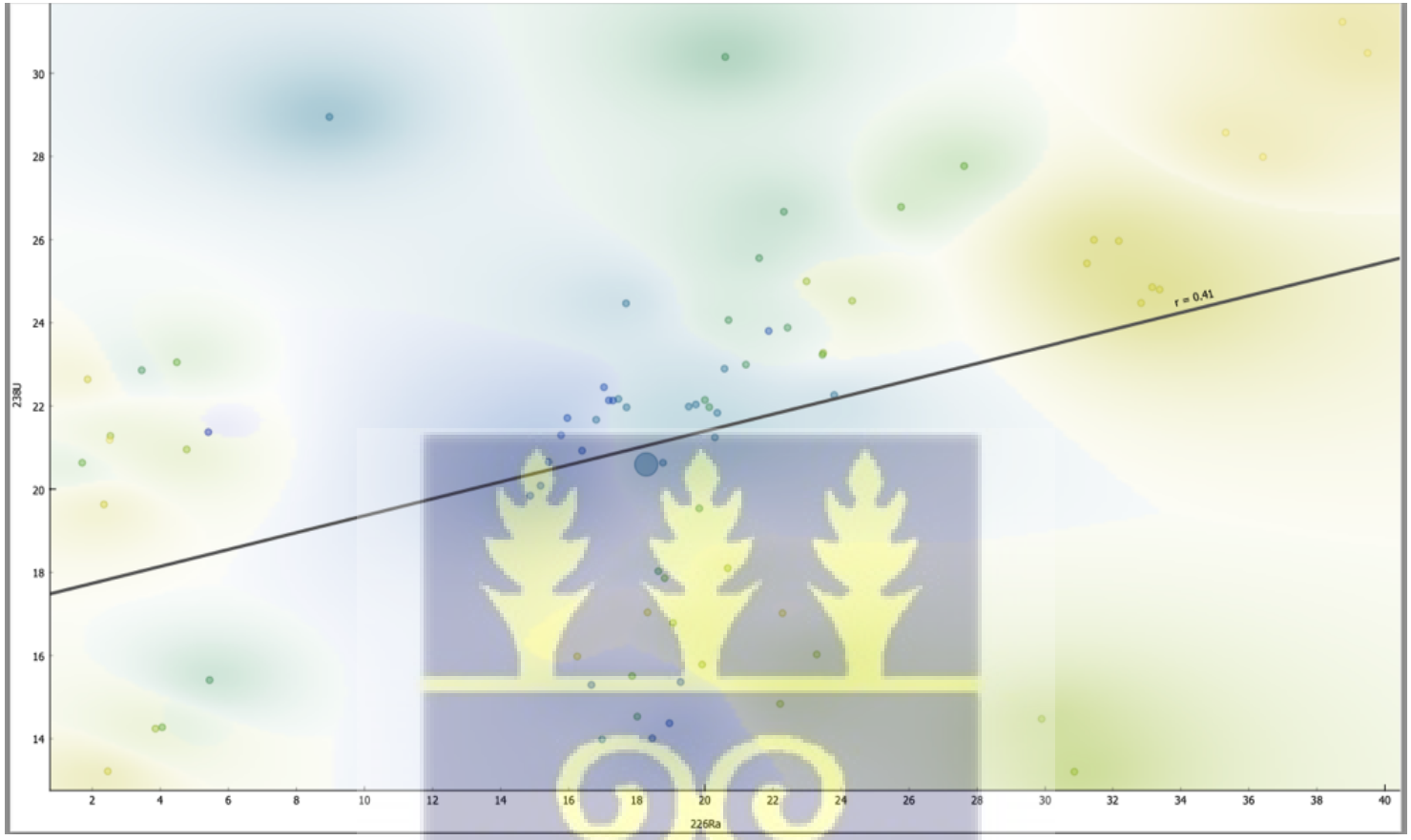

Figure 4.31: Correlation between ^{226}Ra and ^{238}U.

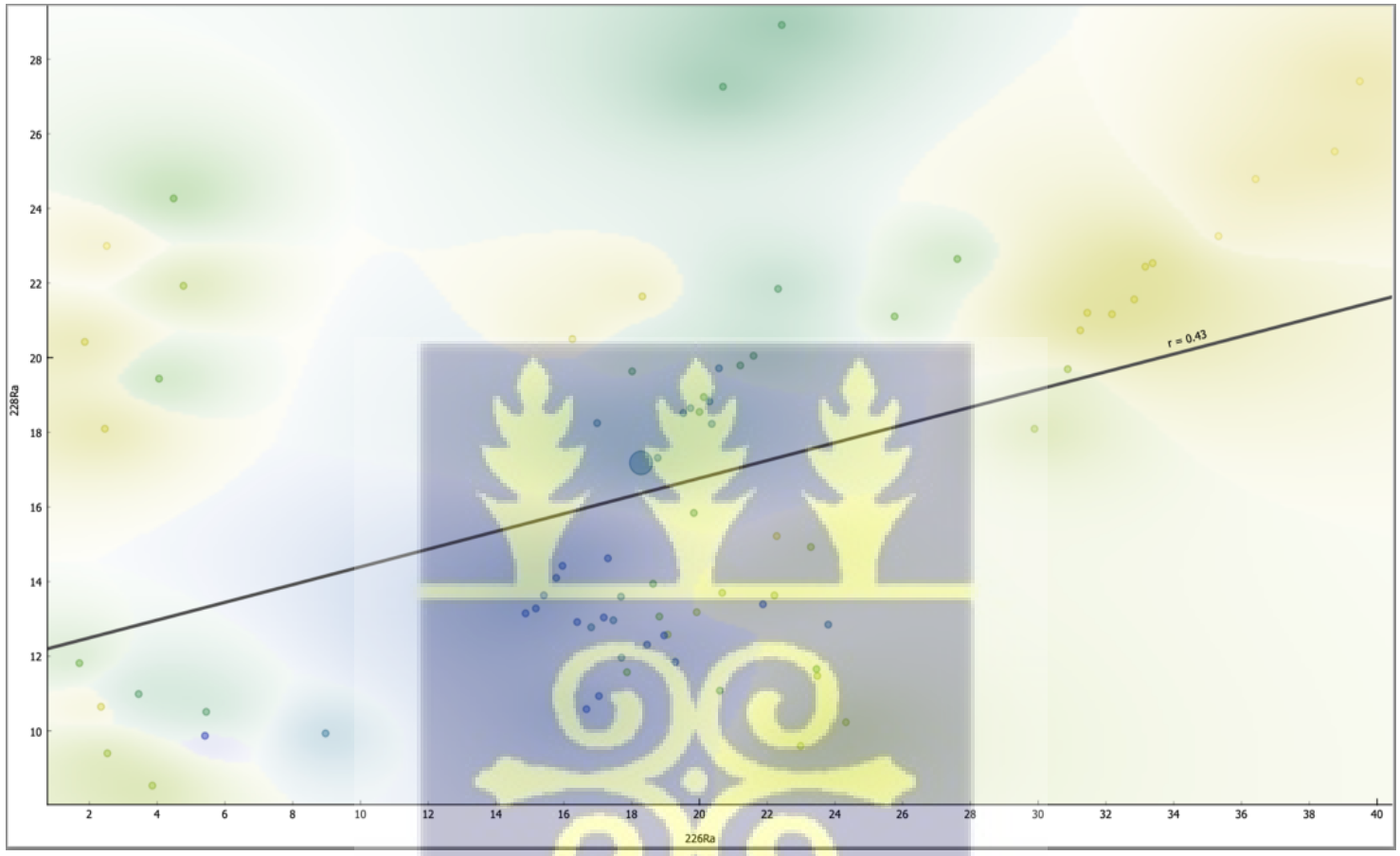

Figure 4.32: Correlation between ^{226}Ra and ^{228}Ra.

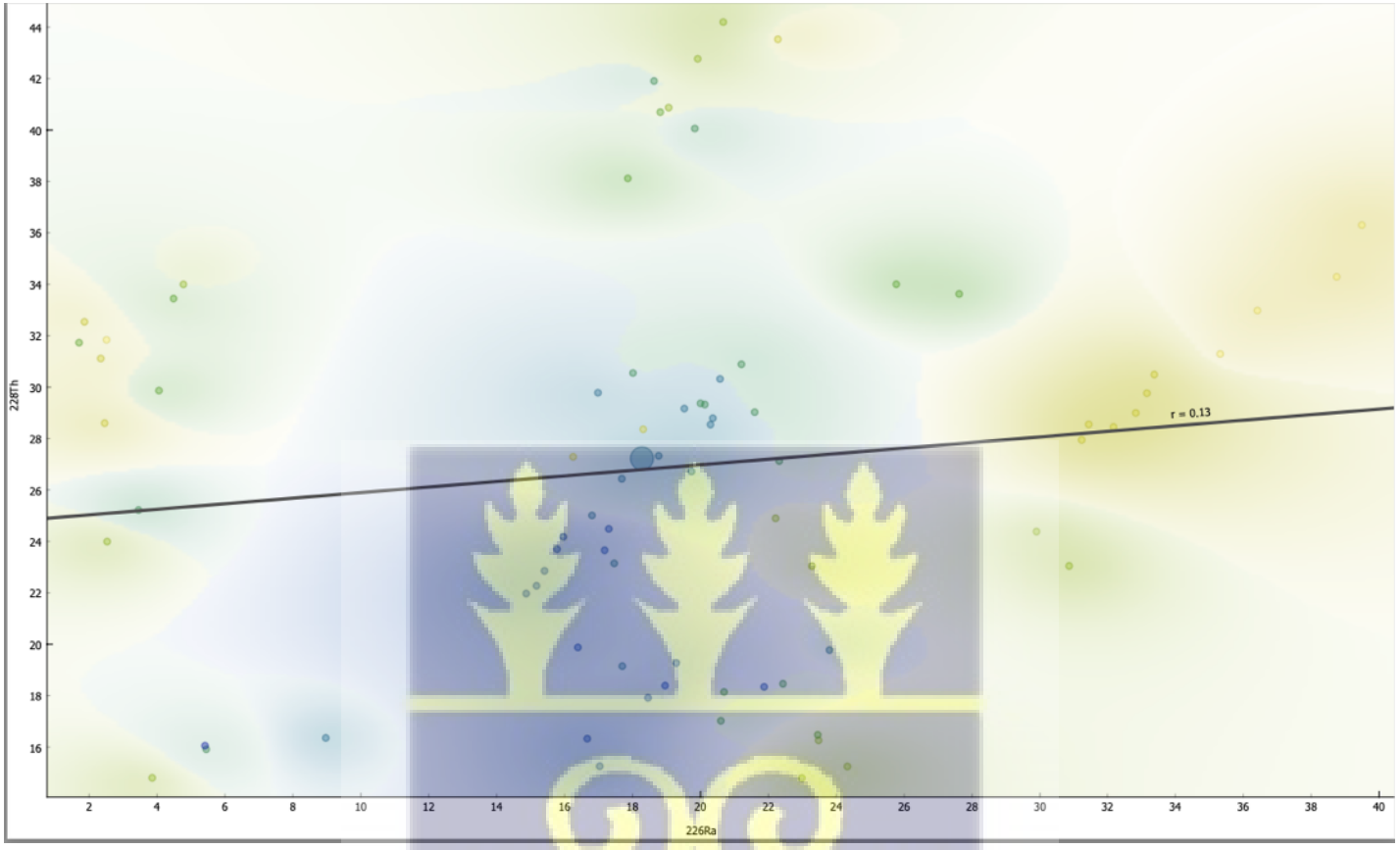

Figure 4.33: Correlation between ^{226}Ra and ^{228}Th.

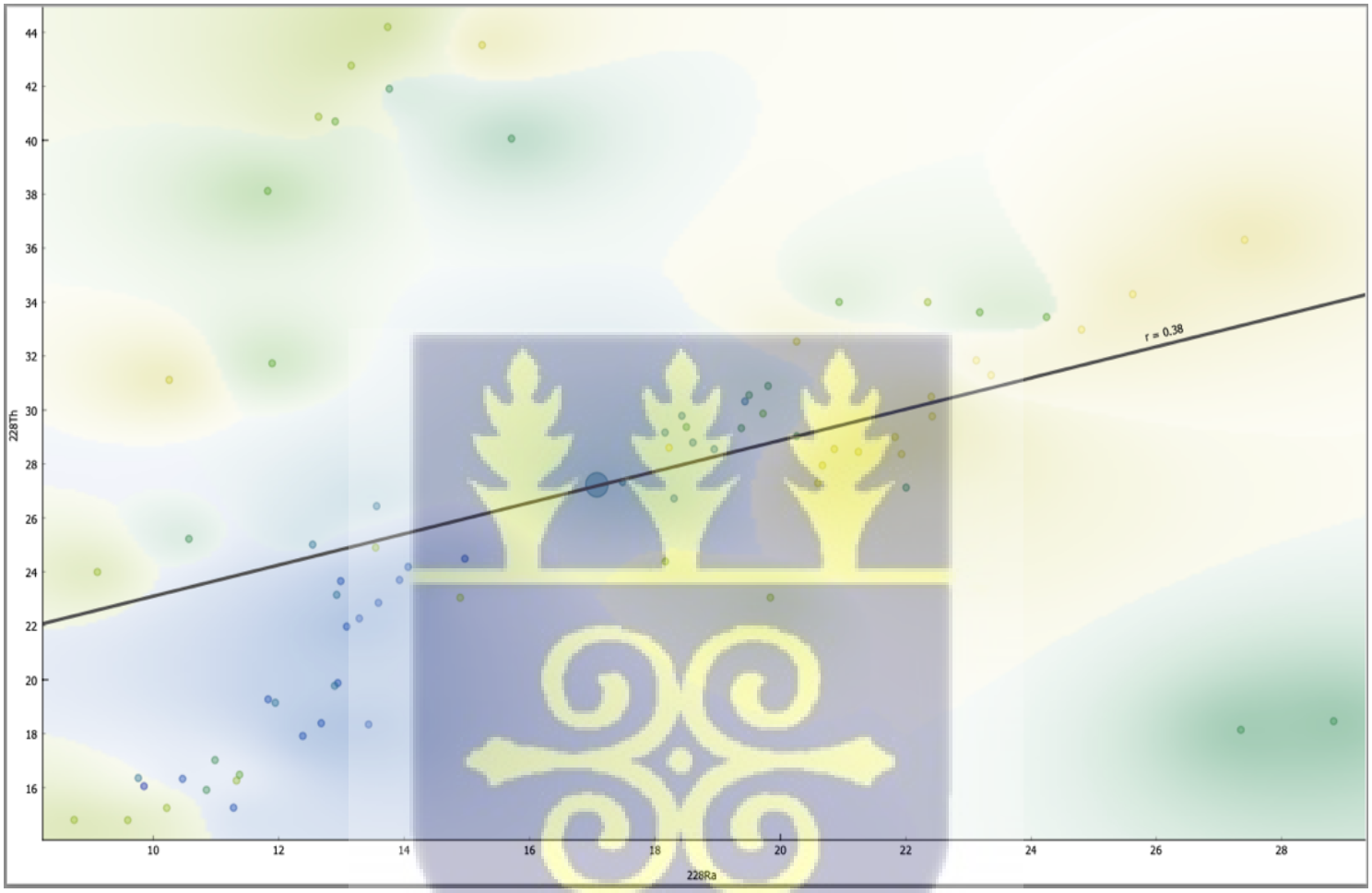

Figure 4.34: Correlation between ^{228}Ra and ^{228}Th.

Figures 4.30 - 4.34 show a linear regression of the activity concentrations of the radionuclides in sea sediment samples. The correlation between ^{226}Ra and ^{238}U and, ^{226}Ra and ^{228}Ra shows a moderately weak relationship with a correlation coefficient of 0.41 and 0.43, respectively. On the other hand, the correlation between ^{226}Ra and ^{228}Th, and ^{228}Ra and ^{228}Th gave a non-significant weak correlation with a correlation coefficient of 0.13 and 0.38, respectively.

CHAPTER FIVE

DISCUSSION

The results of the study area were analyzed, compared, and evaluated to provide data on the radiological risk posed to the environment and inhabitants of Ghana's western coast prior to the proposed construction of a nuclear power facility, taking into consideration the current oil and gas activities. This was done using gamma-ray spectrometry to determine the activity concentrations of natural radionuclides in beach sand, sea sediment, and seawater samples, and alpha spectrometry for activity determination in beach sand and sea sediment.

Concentration levels of ^{238}U, ^{232}Th, ^{226}Ra, ^{228}Ra, ^{228}Th and ^{40}K were determined from four different sampling locations namely, Sekondi-Takoradi, Axim, Beyin and Half-Asini. The total number of samples collected was eighty (80) beach sand samples, eighty (80) sea sediment samples and eighty (80) sea water samples. The calculated activity concentration results from the gamma-ray spectrometry analysis for beach sand samples provided average values of 21.97±3.6 $Bqkg^{-1}$ for ^{238}U; 22.41±4.5 $Bqkg^{-1}$ for ^{232}Th; 344.98±90.7 $Bqkg^{-1}$ for ^{40}K, 21.31±1.8 $Bqkg^{-1}$ for ^{226}Ra; 20.65±6.4 $Bqkg^{-1}$ for ^{228}Ra and 20.42±2.4 $Bqkg^{-1}$ for ^{228}Th (Figure 4.6). Sediment samples also provided average values of 21.24±3.8 $Bqkg^{-1}$ for ^{238}U; 21.77±3.7 $Bqkg^{-1}$ for ^{232}Th; 305.54±68.4 $Bqkg^{-1}$ for ^{40}K, 19.00±1.4 $Bqkg^{-1}$ for ^{226}Ra; 16.54±4.6 $Bqkg^{-1}$ for ^{228}Ra and 26.86±2.9 $Bqkg^{-1}$ for ^{228}Th (Fig. 4.9). The seawater samples provided values of 1.55±0.6 BqL^{-1} for ^{238}U; 2.05±0.5 BqL^{-1} for ^{232}Th; 11.83±1.6 BqL^{-1} for ^{40}K, 0.86±0.1 BqL^{-1} for ^{226}Ra and 2.65±0.4 BqL^{-1} for ^{228}Th (Figure 4.10).

The estimated activity concentration results from gamma-ray spectrometry analysis of seawater, beach sand, and sediment samples bring to light important knowledge about the

distribution of naturally occurring radionuclides (NORM) along the coastal areas of Western Ghana. ^{238}U in beach sand recorded an average activity concentration of 21.97±3.6 Bqkg^{-1}. ^{238}U and its decay products are common radionuclides present in the earth's crust. These products tend to add to the radiation dose in the environment. The average activity concentration recorded by ^{232}Th was 22.41±4.5 Bqkg^{-1}. ^{232}Th contributes significantly to terrestrial radiation because of its long half-life and decay chain. For ^{40}K, its average activity concentration was 344.98±90.7 Bqkg^{-1}, which is significantly higher comparatively to the activity concentrations of the other radionuclides. This is because potassium is naturally abundant in the earth's crust and as such very prevalent in sands (UNSCEAR, 2000). Although ^{40}K is a weak beta and strong gamma emitter, its enormous abundance in nature makes it a substantial contributor to background radiation levels. The observed activity concentrations for ^{226}Ra and ^{228}Ra were 21.31±1.8 Bqkg^{-1} and 20.65±6.4 Bqkg^{-1}, respectively.

Sediment samples provide similar activity concentrations comparatively to those of beach sands, which recorded values of 21.24±3.8 Bqkg^{-1} for ^{238}U and 21.77±3.7 Bqkg^{-1} for ^{232}Th. This implies that both sediments and sands are from similar geological sources. The lower concentrations can be attributed to the physical and chemical processes involved in the deposition of sediment and possible leachate of radionuclides from these materials (UNSCEAR 2000). The ^{40}K concentration in sediments is lower compared to that of beach sand with value recorded at 305.54±68.4 Bqkg^{-1}. This difference can be attributed to the diverse nature of the composition of minerals and the likelihood of potassium accumulating in sediment or leaching out into surrounding waters (Qureshi et al., 2014). The radium isotopes and thorium also show lower activity concentrations in sediment in contrast to beach sand. The values are 19.00±1.4 Bqkg^{-1} for ^{226}Ra, 16.54±4.6 Bqkg^{-1} for ^{228}Ra, and 26.86±2.9 Bqkg^{-1} for ^{228}Th. These lower results are

indicative of the natural variations in the distribution of radionuclides in sediment, which is inclined to accumulate heavier elements such as thorium (Ravisankar et al., 2015).

^{238}U recorded 1.55±0.6 BqL^{-1} activity concentration in sea water, whereas ^{232}Th recorded 2.05±0.5 BqL^{-1} activity concentration. When compared to sea sediment and beach sand, these levels are noticeably lower. This could be explained by dilution of radionuclides in water. The elevated activity concentration of thorium in contrast to uranium implies variations in solubility. Higher amounts of thorium can be found in sediment because it is less soluble and frequently persists in particulate form. ^{40}K recorded an activity concentration of 11.83±1.6 BqL^{-1}in seawater. This value is lower compared to sand and sediment, nonetheless, it is consistent with the soluble behavior of potassium in marine environments (UNSCEAR, 2000). Radium isotopes recorded activity concentrations of 0.86±0.1 $BqL^{-1}$for ^{226}Ra and 2.65±0.4 $BqL^{-1}$for ^{228}Th. These low levels in seawater are due to dilution, but the presence of ^{228}Th suggests a connection with thorium decay in the environment, which may be associated with the solid particulate matter suspended in sea water.

These results imply that the radionuclide concentrations in beach sand, sediment, and seawater are within typical ranges for natural background radiation. The high ^{40}K levels in beach sand and sediments are consistent with the widespread abundance of potassium in nature, while uranium and thorium series radionuclides are found at lower, but still significant, concentrations. The findings demonstrate the variations in radionuclide concentrations found in several environmental samples, including water, sediment, and sand. The processes of sedimentation in marine environments, mineral composition, and sediment transport systems may all have an impact on differences in radionuclide levels between sea sediments and beach sands. Because radionuclides

are less concentrated in dissolved forms, seawater concentrations are often substantially lower (UNSCEAR, 2000)

The mean absorbed dose rate (D) calculated for beach sand was 36.62 $nGyy^{-1}$, which was lower than the worldwide mean absorbed dose rate of 84 $nGyy^{-1}$. The mean estimated radium equivalent activity (Ra_{eq}) for beach sand was 77.12 $Bqkg^{-1}$ with the estimated mean annual effective dose (AED) from beach sand samples being 0.11 mSv y^{-1}. The average annual gonadal dose (AGD) evaluated from sand samples was 259.85 μSvy^{-1}, which is lower than the recommended mean worldwide value of 415.65 μSvy^{-1}. The external hazard index (H_{ext}) for beach sand was calculated to be 0.21, while the internal hazard index was 0.27. The activity utilization index and the gamma representative level index which ensure the suitability of materials containing NORM for various applications, such as building construction and assess the potential gamma radiation exposure risk from building materials or soils containing NORM, respectively was also determined with an average value of 0.47 and 0.11. The mean Ra_{eq} values for beach sand were all below the globally accepted value of 370 $Bqkg^{-1}$, therefore considered safe to be used as building materials. The average H_{ext} value for beach sand was found to be below the globally recommended value of one (Beretka & Mathew, 1985; NEA-OECD, 1979). The mean estimated cancer risk for beach sand was calculated to be 0.17×10^{-3}.

On the results of the estimated absorbed dose rate (D) for sea sediment, the average value was 35.41 $nGyy^{-1}$, which was also lower than the worldwide absorbed dose rate of 84 $nGyy^{-1}$. The average estimated radium equivalent activity (Ra_{eq}) for sea sediment was 75.29 $Bqkg^{-1}$. The average estimated annual effective dose (AED) was 0.11 mSv y^{-1}. The average estimated annual gonadal dose (AGD) was 250.55 μSvy^{-1}, which was lower than the recommended worldwide value

of 415.65 μSvy^{-1} (Penabei et al., 2018). The external hazard index (H_{ext}) for sediment was 0.20, while the internal hazard index was 0.26 whilst the activity utilization index and the representative level index were determined with average values of 0.48 and 0.12, respectively. All the hazard indices show that the samples from the western coast area have acceptable indices with no significant hazard (UNSCEAR, 2000). The risk of inhabitants getting cancer from exposure to sea sediment was 0.15×10^{-3}.

Coastal dwellers are at risk of getting cancer when radionuclides in sea water enter the human body through seafood consumption or incidental ingestion during recreational activities. Marine aerosols containing radionuclides can also be inhaled, though this is generally less significant compared to other pathways. Furthermore, beach sand and sea sediment used in construction, such as sand-crate, can lead to exposure if the materials contain significant levels of radionuclides. As well as soil with significant levels of radionuclides used for agriculture can enter the food chain. The obtained values, however, are within the globally accepted mean value of 0.29×10^{-3} as recommended by UNSCEAR (2000).

Comparing the results of the activity concentrations for the different locations selected for the study, it was observed that ^{40}K recorded the highest mean concentration value of 649.8 Bqkg^{-1} for beach sand, in the Sekondi-Takoradi. This was followed by the Half-Asini area, where also ^{40}K recorded the highest mean concentration value for beach sand and sediment. The values of ^{40}K predominates over the other radionuclides of interest because of its higher natural abundance in mainland rocks and normally with higher concentration levels in most minerals. There is a substantial disparity in the concentration levels between ^{40}K and the other radionuclides in the Sekondi-Takoradi area. The relatively high value of ^{40}K concentration observed in sand from

Sekondi-Takoradi can be ascribed to the geological properties of the rocks and beach sand, which are mostly shales and sandstone (Fares, 2017). Anthropogenic activities such as farming may also add to the levels of natural radioactivity (^{40}K) in the study area, especially when it comes to the use of artificial fertilizers for agricultural activities along the coast which can leach into the soil (Khan et al., 2018). Generally, the average activities of the radionuclides along the study area were all within the recommended international standards except ^{40}K which exceeded the average recommended value of 400 $Bqkg^{-1}$ (UNSCEAR, 2000). The high values of the activity concentrations calculated in the soil samples for the different natural radionuclides in Sekondi-Takoradi imply high values of the associated hazard indices expected and vice versa. However, the estimated values of all the indices were within the global recommended values. The other study areas of Axim, Beyin and Half-Asini recorded low average values of activity concentrations compared to Sekondi-Takoradi. Axim and Half-Asini, on the other hand, recorded activity concentrations of 32.5 $Bqkg^{-1}$ and 32.2 $Bqkg^{-1}$ for ^{232}Th and ^{228}Th, which exceeds the globally accepted average value of 30 $Bqkg^{-1}$ according to UNSCEAR (2000). The overall average values of all the parameters for the different study areas of the western coast of Ghana were within the accepted levels worldwide.

On the other hand, the average activity concentration of beach sand estimated using the alpha spectrometry analysis for ^{232}Th, ^{238}U, ^{234}U and ^{230}Th were 1.10 ±0.3 $Bq.kg^{-1}$, 2.02±0.6 $Bq.kg^{-1}$, 1.34±0.7 $Bq.kg^{-1}$, and 1.66±0.8 $Bq.kg^{-1}$, respectively. While the average activity concentration of sea sediment estimated for ^{232}Th, ^{238}U, ^{234}U and ^{230}Th were 2.69±0.4 $Bq.kg^{-1}$, 3.11±0.8 $Bq.kg^{-1}$, 1.53±0.6 $Bq.kg^{-1}$, and 2.23±0.8 $Bq.kg^{-1}$, respectively.

The activity concentrations recorded for beach sand and sea sediment that were analyzed using gamma spectrometry analysis were higher compared to the activity concentrations of the same

samples (i.e. beach sand and sea sediment) estimated from the alpha spectrometry analysis. This contrast may be attributed to differences in how both techniques detect radionuclides. This significant difference may arise due to the different methodologies, where, in gamma spectrometry analysis, the HPGe detector identifies a broader spectrum of radionuclides, including daughters of the decay series, while alpha spectrometry focuses on only alpha-emitting isotopes like ^{234}U, ^{230}Th, ^{238}U and ^{232}Th. Furthermore, environmental factors such as the composition and form of sea sediment and beach sand may influence the distribution and retention of natural radionuclides. Beach sand may contain more mineral grains such as monazite and zircon that trap radionuclides such as uranium and thorium (Ravisankar et al., 2015; Qureshi et al., 2014). This may increase the activity concentration readings of beach sand in gamma spectrometry analysis. However, sea sediments have fine particle size, therefore its ability to retain radionuclides is low. In addition, the mobile nature of some radionuclides such as ^{226}Ra and ^{228}Ra in aquatic environments may lead to lower concentrations in solid sediments.

Generally, statistical data from this research revealed important trends in the distribution of radionuclides in coastal sand and sediment (Table 4.19 and 4.20). The low standard deviation compared to the mean indicates a uniform distribution of radionuclide concentrations in the samples. This suggests a lack of extreme outliers. While the skewness and kurtosis provide insights into the shape and spread of these distributions, the homogeneity of radionuclides implies stable background radiation levels. However, the presence of skewed or leptokurtic distributions shows the potential for occasional higher concentrations that may need further investigation.

An empirical model based on correlations and linear regressions from the analysis of experimental data was developed. This is important in assessing the risk of exposure to naturally

occurring radioactive materials (NORM). Empirical models provide several significant benefits for risk assessment and management in environments contaminated with radioactive materials. The multiple linear regression model for beach sand (Figures 4.12 and 4.13) provides insights into the relationships between ^{228}Ra as the response variable, and ^{232}Th, ^{228}Th, and ^{40}K, as predictor variables to assess the risk of exposure to NORM. The statistical significance and practical implications of the coefficients play important roles in how this model impacts risk assessment. When the levels of ^{232}Th, ^{228}Th, and ^{40}K are all zero, the intercept of -4.302428 denotes the expected value of ^{228}Ra. It serves as the baseline estimate for ^{228}Ra when other radionuclides are absent. ^{232}Th coefficient of 1.527277 indicates that a one-unit increase in ^{232}Th is associated with an increase of approximately 1.53 units in ^{228}Ra, assuming the other variables are held constant. This strong positive relationship indicates that ^{232}Th plays an important role in predicting ^{228}Ra levels. Higher concentrations of ^{232}Th may lead to elevated levels of ^{228}Ra, which can increase the risk of potential radiation exposure. The strong correlation with ^{232}Th suggests that monitoring ^{232}Th can provide important information about overall radiation risk since ^{228}Ra is a significant contributor to radiation exposure. Areas with high ^{232}Th concentrations may need closer scrutiny due to the associated rise in ^{228}Ra levels. The coefficient (0.003505) for ^{40}K is much smaller, indicating that a one-unit increase in ^{40}K only results in a 0.0035-unit increase in ^{228}Ra. Nonetheless, the p-value of 0.62995 indicates that the relationship is not significant statistically. Even though ^{40}K is a naturally occurring radionuclide, its weak relationship with ^{228}Ra and statistical non-significance implies that ^{40}K does not play a key role in estimating ^{228}Ra levels. As a result, ^{40}K is unlikely to significantly contribute to the risk of radiation exposure associated with ^{228}Ra. The low p-value of 6.34e-05 for ^{232}Th shows that the relationship between ^{232}Th and ^{228}Ra is statistically significant. This means that the observed effect is unlikely to be because of random

chance which makes ^{232}Th a strong predictor in the model. The high p-value of 0.62995 for ^{40}K, however, shows that this variable does not significantly contribute to predicting ^{228}Ra concentrations. Due to this, the contribution of ^{40}K to the risk of radiation is minimal. The Multiple R-squared value of 0.9936 implies that the model explains 99.36% of the variability in ^{228}Ra. While this indicates that the model fits the data well, the high R-squared value also raises concerns about overfitting. The very low p-value of 0.0004895 from the F-test suggests that the model as a whole is statistically significant, meaning that the predictor variables together have a strong relationship with ^{228}Ra. The model's statistical significance validates its usefulness for understanding the relationships between the radionuclides, which is essential for assessing exposure risks.

From Figures 4.14 and 4.15, the coefficient of ^{232}Th suggests that there is a predicted increase of 1.07161 units in ^{228}Ra for every unit increase in ^{232}Th if other variables remain constant. This strong relationship implies that ^{232}Th is an important predictor of ^{228}Ra. ^{232}Th is related to ^{228}Ra and, therefore can contribute significantly to radiation exposure. An increase in ^{232}Th directly increases ^{228}Ra concentrations as both are naturally occurring radioactive materials. This increases the potential risk of radiation exposure in the environment. It is eminent in risk assessment because areas with higher concentrations of ^{232}Th will have increased levels of ^{228}Ra, which may pose a health risk to the local population due to prolonged exposure. The small p-value for ^{232}Th which is less than 2e-16 indicates that the relationship between ^{232}Th and ^{228}Ra is statistically significant. This high level of significance emphasizes that ^{232}Th is a critical variable in predicting ^{228}Ra levels. Therefore, ^{232}Th should be included in environmental monitoring programs, specifically in areas where exposure to NORM could pose health risks to humans and ecosystems. The model's statistical significance confirms that the relationships are valid, strengthening its use for predicting ^{228}Ra levels based on ^{232}Th concentrations.

The correlation studies between ^{228}Ra and ^{232}Th as shown in Figure 4.16, with a coefficient (r) of 0.81 imply a strong positive relationship between ^{228}Ra and ^{232}Th. This suggests that as ^{232}Th levels increase, ^{228}Ra levels tend to increase significantly as well. A strong correlation implies a close association between these two radionuclides in environmental samples. ^{228}Ra and ^{232}Th are both radioactive and contribute to radiation exposure, therefore the strong correlation indicates that monitoring ^{232}Th can effectively show the existence of ^{228}Ra. This is useful for environmental monitoring because instead of measuring multiple radionuclides separately, it may be sufficient to monitor ^{232}Th to estimate ^{228}Ra-related exposure risks. Both ^{228}Ra and ^{232}Th are part of radioactive decay chains and can contribute to internal and external radiation exposure. This can increase cancer risk and other health issues if concentrations are high. Areas with elevated ^{232}Th levels are likely to have elevated ^{228}Ra levels as well from the strong correlation. This increases the total radiation dose to which individuals are exposed. The strong relationship between these radionuclides also allows for more goal-oriented radiation protection strategies. For instance, if ^{232}Th is present in high concentrations in soil or sediment, one can infer higher levels of ^{228}Ra and take appropriate safety measures.

The correlation between ^{40}K and ^{232}Th as shown in Figure 4.17, with a coefficient of 0.41, shows a moderate positive relationship between ^{40}K and ^{232}Th. This indicates a tendency for ^{40}K levels to increase as ^{232}Th increases. However, the relationship is not as strong as that between ^{228}Ra and ^{232}Th. ^{40}K is influenced by several variables not related to ^{232}Th. The moderate association suggests a weaker relationship between ^{40}K and ^{232}Th than between ^{228}Ra and ^{232}Th. In comparison to ^{228}Ra, ^{40}K levels are a less accurate predictor of radiation exposure, even though they can give some indication of the presence of ^{232}Th. While ^{40}K does contribute to total radiation exposure, its lesser connection indicates that, to get a precise estimate of total radiation exposure,

it might need to be monitored separately from ^{232}Th. Risk assessments in settings where ^{40}K concentrations vary independently from other radionuclides, such as ^{232}Th, may find this to be significant.

^{232}Th and ^{228}Ra are alpha-emitting radionuclides. They can pose significant health risks if inhaled or ingested over time, leading to radiation exposure to internal organs like the lungs, liver, and bones. The strong correlation indicates that areas with high ^{232}Th likely also have high ^{228}Ra levels. Therefore, the risk of exposure to harmful alpha radiation is increased in such areas. ^{40}K, although a naturally occurring beta and gamma emitter, its moderate correlation with ^{232}Th means that the overall exposure risk from ^{40}K can vary independently of ^{232}Th levels. Therefore, radiation protection strategies need to account for the separate behavior of ^{40}K in the environment.

The values from the residual plots and regression model between ^{228}Th and ^{232}Th (Figures 4.18 and 4.19) also give information on the model's ability to predict ^{232}Th based on ^{228}Th. The standard error of residuals given as 4.327, indicates the typical size of the errors between the model's predictions and the actual observed values. This value suggests that the predictions of the model can deviate by an average of 4.327 units from the observed values. A higher residual standard error suggests less accurate predictions. For risk assessment, this means that the model may not precisely predict ^{232}Th concentrations based solely on ^{228}Th levels. The high value of the Multiple R-squared given as 0.9487, explains 94.87% of the variance in ^{232}Th based on ^{228}Th. This suggests that the relationship between the two radionuclides is strong. The p-value of 0.07999 is higher than the conventional significance level of 0.05, meaning the model is not statistically significant. This means that the relationship between ^{228}Th and ^{232}Th may not be strong enough to use this model for reliable predictions. Without statistical significance, we cannot confidently rely on the model to predict ^{232}Th concentrations based on ^{228}Th levels. It suggests that the relationship between

^{228}Th and ^{232}Th might not be a robust indicator of radiation risk. Additional variables or different models may be required to accurately assess the presence and concentration of ^{232}Th. While the model shows a strong relationship between ^{228}Th and ^{232}Th, (with a high multiple R-squared), the large residuals, non-significant p-value, and adjusted R-squared show that this relationship might not be reliable for precise predictions. This introduces uncertainty in the assessment of radiation risks, especially when predicting the presence and concentrations of ^{232}Th based on ^{228}Th. For risk assessment of NORM, this indicates that relying only on this model may not provide accurate estimates of radioactive exposure, and the variability in residuals could lead to inconsistent predictions.

The multiple linear regression between ^{40}K and ^{232}Th as shown in Figure 4.20 and 4.21 depicts a statistically significant relationship with a low p-value (0.000164) suggesting a reliable positive correlation between the two radionuclides. This implies that higher levels of ^{232}Th are generally associated with higher levels of ^{40}K in beach sand. Since both radionuclides contribute to natural radioactivity, the presence of one could help predict the levels of the other. ^{40}K and ^{232}Th are both contributors to natural background radiation, and their concentrations are critical in assessing the total radiation dose to individuals exposed to beach sand containing NORM. The model's statistically significant but weak relationship between these radionuclides suggests that there may be some co-occurrence, but the variability in ^{40}K levels requires further investigation. The fact that ^{232}Th explains only about 16.74% of the variability in ^{40}K suggests that other environmental or geochemical factors may play a role in ^{40}K distribution.

The linear regression analysis involving the radionuclides ^{228}Ra, ^{232}Th, ^{228}Th, ^{40}K, and ^{226}Ra in sea sediment also provides significant insights in the assessment of risk. Residual plots (Figures

4.23 and 4.24) and summary statistics of the residuals provide insight into how well the model fits the data and whether the errors are normally distributed. A good fit implies that the model is dependable in predicting ^{228}Ra concentrations. The negative intercept of -1.456544 means that without any contribution from these radionuclides, the model predicts a slightly negative value of ^{228}Ra. The coefficient for ^{232}Th given as 1.680992 shows that a unit increase in ^{232}Th is associated with an increase of about 1.68 units in ^{228}Ra, with other variables constant. This association is statistically significant, as indicated by the low p-value of less than 0.001. Since ^{232}Th and ^{228}Ra are both radioactive, the positive correlation suggests that there may be a relationship between higher ^{232}Th and higher ^{228}Ra levels in the sediment. This indicates that because of the combined presence of these radionuclides, places with high concentrations of ^{232}Th may present a greater radiation risk. When other variables are maintained constant, a negative coefficient for ^{228}Th (-0.753465) indicates that ^{228}Ra declines by roughly 0.75 units for every unit rise in ^{228}Th. The p-value indicates that this is statistically significant. This inverse relationship may indicate some form of dynamic balance between ^{228}Ra and ^{228}Th in sediment environments, possibly because of differences in geochemical behaviors or decay processes. The interaction between radionuclides in this way is important to understand for accurate dose calculations and long-term risk predictions. The coefficient for ^{40}K (0.004029) is very small but positive, indicating that a one-unit increase in ^{40}K results in a 0.004-unit increase in ^{228}Ra. Even though statistically significant with a p-value of 0.0134, the effect size is very small. The weak relationship suggests that ^{40}K is not a major contributor to ^{228}Ra levels in the sediment, however, it still plays a small role. ^{40}K is a naturally occurring radionuclide itself and contributes to radiation exposure. A small positive coefficient of. 0.022 suggests that an increase in ^{226}Ra is associated with a slight increase in ^{228}Ra, but the high p-value (0.5404) indicates that this relationship is not statistically significant. Since ^{226}Ra is not a

significant predictor of ^{228}Ra in this model, its role in the variability of ^{228}Ra is minimal. However, ^{226}Ra is a known contributor to radiation exposure, and while its relationship to ^{228}Ra might not be strong, it still poses a radiological risk on its own. With an R-squared of 75.78%, the model explains a large portion of the variability in ^{228}Ra, making it a useful tool for predicting radiation levels in sediments where NORM is present. The statistically significant relationship between ^{228}Ra and both ^{232}Th and ^{40}K with a p-value of less than 2.2e-16 highlights the importance of these radionuclides in determining ^{228}Ra levels, which can help in understanding the geochemical processes influencing radionuclide distribution.

The linear regression model between ^{228}Ra and ^{232}Th in sea sediment (Figures 4.25 and 4.26) reveals a strong, positive correlation coefficient of 0.69661 is critical because both radionuclides are contributors to radiation dose. Higher concentrations of ^{232}Th are strongly associated with elevated levels of ^{228}Ra, which suggests that areas with high ^{232}Th concentrations are likely to pose a greater radiological risk. This relationship allows for a more accurate estimation of ^{228}Ra levels based on ^{232}Th measurements, which is essential for evaluating radiation exposure in coastal environments where NORM is present. The F-statistic and p-value of 1.302e-12 shows that the model is statistically significant. The model's statistical significance indicates that ^{232}Th levels have an impact on ^{228}Ra concentrations. This means that measuring ^{232}Th levels can provide beneficial information for estimating ^{228}Ra-related risks of radiation exposure. However, the moderate R-squared values indicate the need to consider additional radionuclides or environmental variables. The model explains about 47.75% of the variation in ^{228}Ra, indicating ^{232}Th is an important but not the sole predictor of ^{228}Ra concentrations in sea sediment. This indicates that other radionuclides or environmental variables may also contribute to the variability of ^{228}Ra. The

statistically significant positive relationship between ^{232}Th and ^{228}Ra is important for NORM risk assessment, as both radionuclides are major contributors to radiation exposure.

The relationship between ^{40}K and ^{232}Th in sea sediment is examined using a basic linear regression model, which has low statistical significance and predictive power (Figures 4.27 and 4.28). Based on ^{232}Th concentrations, the model only explains 2% of the variability in ^{40}K, indicating that ^{232}Th is not a very good predictor of ^{40}K. This implies that to comprehend ^{40}K levels in sea sediment and the related radiation dangers, other variables or radionuclides must be taken into account. The statistical significance of the link between ^{232}Th and ^{40}K is not supported by the p-value of 0.2103 for ^{232}Th. This shows there is no strong correlation between these radionuclides. The residual standard error of 182 and the low R-squared (0.02004 and 0.00748) values show that the model is not a good fit for the data. The residual plots (Figures 4.27 and 4.28) represent the differences between observed and predicted values of ^{40}K. The wide range of residuals suggests that the model does not fit the data well. And as such it cannot be used to estimate ^{40}K concentrations or radiation exposure based on ^{232}Th levels.

The linear regression model between ^{232}Th and ^{228}Th as shown in Figure 4.29 and Figure 4.30 provides a strong, statistically significant relationship. This positive, significant relationship between ^{232}Th and ^{228}Th (as indicated by the coefficient of 1.35219) reflects the fact that they are both part of the same decay chain. ^{228}Th is a decay product of ^{232}Th from the thorium decay series. The correlation between these radionuclides is relevant for assessing NORM risk because both contribute to radiation exposure, especially through their gamma emissions. Areas with elevated levels of ^{232}Th are likely to also have elevated levels of ^{228}Th, which can increase the total radiation dose in the environment. The high R-squared value (79.29%) and the statistically significant relationship between ^{232}Th and ^{228}Th suggest that ^{232}Th can be used as a reliable indicator of ^{228}Th

levels. This is critical for assessing radiation risks because both radionuclides emit gamma radiation, which can lead to increased external radiation doses in areas with high NORM levels.

The correlations between the radionuclides as shown in Figures 4.31 and 4.32, and as represented by the r-values in the linear regression analysis, depict the relationships among different radioactive elements in sea sediment. The r-value of 0.41 (Figure 4.31) indicates a moderately weak positive correlation between ^{226}Ra and ^{238}U. This suggests that there is some relationship between the activity concentrations of these radionuclides, but it is not strong. The correlation may reflect the fact that ^{226}Ra is part of the uranium decay series and is produced from the decay of ^{238}U, but other factors such as environmental influences, and mobility of radionuclides may weaken this relationship in sea sediment. A moderate correlation between ^{226}Ra and ^{238}U suggests that areas with higher ^{238}U concentrations may also have elevated levels of ^{226}Ra, which is significant for NORM risk because ^{226}Ra is a major contributor to radiation exposure through its gamma and alpha emissions. However, the relatively weak correlation indicates that ^{226}Ra levels cannot be reliably predicted solely based on ^{238}U concentrations, highlighting the need for direct measurements of both radionuclides in NORM risk assessments. The r-value of 0.43 (Figure 4.32) also shows a moderately weak correlation between ^{226}Ra and ^{228}Ra. These radionuclides belong to different decay series. ^{226}Ra is from the uranium series, while ^{228}Ra is from the thorium series, therefore their activities are not directly linked. The moderate correlation may be due to the coexistence of both radionuclides in certain sedimentary environments where both decay chains are present. The moderately weak correlation between ^{226}Ra and ^{228}Ra indicates that the presence of ^{226}Ra does not strongly predict ^{228}Ra levels, but the co-occurrence of both in the environment can contribute to overall radiation exposure. Since both emit gamma radiation, the combined presence of these radionuclides could lead to higher radiation doses, which is relevant for assessing

NORM risks, particularly in regions where both uranium and thorium decay series radionuclides are present. The r-value of 0.13 (Figure 4.33) indicates a very weak and statistically non-significant correlation between ^{226}Ra and ^{228}Th. This is expected, as ^{226}Ra and ^{228}Th belong to different decay series (uranium and thorium, respectively), and their activity concentrations are not directly related. The weak correlation implies that ^{226}Ra and ^{228}Th levels are independent of each other, meaning that the presence of one radionuclide does not imply the presence of the other. In terms of NORM risk, this suggests that both radionuclides should be independently assessed when evaluating radiation exposure, as one cannot be used as a reliable indicator for the other. The r-value of 0.38 (Figure 4.34) reflects a weak correlation between ^{228}Ra and ^{228}Th as well, even though both radionuclides belong to the thorium decay series. This weak correlation might result from environmental processes affecting their mobility and distribution differently in sea sediment. The weak correlation between ^{228}Ra and ^{228}Th suggests that external factors, such as sediment composition, water flow, or chemical interactions (UNSCEAR, 2000), may influence their distribution differently. This has implications for NORM risk, as the levels of ^{228}Ra and ^{228}Th may vary independently, requiring separate assessments for each radionuclide to accurately evaluate radiation exposure risks.

CHAPTER SIX

CONCLUSIONS AND RECOMMENDATIONS

6.1 Summary of the Study Findings

The main aim of this research was to establish the activity concentration levels of ^{238}U, ^{232}Th, ^{40}K,^{226}Ra, ^{228}Ra, and ^{228}Th levels in seawater, beach sand, and sediment as well as assess the human health risk associated with these naturally occurring radionuclides to inhabitants along the coastal area of Western Ghana. The activity concentrations of the radionuclides were determined using alpha spectrometry and high-resolution gamma-ray spectrometry. The result of the study shows that the radiological risk assessed using R programming software is insignificant.

The provided data on the activity concentration of radionuclides (^{238}U, ^{232}Th, ^{226}Ra, ^{228}Ra, ^{228}Th, and ^{40}K) in beach sand, sea sediments, and seawater from four locations (Sekondi-Takoradi, Axim, Beyin, and Half-Asini). A total of 80 samples each of beach sand and sediment, and 80 seawater samples were analysed using gamma-ray spectrometry. Results obtained for beach sand using gamma spectrometry were of 21.97±3.6 $Bqkg^{-1}$ for ^{238}U; 22.41±4.5 $Bqkg^{-1}$ for ^{232}Th; 344.98±90.7 $Bqkg^{-1}$ for ^{40}K, 21.31±1.8 $Bqkg^{-1}$ for ^{226}Ra; 20.65±6.4 $Bqkg^{-1}$ for ^{228}Ra and 20.42±2.4 $Bqkg^{-1}$ for ^{228}Th. Sediment samples also provided average values of 21.24±3.8 $Bqkg^{-1}$ for ^{238}U; 21.77±3.7 $Bqkg^{-1}$ for ^{232}Th; 305.54±68.4 $Bqkg^{-1}$ for ^{40}K, 19.00±1.4 $Bqkg^{-1}$ for ^{226}Ra; 16.54±4.6 $Bqkg^{-1}$ for ^{228}Ra and 26.86±2.9 $Bqkg^{-1}$ for ^{228}Th. The seawater samples provided values of 1.55±0.6 BqL^{-1} for ^{238}U; 2.05±0.5 BqL^{-1} for ^{232}Th; 11.83±1.6 BqL^{-1} for ^{40}K, 0.86±0.1 BqL^{-1} for ^{226}Ra and 2.65±0.4 BqL^{-1} for ^{228Th} (Figure 4.10).

The highest activity concentrations were found in beach sand, especially for ^{40}K, which was much more than in sediments and seawater. While the concentrations of radionuclides, particularly

^{232}Th and its decay products, were lower in sediment than in beach sand, they were nonetheless detectable. The radioactive amounts in sea water were the lowest, reflecting the dilution that occurs naturally in aquatic habitats. However, radionuclides are transported by seawater into sediments and sands, where they eventually build up. This trend is in line with how NORM behaves in coastal environments, where radionuclide concentrations build up in environmental samples like sand and silt, influencing radiation exposure in the region.

The assessment of the radiation hazard indices helped to estimate the potential health risks posed by NORM. The radiation hazard indices for beach sands and sea sediments were within safe limits. For beach sand, the mean absorbed dose rate was 36.62 nGyy^{-1} (below the worldwide average of 84 nGyy^{-1}), with a mean annual effective dose of 0.11 mSvy^{-1} which is below the recommended dose of 1 mSvy^{-1} by ICRP, and a cancer risk of 0.17 × 10^{-3}. The absorbed dose rate recorded for sediments was 35.41 nGyy^{-1}, with similar hazard indices and cancer risk of 0.15 × 10^{-3}.

When the study analyzed the radionuclide activity concentrations in the four locations it discovered that ^{40}K had the highest levels, especially in Sekondi-Takoradi, where the average activity concentration in the beach sand was 649.8 Bqkg^{-1}. This was ascribed to the ^{40}K's inherent abundance in rocks and sands as well as potential inputs from fertilizers used in agriculture. Sekondi-Takoradi's ^{40}K levels were significantly higher than those of other radionuclides and more than the recommended 400 Bqkg^{-1} international limit. All hazard indices stayed under internationally recognized safety limits even with the high ^{40}K.

The other locations, such as Axim and Half-Asini, recorded lower radionuclide concentration levels, except for ^{232}Th and ^{228}Th, which exceeded the worldwide standard of 30 Bqkg^{-1}. However, the total activity concentrations for the western coast of Ghana were within acceptable limits.

Furthermore, results obtained from alpha spectrometry analysis for radionuclides such as ^{232}Th, ^{238}U, ^{234}U, and ^{230}Th in beach sand and sediments were lower compared to the results obtained from gamma spectrometry analysis. This may be attributed to the differences in detection methods of each analysis, environmental factors like grain particle size and the mobile behavior of certain radionuclides like ^{226}Ra and ^{228}Ra. Gamma spectrometry analysis is known to capture a broader range of radionuclides, and as such recorded higher values compared to alpha spectrometry analysis, which is geared towards the determination of solely alpha-emitting isotopes.

This research aimed at developing an empirical model to assess the risk of exposure to NORM by using multiple linear regression to understand the relationships between the natural radionuclides.

The model basically analyzes beach sand, with a focal point on the relationships between ^{228}Ra, as the response variable, and ^{232}Th, ^{228}Th and ^{40}K, as predictor variables. From the regression analysis, ^{232}Th is a significant predictor of ^{228}Ra, with a strong positive correlation. This indicates that as ^{232}Th increases, so does ^{228}Ra which increases the radiation risk. However, ^{40}K has a weaker and statistically non-significant relationship with ^{228}Ra. This suggests that it plays a minimal role in radiation exposure risk from ^{228}Ra. The model's multiple R-squared value of 99.36 % indicates a strong fit. The statistical significance of ^{232}Th as a predictor is validated, which underscores its importance in monitoring and assessing radiation exposure. The high correlation between ^{228}Ra and ^{232}Th with an R-value of 0.81 reinforces the notion that ^{232}Th can serve as a reliable indicator for ^{228}Ra, simplifying the monitoring process.

Additionally, the relationship between ^{228}Th and ^{232}Th is strong, with an R-squared of 94.87 %, the model, however, lacks statistical significance. This suggests that additional factors may be needed for accurate predictions of ^{232}Th levels based on ^{228}Th.

^{232}Th and ^{228}Ra also show a strong positive correlation in sea sediment. This emphasizes the importance of ^{232}Th as a predictor of radiation risk in sediment environments. Nonetheless, other radionuclides such as ^{40}K and ^{226}Ra, from the models created, exhibit weaker relationships. This highlights the need for separate assessments of these radionuclides in comprehensive radiation risks evaluations.

6.2 Conclusion and Recommendations

6.2.1 Conclusion

This study aimed to evaluate the activity concentrations of naturally occurring radionuclides (^{238}U, ^{232}Th, ^{40}K, ^{226}Ra, ^{228}Ra, and ^{228}Th) in seawater, beach sand, and sea sediment along the coastal region of Western Ghana and assess the associated human health risks. The results revealed that the radionuclide concentrations in the environmental samples were within acceptable levels, generally, with beach sand having higher radionuclide concentrations compared to sea sediment and seawater. The concentrations of ^{40}K in beach sand, particularly in Sekondi-Takoradi, exceeded the international recommended levels but not of significant health risks.

The radiation hazard indices such as absorbed dose rates, annual effective doses, radium equivalent activity, activity utilization index, and gamma representative index that were evaluated were well below globally recommended levels for radiation protection of the public, indicating a low radiological risk to the local population of the coast.

The Excess Lifetime Cancer Risk (ELCR) for the reference population was estimated, with values remaining within acceptable risk levels. For beach sand, the cancer risk was calculated at

0.17×10^{-3}, and for sediments, 0.15×10^{-3}. These values suggest that the risk of cancer due to exposure to these radionuclides is minimal for the coastal population.

The empirical model developed for assessing the relationship between radionuclides identified ^{232}Th as a significant predictor of ^{228}Ra levels, which reinforces its importance in radiation exposure risk monitoring. However, the reduced impact of ^{40}K and the presence of multicollinearity among radionuclides like ^{232}Th, ^{228}Th, and ^{40}K could complicate the authenticity of radiation assessments.

The findings of this research have provided baseline data to be used as reference for the current oil and gas production activities and future development in the coastal area of Ghana especially with the envisaged siting of a nuclear power plant. The study has provided comprehensive data on the activity concentration level of naturally occurring radionuclides in seawater, beach sand, and sediments along the coastal areas of Western Ghana. This is imperative for understanding the natural radiological environment of the study area with the potential of contamination from oil and gas activities and the construction of a nuclear power plant. By assessing the current radiation hazard indices and effective dose rates, the study establishes a reference point to measure any future radiological incidents that might arise from industrial activities. This gives way to comparisons between pre- and post-construction environmental radiation levels. Moreover, the evaluation of radiation risks to local populations, including the Excess Lifetime Cancer Risk (ELCR), is essential for understanding the potential health implications of major industrial activities in the study area. Knowledge of the background radiation levels helps in planning safety measures in the area, ensuring public health is not compromised with additional radiation exposure from industrial activities.

Public concerns about radiation risks are a major issue when siting nuclear facilities. This research can be used to reassure the local population that current radiological levels are safe and to design monitoring systems that will promptly detect any deviations from these levels once the plant is operational. Furthermore, high activity concentration of radionuclides in beach sand, sediments, and sea water can influence the suitability of the areas for recreational activities by the inhabitants of the area. Areas with lower natural background radiation levels are preferred to minimize cumulative radiological impacts. Additionally, knowledge of the local geology and radionuclide distribution helps in understanding how radioactive materials from a nuclear plant or the oil and gas industry might interact with the local environment. Since the study shows that radionuclides tend to accumulate more in sand and sediments than in water, this information is vital for assessing long-term risks. It can guide the selection of a site for a nuclear power plant with lower radionuclide accumulation rates, reducing the environmental burden over time.

The empirical model developed in the study, which uses ^{232}Th as a key predictor of ^{228}Ra levels, can be adapted for use in assessing potential radiological risks during the plant's construction and operation phases as well as for the ongoing operational activities of the oil and gas industries. This predictive capability is important for proactive management of radiation exposure risks to workers and the local populace.

Since the study focuses on naturally occurring radioactive materials (NORM), insights into how these materials accumulate in sediments and beach sands will be useful in designing strategies for managing NORM waste and other waste arising from a nuclear power project as well as the oil and gas industry. Proper understanding of how radionuclides behave in the environment can help design effective waste storage and disposal solutions to prevent contamination.

To avoid increased risks, the increased levels of ^{232}Th and ^{228}Ra in certain areas highlight the need for careful planning to prevent unintended interactions between nuclear waste and naturally high-radiation zones. The nuclear power plant and the oil and gas industries can operate within safe limits, by understanding and mitigating the environmental impacts of radiation. This can contribute to a sustainable energy production in future with minimal environmental degradation.

The research confirms that while radionuclide levels vary across different media (seawater, beach sand, and sediments), the radiation hazard indices remain within safe limits for the inhabitants along Western Ghana's coastal areas. Also, it provides critical data and insights that are essential for informed decision-making when operating a nuclear power plant or an oil and gas industry. It ensures a thorough understanding of the existing radiological environment, that health and safety risks are minimized, and that regulatory requirements are met, promoting the safe and sustainable operation of nuclear facilities along the coast.

6.2.2 Recommendations

6.2.2.1 Regulatory Authorities

Monitoring of radionuclide concentrations in sea water, beach sand, and sediments regularly by the Nuclear Regulatory Authority (NRA) and the Environmental Protection Agency (EPA) is essential to ensure the protection of the public and the environment. This will also help ensure that with the emergence of a nuclear power plant and the ongoing activities of the oil and gas industries, their operations will be within acceptable levels, and any unexpected radiological changes are promptly addressed.

Given the model's indication of ^{232}Th as a major predictor of ^{228}Ra, monitoring ^{232}Th levels should be emphasized. The empirical model developed in the study to assess potential radiation exposure risks can help forecast radiological impacts and guide mitigation strategies for oil and gas activities, as well as during the construction and operation of the nuclear power plant.

Findings from this study can be integrated into policy using outcomes from the predictive modelling to inform coastal zone management policies, marine pollution control, and nuclear site planning.

6.2.2.2 Oil and Gas Industries

The oil and gas industries can use this predictive model to estimate and forecast potential radiological impacts based on the parameters used in this study for beach sand, sediments and sea water. They can also use the assessment indices such as radium equivalent activity, gamma representative index, and hazard indices to quantify environmental safety margins with reference to the international acceptable levels of NORM.

6.2.2.3 Research Institutions and Academic Bodies

Periodic reassessment of hazard indices such as the radiation hazard indices, radium equivalent activity, and other safety parameters. This will help to reflect the most current data on environmental radioactivity to ensure that any emerging risks are identified early and addressed in a timely manner.

Further research and refining of the predictive model would enhance the reliability of future risk assessments. Machine learning methods such as random forest, support vector machines can be integrated in future research for more robust predictions.

REFERENCES

Abbasi, A., Algethami, M., Bawazeer, O., Zakaly, H.M.H. (2022). Distribution of natural and anthropogenic radionuclides and associated radiation indices in the Southwestern coastline of Caspian Sea. Mar. Pollut. Bull. 2022, 178, 113593.

Abbasi, A., Zakaly, H.M.H., Mirekhtiary, F. (2020). Baseline levels of natural radionuclides concentration in sediments East coastline of North Cyprus. Mar. Pollut. Bull. 2020, 161, 111793.

Adebiyi, F. M., Ore, O. T., Adeola, A. O., Durodola, S. S., Akeremale, O. F., Olubodun, K. O., & Akeremale, O. K. (2021). Occurrence and remediation of naturally occurring radioactive materials in Nigeria: a review. Environmental Chemistry Letters, 19(4), 3243–3262. https://doi.org/10.1007/s10311-021-01237-4

Adukpo, O. K., Faanu, A., Lawluvi, H., Tettey-Larbi, L., Emi-Reynolds, G., Darko, E. O., Kansaana, C., Kpeglo, D. O., Awudu, A. R., Glover, E. T., Amoah, P. A., Efa, A. O., Agyemang, L. A., Agyeman, B. K., Kpordzro, R., & Doe, A. I. (2015). Distribution and assessment of radionuclides in sediments, soil and water from the lower basin of river Pra in the Central and Western Regions of Ghana. Journal of Radioanalytical and Nuclear Chemistry, 303(3), 1679–1685. https://doi.org/10.1007/s10967-014-3637-5

Agyekum, E.B., 2020. Energy poverty in energy rich Ghana: a SWOT analytical approach for the development of Ghana's renewable energy. Sustainable Energy Technol. Assess. 40, 100760. https://doi.org/10.1016/j.seta.2020.100760.

Agyekum, E.B., Velkin, V.I., 2020. Optimization and techno-economic assessment of concentrated solar power (CSP) in South-Western Africa: a case study on Ghana. Sustainable Energy Technol. Assess. 40, 100763. https://doi.org/10.1016/j.seta.2020.100763.

Ahmad, F., Morris, K., Law, G. T. W., Taylor, K. G., & Shaw, S. (2021). Fate of radium on the discharge of oil and gas produced water to the marine environment. Chemosphere, 273, 129550. https://doi.org/10.1016/j.chemosphere.2021.129550

Ahmed, A., Tariq, S., Ud, K., Manzoor, S., Calligaris, C., & Waheed, A. (2014). ScienceDirect Evaluation of excessive lifetime cancer risk due to natural radioactivity in the rivers sediments of Northern Pakistan. Journal of Radiation Research and Applied Sciences, 7(4), 438–447. https://doi.org/10.1016/j.jrras.2014.07.008.

Alam, M.N., Chowdhury, M.I., Kamal, M., Ghose, S., Islam, M.N., Mustafa, M.N., Miah, M.M.H., Ansary, M.M. (1999). The ^{226}Ra, ^{232}Th and ^{40}K activities in beach sand minerals and beach soils of Cox's Bazar, Bangladesh. J. Environ. Radioact. 46, 243–250.

Alshahri, F. (2017). Radioactivity of ^{226}Ra, ^{232}Th, ^{40}K and ^{137}Cs in beach sand and sediment near to desalination plant in eastern Saudi Arabia: Assessment of radiological impacts. J. King Saud Univ. Sci. 29(2), 174–181.

Ajayi, T. R., Torto, N., Tchokossa, P., & Akinlua, A. (2009). Natural radioactivity and trace metals in crude oils: Implication for health. Environmental Geochemistry and Health, 31(1), 61–69. https://doi.org/10.1007/s10653-008-9155-z

Aközcan, S., Külahcı, F. and Mercan, Y. (2018). A suggestion to radiological hazards characterization of ^{226}Ra, ^{232}Th, ^{40}K and ^{137}Cs: spatial distribution modelling, Journal of Hazardous Materials, Volume 353, Pages 476-489, ISSN 0304-3894, https://doi.org/10.1016/j.jhazmat.2018.04.042. (https://www.sciencedirect.com/science/article/pii/S0304389418302747)

Al-Mur, B. A., & Gad, A. (2022). Radiation Hazard from Natural Radioactivity in the Marine Sediment of Jeddah Coast, Red Sea, Saudi Arabia. Journal of Marine Science and Engineering, 10(8), 1145. https://doi.org/10.3390/jmse10081145.

Al Nabhani, K. (2021). Applications of Nuclear and Radioisotope Technology: For peace and sustainable development. History of the atom and the emergence of nuclear energy. Pg 1-52. Academic Press.

Alnabhani, K., Khan, F., & Yang, M. (2015). Technologically Enhanced Naturally Occurring Radioactive Materials in Oil and Gas Production: A Silent Killer, Process Safety and Environmental Protection. https://doi.org/10.1016/j.psep.2015.09.014

Amin, Y.M., Mahat, R.H., Nor, R.M., Khandaker, M.U., Takleef, G.H., Bradley, D.A., (2013). The presence of natural radioactivity and Cs-137 in the South China Sea bordering Peninsular Malaysia. Radiat. Prot. Dos. 156, 475–480.

Amoasah, G. (2010). The Potential Impacts of Oil and Gas Exploration and Production on the Coastal Zone of Ghana. An Ecosystem Services Approach. February, 1–76.

Amwaalanga, M.N.N., Onjefu, S.A., Zivuku, M., Hamunyela, R.H. (2019). Assessment of natural radioactivity levels and radiation hazards in shore sediments from the Zambezi River, Namibia. Int. Sci. Technol. J. Namibia. 13(4), 59–67.

Australian Petroleum Production & Exploration Association (APPEA) Limited (2002). Guidelines for Naturally Occurring Radioactive Materials, APPEA, Australia.

ASTM (1983) Standard Method for sampling surface soils for radionuclides, American Society for Testing Materials, Report No. C (PA: ASTM), 983–998

ASTM (1986) Recommended practice for investigation and sampling soil and rock for engineering purposes, In: Annal book of ASTM standards; (04/08), American Society for Testing Materials, Report No. D, 420 (PA: ASTM, 109–113

Avwiri, G. O., & Ononugbo, C. O. (2011). Assessment of naturally occurring radioactive material (norm) content of hydrocarbon exploration and production activities in ogba / egbema / ndoni oil / gas Assessment of naturally occurring radioactive material (NORM) content of hydrocarbon explorat. Indian Journal of Innovations Development, 1(1), 9–14.

Awad, M., El Mezayen, A.M., El Azab, A., Alfi, S.M., Ali, H.H., Hanfi, M.Y. (2022). Radioactive risk assessment of beach sand along the coastline of Mediterranean Sea at El-Arish area, North Sinai, Egypt. Mar. Pollut. Bull. 177, 113494.

Barzehkar, M., Dinan, N.M., Salemi, A., (2016). Environmental capability evaluation for nuclear power plant site selection: a case study of Sahar Khiz Region in Gilan Province, Iran. Environ. Earth Sci. 75, 1016. https://doi.org/10.1007/s12665-016-5825-9.

Baskurt, Z. M., & Aydin, C. C. (2018). Nuclear power plant site selection by Weighted Linear Combination in GIS environment, Edirne, Turkey. Progress in Nuclear Energy, 104, 85–101. https://doi.org/10.1016/j.pnucene.2017.09.004

Beretka, J. and Mathew, P. J. (1985).Natural Radioactivity of Australian Building Materials, industrial waste and by-products, Health Phys Vol. 48(1985): 87-95.

Bland, M. (2006). Mean and standard deviation. Applied Biostatistics. Health Sciences MSc. Programme.

Botwe, B. O., Schirone, A., Delbono, I., Barsanti, M., Delfanti, R., Kelderman, P., Nyarko, E., & Lens, P. N. L. (2017). Radioactivity concentrations and their radiological significance in sediments of the Tema Harbour (Greater Accra, Ghana). Journal of Radiation Research and Applied Sciences, 10(1), 63–71. https://doi.org/10.1016/j.jrras.2016.12.002

Bourguignon, D., & Scholz, N. (2016). Chernobyl 30 years on: Soviet apocalypse. Economist (United Kingdom), 412(8983).

Boye, C. B. (2015). Causes and Trends in Shoreline Change in the Western Region of Ghana Department of Marine and Fisheries Sciences, University of Ghana. Mrs Cynthia Borkai Boye. 10359290.

Boye, C. B., & Fiadonu, E. B. (2020). Lithological effects on rocky coastline stability. Heliyon, 6(3), e03539. https://doi.org/10.1016/j.heliyon.2020.e03539

Cao, Y., Lin, J., Zhai, K., Jiang, W., Zou, H., Ren, H., Wang, P., Gao, X., Zhang, M., Yu, S., Zhao, Y., Xuan, Z., Zhang, D., Liu, Y., & Lou, X. (2022). Long-term investigation of environmental radioactivity levels and public health around the Qinshan Nuclear Power Plant, China. Scientific Reports, 12(1), 1–12. https://doi.org/10.1038/s41598-022-09091-2

Cember, H. and Johnson, T.E. (2009). Introduction to Health Physics (4th edition), New York: McGraw-Hill Companies, Inc.

Chambers, D. B. (2015). Radiological protection in North American naturally occurring radioactive material industries. Annals of the ICRP, 44, 202–213. https://doi.org/10.1177/0146645315572300

Chu, S. Y. F., Ekstro¨m, L. P., Firestone, R. B. (1999). The Lund/LBNL Nuclear Data Search. http://nucleardata.nuclear.lu.se/nucleardata/toi/.

Chowdhury, S., Husain, T., Veitch, B., Bose, N. & Sadiq, R. (2004) Human Health Risk Assessment of Naturally Occurring Radioactive Materials in Produced Water—A Case Study, Human and Ecological Risk Assessment: An International Journal, 10:6, 1155-1171, DOI: 10.1080/10807030490887203. http://dx.doi.org/10.1080/10807030490887203

Chowdhury, M.I., Alam, M.N. and Hazari, S.K.S. (1999). "Distribution of Radionuclides in the River Sediments and Coastal Soils of Chittagong, Bangladesh and Evalution of the Radiation Hazard", Applied Radiation and Isotope 51: 747-75

CNSC (2019). Introduction to Radiation. Types and Sources of Radiation (November 2019), 1–3.

Darko, E. O and Faanu, A. (2007). Baseline radioactivity measurements in the vicinity of a Gold Treatment Plant, Journal of Applied Science and Technology, Vol. 10, NO 1&2, Ghana.

Diab, H. M., Ramadan, A. B., Monged, M. H. E., Shahin, M. (2019). Environmental assessment of radionuclides levels and some heavy metals pollution along Gulf of Suez, Egypt. Environmental Science and Pollution Research 26(March 2019):1-13. DOI:10.1007/s11356-019-04610-7.

Dołhańczuk-Śródka, A. (2012). Estimation of external gamma radiation dose in the area of Bory Stobrawskie forests (PL). Environmental Monitoring and Assessment, 184(9), 5773–5779. https://doi.org/10.1007/s10661-011-2380-4.

Donya, M., Radford, M., ElGuindy, A., Firmind, D., Yacoub, M. H. (2014). Radiation in medicine: Origins, risks and aspirations, Global Cardiology Science and Practice 2014:57. http://dx.doi.org/105339/gcsp.2014.57.

Doyi, I.Essumang, D. K., Dampare, S. B., Duah, D. & Glover E. T. (2015). Technologically Enhanced Naturally Occurring Radioactive materials (TENORM) in the Oil andGas Industry: A Review. Reviews of Environmental Contamination and Toxicology. DOI:10.1007/398_2015_5005.

El-Gamal, A., Nasr, S., El-Taher, A. (2007). Study of the spatial distribution of natural radioactivity in the upper Egypt Nile River sediments. Radiat. Meas. 42, 457–465.

Emam, E. A., Moawad, T. M., & Aboul-Gheit, N. A. K. (2014). Evaluating the characteristics of offshore oilfield produced water. Petroleum and Coal, 56(4), 363–372.

Ennison, I., Akiti, T., Amponsah, P., Osae, S. &Gbadago J. K. (2013). Determination of Suitable Sites for Nuclear Power Plants in Ghana:-The Issues Involved. Environmental Research Engineering and Management 62(4). DOI:10.5755/j01.erem.62.4.2655.

Faanu, A., Darko, E. O., & Ephraim, J. H. (2012). Determination of natural radioactivity and hazard in soil and rock samples in a mining area in Ghana. West African Journal of Applied Ecology, 19(1), 77–92.

Fares, S. (2017). Measurements of natural radioactivity level in black sand and sediment samples of the Temsah Lake beach in Suez Canal region in Egypt. Journal of Radiation Research and Applied Sciences, 10(3), 194–203. https://doi.org/10.1016/j.jrras.2017.04.00.

Fentiman, I. S.,Deshmane, V., Tong, D., Winter, P. J., Mayles, H., & Chaudary, M. A. (2004). Caesium (137) implant as sole radiation therapy for operable breast cancer. British Journal of Surgery, 911, 116-116.

Ferson, S. (1996). What Monte Carlo methods cannot do. Human and Ecological Risk Assessment 2, 990-1007.

GSS (2021). Population and Housing census, Western region of Ghana.

GSS (2012). Population and Housing Census, District Analytical Report, Sekondi-Takoradi Metropolitan.

Glubrecht, H. (1977). Future trends in the application of isotopes and radiation. IAEA Bulletin, 19(6), 38–47. http://www.iaea.org/Publications/Magazines/Bulletin/Bull196/19605093847.pdf

Gonzales, & A.J., Anderer, J. (1989). Radiation Versus Radiation.. Nuclear Energy in Perspective, IAEA Bulletin, Quarte. Journal of the International Atomic Energy Agency, 31(2), 21–31.

Guyonnet, D., Come, B., Perrochet, P., Parriaux, A. (1999). Comparing two methods for addressing uncertainty in risk assessments. Journal of Environmental Engineering 125(7), 660-667.

Harb, S. (2008). Natural Radioactivity and external gamma radiation exposure at the coastal Red Sea in Egypt. Radiat. Prot. Dosimetry. 130, 376–384.

Hamlat, S., Thompson, P., Rinker, M., St-Amant, N., Pan, P., Peters, K., Dagher, E., Jovanovic, S., & Sauvé (2018). Independent environmental monitoring and public dose assessment around the Canadian Nuclear Power Plants. *J Radioanal Nucl Chem***317**, 325–335. https://doi.org/10.1007/s10967-018-5903-4

Hammonds, J. S., Hoffman, F. O., & Bartell, S. M. (1994). An Introductory Guide to Uncertainty Analysis in Environmental and Health Risk Assessment. Energy, 47(3). https://doi.org/10.2172/10127301.

Hartwell, J. K. (1975). Detection limits for radioanalytical counting techniques. Atlantic Richfield Handford Company. Richland, Washington, 99352. ARH-SA-215.

Hasselberg, A. E., Wessels, L., Aakre, I., Reich, F., Atter, A., Steiner-Asiedu, M., Amponsah, S., Pucher, J., & Kjellevold, M. (2020). Composition of nutrients, heavy metals, polycyclic aromatic hydrocarbons and microbiological quality in processed small indigenous fish

species from Ghana: Implications for food security. PLoS ONE, 15(11 November), 1–25. https://doi.org/10.1371/journal.pone.0242086.

IAEA (2011). Disposal of Radioactive Waste. Specific Safety Requirements. IAEA Safety Standardf Series No. SSR-5.

IAEA (2012). SAFETY STANDARDS Nuclear Power Plants SSR-2/1. English.

IAEA (1989). Measurement of Radionuclides in Food and Environment: A Guidebook, IAEA-Technical Reports Series No. 295, Austria.

International Agency for Research on Cancer (1988). Man Made Mineral Fibers and Radon, IARC Monographs Vol. 43, IARC, Lyon.

ICRP (2021). Optimisation *in Digital Radiology Part 1*, ICRP Task Group 108, ICRP Publication.

ICRP (1993). Protection against Radon-222 at home and at work, Publication 65, Pergamon Press, Oxford.

ICRP (2007). The 2007 Recommendations of the International Commission on Radiological Protection. ICRP Publication 103. Ann. ICRP 37(2–4).

ICRP (1981). Limits on Inhalation of Radon Daughters by Workers, Publication 32, Pergamon Press, Oxford.

ICRP (1979). Limits for Intakes of Radionuclides by Workers. Part 1. Annals of the ICRP, 2, ICRP Publication 30.

Ite, A. E., Ibok, U. J., Ite, U. M., & Petters, S. W. (2013). Petroleum Exploration and Production: Past and Present Environmental Issues in the Nigeria's Niger Delta. American Journal of Environmental Protection, 1(4), 78–90. https://doi.org/10.12691/env-1-4-2.

Iqbal, J., M. Howari, F., Mohamed, A.-M. O., & Paleologos, E. K. (2021). Assessment of radiation pollution from nuclear power plants. In Pollution Assessment for Sustainable Practices in

Applied Sciences and Engineering (Issue March 2011). Elsevier Inc. https://doi.org/10.1016/b978-0-12-809582-9.00020-7.

Jasaitis, D., Klima, V., Pečiulienė, M., Vasiliauskienė, V., Konstantinova, M. (2020). Comparative assessment of radiation background due to natural and artificial radionuclides in soil in specific areas on the territories of state of Washington (USA) and Lithuania. Water Air Soil Pollut 231(7):1–10. https:// doi. org/ 10. 1007/ s11270- 020- 04730-8.

Kamunda, C., & Madhuku, M. (2017). Human Health Risk Assessment of Environmental Radionuclides and Heavy Metals around a Gold Mining Area in Gauteng Province, South Africa. May, 192.

Kathren, R. L. (1998). NORM sources and their origins. Applied Radiation and Isotopes 49(1998): 149-168.

Khandaker, M. U., Jojo, P. J., & Kassim, H. A. (2012). Determination of Primordial Radionuclides in Natural Samples Using HPGe Gamma-Ray Spectrometry. APCBEE Procedia, 1(January), 187–192. https://doi.org/10.1016/j.apcbee.2012.03.030.

Khan M.N., Mobin M., Abbas Z.K. and Alamri S.A. (2018) Fertilizers and Their Contaminants in Soils, Surface and Groundwater. In: Dominick A. DellaSala, and Michael I. Goldstein (eds.) The Encyclopedia of the Anthropocene, vol. 5, p. 225-240. Oxford: Elsevier.

Kpeglo, D. O., Mantero, J., Darko, E., Faanu, A., Amoatey, E., Manjón, G., Vioque, I. & García-Tenorio, R. (2019). Assessment of natural radioactivity levels and associated radiological hazard in scale and sludge from Jubilee oilfield of Ghana. International Journal of Low Radiation. 21. 143-157.

Kpeglo, David Okoh. (2015). Radiation Exposure to Natural Radioactivity in Crude Oil and Petroleum Waste from Oil Fields in Ghana ; Modelling , Risk Assessment and Regulatory Control. PhD Dissertation, University of Ghana, Accra, Ghana.

Korkulu, Z. & Özkan, N. (2013) Determination of natural radioactivity levels of beach sand samples in the black seacoast of Kocaeli (Turkey). Radiat. Phys. Chem. 2013, 88, 27–31.

Kurnaz, A., Küçükömeroğlu, B., Keser, R., Okumusoglu, N. T., Korkmaz, F., Karahan, G., & Çevik, U. (2007). Determination of radioactivity levels and hazards of soil and sediment samples in Fi{dotless}rti{dotless}na Valley (Rize, Turkey). Applied Radiation and Isotopes, 65(11), 1281–1289. https://doi.org/10.1016/j.apradiso.2007.06.001.

Lawluvi, H. (2016). Multivariate Statistical Classification of Beach Sand along the Coastal Belt of Ghana using Natural Radioactivity Data. PhD Dissertation, University of Ghana, Accra, Ghana.

Lawluvi, H., Darko, E. O., Schandorf, C., & Faanu, A. (2015). Radiological Hazard Assessment of Beach Sands from Landing Beaches in the Volta Region of Ghana SDRP Journal of Earth Sciences & Environmental Studies. 1(1), 1–5.

Lehritani M, Mantero J, Casacuberta N, Masqué P, García-Tenorio R (2012). Comparison of two Sequential Separation Methods for U and Th determination in environmental samples by alpha-particle spectrometry. Radiochimica Acta 100:431-438.

Lilley, J. (2001). Nuclear Physics: Principles and Applications, Chichester: John Wiley & Sons, Ltd. Issue (7).

Lin, W., Feng, Y., Yu, K., Lan, W., Wang, Y., Mo, Z., Ning, Q., Feng, L., He, X., Huang, Y. (2020). Long-lived radionuclides in marine sediments from the Beibu Gulf, South China Sea: Spatial distribution, controlling factors, and proxy for transport pathway. Mar. Geol. 2020, 424, 106157.

Mamont-Ciesla, K., Gwiazdowski, B., Biernacka, M., Zak, A. (1982). Radioactivity of building materials in Poland. In: Vohra, G., Pillai, K.C., Sadavisan, S. (Eds.), Natural Radiation Environment. Halsted Press, New York, p. 551.

Martin, A. and Harbison, S. (2006). An Introduction to Radiation Protection (5th edition), London: Hodder Arnold.

Mays, C.W., Rowland, R.E., and Stehney, A.F. (1985). A Cancer Risk from the Lifetime Intake of Ra and U Isotopes, Health Physics, 48, 635-647.

Meinhold, A.F., Hamilton, L.D., (1993). "Radium concentration factors and their use in health and environmental risk assessment", Environmental Science Research, Vol. 46 Issue (5). (Ray, J.P., Engelhart, F.R., Eds), Kluwer Academic, Dordrecht 293–302.

Ministry of The Environment Government of Japan. (2018). Various Forms of Exposure. Basic Knowledge and Health Effects of Radiation, 1, 23–75.

NCRP (1987). National Council on Radiation Protection and Measurements. A handbook of radioactivity measurement procedures. Recommendations of the NCRP, NCRP Report. No. 58, Bethesda MD 20814.

NEA-OECD. (1979). Exposure to Radiation from Natural Radioactivity in Building Materials. Report by NEA Group of Experts of the Nuclear Energy Agency. OECD, Paris, France.

Noz, M. E. & Maguire, G. Q. (2007). Radiation Protection in the Health Sciences (With Problem Solutions Manual) Second Edition. World Scientific Publishing Co. Pte. Ltd. Page 69.

NRC/NAS (1992). Issues in Risk Assessment, Vol. 3. Ecological Risk Assessment, National Research Council/National Academy of Sciences. Academy Press. Washington. D.C.

Nuclear Power Ghana (2022). NPA identifies four sites for Ghana's first nuclear plant. Ghana, Accra, Nuclear Power Ghana [cited May 2]. Available from www.nuclearpowergh.com.

Nyarko, E., Botwe, B. O., Ansong, J. E., Delfanti, R., Barsanti, M., Schirone, A., & Delbono, I. (2011). Determination of 210 Pb , 226 Ra and 137 Cs in Beach Sands along the Coastline of Ghana. African Journal Environment Pollution Health, 9(2), 17–23.

Ononugbo, C. P., & Anyalebechi, C. D. (2018). Natural Radioactivity Levels and Radiological Risk Assessment of Surface Water from Coastal Communities of Ndokwa East , Delta State , Nigeria. April. https://doi.org/10.9734/PSIJ/2017/31782.

Omeje, M., Olusegun, O.A., Emmanuel, S.J., Ijeh, I.B., Terhile, M.T.A., Emeka, E.O., Omeje, A.U., Adeleye, B.N., Orosun, M.M., Oha, A.I., Ogunrinola, I.E., Ahuekwe, E.F., Saeed, M.A. (2021). Measurements of seasonal variations of radioactivity distributions in riverine

soil sediment of Ado-Odo Ota, south-west Nigeria: probabilistic approach using Monte Carlo. Radiat. Protect. Dosim. 193 (2), 76–89.

Onjefu, S. A., Kauluma, A. N. I., Zivuku, M., Ejembi, E., Hamunyela, R. H., Tyobeka, B. M. (2022). Assessment of radioactivity levels in shore sediments along the coastline of the orange river, Oranjemund, Namibia. https://doi.org/10.1016/j.heliyon.2022.e10579.

Penabei, S., Bongue, D., Maleka, P., Dlamini, T., Saïdou, Guembou Shouop, C. J., Halawlaw, Y. I., Ngwa Ebongue, A., & Kwato Njock, M. G. (2018). Assessment of natural radioactivity levels and the associated radiological hazards in some building materials from Mayo-Kebbi region, Chad. Radioprotection, 53(4), 265–278. https://doi.org/10.1051/radiopro/2018030

Powell, B. A., Hughes, L. D., Aurelie, M., Soreefan, A., Falta, D., Wall, M., et al. (2007). Elevated concentrations of primordial radionuclides in sediments from the Reedy River and surrounding creeks in Simpsonville, South Carolina. Journal of Environmental Radioactivity, 94, 121e128.

Qureshi, A. A, Tariq, S., Kamal U. D., Manzoor S., Chiara Calligaris, C., Waheed A. (2014). Evaluation of excessive lifetime cancer risk due to natural radioactivity in the river sediments of Northern Pakistan. Journal of Radiation Research and Applied Sciences 7 (2014) 438-447.

Radomirovic´, M., Stankovic´, S., Mandic´, M., Jovic´, M., Mandic´, L.J., Dragovic´, S., Onjia, A., (2021). Spatial distribution, radiological risk assessment and positive matrix factorization of gamma-emitting radionuclides in the sediment of the Boka Kotorska Bay. Mar. Pollut. Bull. 2021, 169, 112491.

Ravisankar, R., Chandramohan, J., Chandrasekaran, A., Prakash, J. P., Vijayalakshmi, I., Vijayagopal, P., & Venkatraman, B. (2015). Assessments of radioactivity concentration of natural radionuclides and radiological hazard indices in sediment samples from the East coast of Tamilnadu , India with statistical approach. Marine Pollution Bulletin. https://doi.org/10.1016/j.marpolbul.2015.05.058.

Ravisankar, R., Sivakumar, S., Chandrasekaran, A., Prince Prakash Jebakumar, J., Vijayalakshmi, I., Vijayagopal, P., Venkatraman, B. (2014). Spatial distribution of gamma radioactivity levels and radiological hazard indices in the East coastal sediments of Tamilnadu, India with statistical approach. Radiat. Phys. Chem. 103, 89–98.

Razak, A. (2015). University of Ghana http://ugspace.ug.edu.gh Naturally Occurring Radioactive Materials in Mining : Dose. 10213258.

Roucher, R.S., Agras, J., Mills, D., Harrod, M., Chestnut, L. (2002). Quantifying Public Health Risk Reduction Benefits. AWWA Research Foundation and AWWA, Denver, USA. ISBN 1-58321-192-6.

Saad, H. R., & Al-Azmi (2002). Radioactivity concentrations in sediments and their correlation to the coastal structure in Kuwait. Appl Radiat Isot 56:991-997. https://doi.org/10.1016/S0969 - 8043(02)00061.

SAEPA. (2017). Naturally occurring radioactive material (NORM). December.

Santawamaitre, T. (2007). The Measurement of Naturally Occuring Radioactive Material (NORM) And Neutron Activation Analysis in Environmental Samples. 235, 245. http://digilib.unila.ac.id/11478/16/16. BAB II.pdf.

Smith, K. P. (1992). An Overview of Naturally Occurring Radioactive Materials (NORM) in the Petroleum Industry MASTER Office of Domestic and InternationalEnergy Policy.

Stanley, F. K. T., Irvine, J. L., Jacques, W. R., Salgia, S. R., Innes, D. G., Winquist, B. D., Torr, D., Brenner, D. R., & Goodarzi, A. A. (2019). Radon exposure is rising steadily within the modern North American residential environment, and is increasingly uniform across seasons. Scientific Reports, 9(1), 1–17. https://doi.org/10.1038/s41598-019-54891-8.

Tadmor, J. (1986). Radioactivity from coal-fired power plants: A review, Journal of Environmental Radioactivity, Volume 4, Issue 3, Pages 177-204, ISSN 0265-

931X,https://doi.org/10.1016/0265-931X(86)90010-X. (https://www.sciencedirect.com/science/article/pii/0265931X8690010X).

Taskin, H., Karavus, M., Ay, P., Topuzoglu, A., Hindiroglu, S. and Karahan, G. (2009). Radionuclide concentrations in soil and lifetime cancer risk due to the gamma radioactivity in Kirlareli, Turkey. J. Environ. Radioact. 100, 49–53.

Thangam, V., Rajalakshmi, A., Chandrasekaran, A., Arun, A., Viswanathan, S., Venkatraman, B., Bera, S. (2022). Determination of natural radioactivity in beach sands collected along the coastal area of Tamilnadu, India using gamma ray spectrometry. J. Radioanal. Nucl. Chem. 331, 1207–1223.Issue (1).

Thorne, M. C. (2003). Background radiation: natural and man-made. A review. Journal of Raiological Protection. J. Radiol. Prot. 23 (2003) 29-42. Issue (3).

TRACERCO. (2007). Module 14: Naturally occurring radioactive material in oil production, radiological safety course (pp. 1–11).

Tsabaris, C., Eleftheriou, G., Kapsimalis, V., Anagnostou, C., Vlastou, R., Durmishi, C., Kedhi, M., Kalfas, C.A. (2007). Radioactivity levels of recent sediments in the Butrint Lagoon and the adjacent coast of Albania. Appl. Radiat. Isot. 65 (4), 445– 453.

Ugbede, F., O. (2020). Distribution of 40K, 238U and 232Th and associated radiological risks in river sediments across Enugu East, Nigeria. Environmental Nanotechnology, Monitoring and Management 14 (2020) 100317.

UNSCEAR (2008). "Sources and Effects of Ionizing Radiation", UNSCEAR 2006 Report Vol.1 to the General Assembly, with scientific annexes, United Nations Sales Publication, United Nations, New York.

UNSCEAR (2000). Sources, Effects and Risks of Ionizing Radiation. Report to the General Assembly. United Nations, New York.

UNSCEAR (1993). Sources, Effects and Risks of Ionizing Radiation. United Nations, NewYork.

USEPA (1996). Summary Report for the Workshop on Monte Carlo Analysis, Risk Assessment Forum. USEPA, US Environmental Protection Agency, Washington, DC. EPA-630-R-96-010.

USEPA (1998), Guidelines for Ecological Risk Assessment. US Environmental Protection Agency EPA/630IR -95/002F. Risk Assessment Forum, Washington. DC. USA

Vearrier, D., Curtis, J. A., & Greenberg, M. I. (2009). Technologically enhanced naturally occurring radioactive materials. Clinical Toxicology, 47(5), 393–406. https://doi.org/10.1080/15563650902997849.

Wanty, R. B., and Shoen, R., (1993). A Review of the Chemical Processess Affecting the Mobility of Radionuclides in Natural waters, With Applications, in Gunderson, L.C.S, and Wanty, R. B..eds., Field Studies of Radon in Rocks, Soils and Water:Boca Raton, Florida, C. K. Smoley, p. 334.

WHO (1993). Indoor Air Quality: A Risk Based Approach to Health Criteria for Radon Indoors, Doc. BUR/ICP/CEH 108 (S), World Health Organization Regional Office for Europe, Copenhagen.

World Nuclear Association, (2020). Emerging Nuclear Energy Countries | New Nuclear Build Countries - World Nuclear Association [WWW Document]. URL <https://www.world-nuclear.org/information-library/country-profiles/others/emerging-nuclear-energy-countries.aspx> (accessed 11.5.23).

Yii, M.W., Zaharudin, A. and Abdul-Kadir, I. (2009), Distribution of naturally occurring radionuclides activity concentration in East Malaysian marine sediment, Applied Radiation and Isotopes, Volume 67, Issue 4, 2009, Pages 630-635, ISSN 0969-8043,

https://doi.org/10.1016/j.apradiso.2008.11.019.
(https://www.sciencedirect.com/science/article/pii/S0969804308005265).

Zimmermann, H.J., (2001). Fuzzy Set Theory-and Its Applications, fourth ed. Kluwer Academic Publishers, Norwell, Massachusetts.

APPENDICES

APPENDIX A: Hazard parameters associated with coastal sand from Sekondi-Takoradi.

Sample ID	Dr(nGy^{-1})	Raeq	Hin	Hex	AED (mSvy^{-1})	AGD (uSvy^{-1})	RLI	AUI	ELCR ($\times 10^{-3}$)
TK 1	59,39	119,65	0,3858	0,3231	0,0728	430,47	0,0921	0,5377	0,2549
TK 2	51,85	104,45	0,3369	0,2821	0,0636	375,84	0,1055	0,4693	0,2226
TK 3	47,8	96,85	0,3337	0,2616	0,0586	344,13	0,1066	0,4777	0,2052
TK 4	47,66	98,62	0,3222	0,2663	0,0584	341,92	0,0916	0,5287	0,2046
TK 5	51,83	107,82	0,343	0,2911	0,0636	371,98	0,0876	0,5832	0,2225
TK 6	56,97	118,49	0,377	0,32	0,0699	408,84	0,0798	0,6407	0,2445
TK 7	49,49	102,95	0,3275	0,278	0,0607	355,19	0,0918	0,557	0,2124
TK 8	50,07	104,14	0,3312	0,2812	0,0614	359,33	0,0918	0,563	0,2149
TK 9	54,41	113,18	0,3599	0,3056	0,0667	390,48	0,0836	0,6121	0,2336
TK 10	52,82	109,14	0,3669	0,2947	0,0648	378,39	0,0801	0,5921	0,2267
TK 11	59,28	119,25	0,388	0,322	0,072	429,65	0,093	0,535	0,254
TK 12	52,04	104,72	0,342	0,283	0,064	377,05	0,105	0,472	0,223
TK 13	49,04	99,58	0,344	0,269	0,06	352,6	0,101	0,501	0,21
TK 14	49,92	102,65	0,336	0,278	0,061	354,02	0,086	0,563	0,212
TK 15	51,74	107,45	0,346	0,29	0,063	371,19	0,085	0,58	0,222
TK 16	56,51	117,27	0,376	0,317	0,069	405,56	0,079	0,631	0,243
TK 17	48,87	103,85	0,372	0,281	0,061	357,95	0,094	0,563	0,214
TK 18	50,19	104,62	0,328	0,283	0,062	360,35	0,094	0,567	0,215
TK 19	55,93	116,67	0,373	0,315	0,069	400,82	0,079	0,644	0,24
TK 20	52,65	108,56	0,369	0,293	0,065	377,01	0,08	0,59	0,226
Mean	52,42	108,00	0,35	0,29	0,06	377,14	0,09	0,56	0,23
Max	59,39	119,65	0,39	0,32	0,07	430,47	0,11	0,64	0,25
Min	47,66	96,85	0,32	0,26	0,06	341,92	0,08	0,47	0,20

APPENDIX B: Hazard parameters associated with coastal sand in Axim.

Sample ID	Dr(nGy^{-1})	Raeq	Hin	Hex	AED (mSvy^{-1})	AGD (uSvy^{-1})	RLI	AUI	ELCR ($\times 10^{-3}$)
AX 1	22,33	46,52	0,1602	0,1256	0,0274	159,21	0,2332	0,2682	0,0959
AX 2	17,18	37,19	0,1177	0,1004	0,0211	121,57	0,1477	0,244	0,0737
AX 3	22,32	47,51	0,177	0,1283	0,0274	156,8	0,1477	0,3203	0,9581
AX 4	27,45	60,08	0,2177	0,1623	0,0337	191,22	0,1053	0,4459	0,1178
AX 5	25,41	54,11	0,1726	0,1461	0,0312	180,75	0,1609	0,3309	0,109
AX 6	27,18	58,59	0,1977	0,1582	0,0333	191,63	0,1237	0,3918	0.1166
AX 7	24,19	51,35	0,1806	0,1387	0,0297	170,97	0,1408	0,3292	0,1038
AX 8	26,72	56,74	0,1995	0,1532	0,0328	188,88	0,1274	0,3639	0,1148
AX 9	23,34	48,97	0,1771	0,1323	0,0286	165,31	0,1566	0,3029	0,1002
AX 10	24,51	51,41	0,1862	0,1389	0,0301	173,54	0,1492	0,3182	0,1052
AX 11	22,7	47,25	0,165	0,128	0,028	161,62	0,172	0,275	0,097
AX 12	17,06	36,83	0,12	0,099	0,021	120,61	0,215	0,241	0,073
AX 13	22,19	47,18	0,179	0,127	0,027	155,73	0,153	0,319	0,095
AX 14	27,31	59,62	0,219	0,161	0,033	190,18	0,106	0,442	0,117
AX 15	28,17	59,89	0,209	0,162	0,035	199,09	0,121	0,385	0,121
AX 16	26,68	57,3	0,198	0,155	0,033	188,04	0,123	0,383	0,115
AX 17	24,07	50,93	0,183	0,138	0,03	170,04	0,143	0,326	0,103
AX 18	26,54	56,18	0,203	0,152	0,033	187,42	0,129	0,361	0,114
AX 19	24,54	51,74	0,188	0,14	0,03	173,4	0,143	0,328	0,105
AX 20	24,74	52,08	0,186	0,141	0,03	175,18	0,144	0,324	0,106
mean	24,23	51,57	0,18	0,14	0,03	171,06	0,15	0,33	0,15
max	28,17	60,08	0,22	0,16	0,04	199,09	0,23	0,45	0,96
min	17,06	36,83	0,12	0,10	0,02	120,61	0,11	0,24	0,07

APPENDIX C: Hazard parameters associated with coastal sand in Beyin.

Sample ID	Dr(nGy^{-1})	Raeq	Hin	Hex	AED (mSvy^{-1})	AGD (uSvy^{-1})	RLI	AUI	ELCR ($\times 10^{-3}$)
BN 1	25,77	56,12	0,2002	0,1516	0,0316	180,2	0,1158	0,4043	0,1106
BN 2	42,76	94,21	0,3423	0,2545	0,0524	297,08	0,0662	0,7176	0,1835
BN 3	42,53	91,95	0,3565	0,2484	0,0522	295,83	0,071	0,6783	0,1825
BN 4	29,74	63,51	0,2375	0,1715	0,0364	208,61	0,1086	0,435	0,1277
BN 5	38,86	84,31	0,2869	0,2277	0,0477	273,14	0,0832	0,5824	0,1668
BN 6	41,48	90,69	0,3257	0,2449	0,0506	298,25	0,0704	0,6672	0,178
BN 7	43,72	92,98	0,3341	0,2511	0,0536	308,22	0,0761	0,6097	0,1877
BN 8	21,76	46,81	0,1746	0,1264	0,0267	152,18	0,1415	0,3305	0,0934
BN 9	32,63	69,25	0,2419	0,187	0,04	230,8	0,1052	0,4413	0,1401
BN 10	31,33	67,25	0,2416	0,1816	0,0384	220,09	0,1008	0,459	0,1345
BN 11	27,07	59,05	0,211	0,159	0,033	189,08	0,109	0,429	0,116
BN 12	43,43	95,59	0,351	0,258	0,053	301,55	0,065	0,73	0,186
BN 13	43,78	94,79	0,367	0,256	0,053	304,43	0,068	0,702	0,188
BN 14	31	66,33	0,248	0,179	0,038	217,24	0,103	0,459	0,133
BN 15	40,27	87,49	0,3	0,236	0,049	282,78	0,079	0,61	0,173
BN 16	48,45	104,15	0,364	0,281	0,059	340,99	0,066	0,703	0,208
BN 17	36,65	80,74	0,304	0,218	0,045	253,31	0,076	0,628	0,157
BN 18	23,38	50,49	0,189	0,136	0,029	163,26	0,129	0,362	0,101
BN 19	32,64	69,38	0,238	0,187	0,04	231,08	0,107	0,44	0,14
BN 20	32,58	70,12	0,251	0,189	0,04	228,73	0,11	0,483	0,141
mean	35,49	76,76	0,28	0,21	0,04	248,84	0,09	0,54	0,15
max	48,45	104,15	0,37	0,28	0,06	340,99	0,14	0,73	0,21
min	21,76	46,81	0,17	0,13	0,03	152,18	0,07	0,33	0,09

APPENDIX D: Hazard parameters associated with coastal sand in Half-Asini.

Sample ID	Dr(nGy-1)	Raeq	Hin	Hex	AED ($mSvy^{-1}$)	AGD ($uSvy^{-1}$)	RLI	AUI	ELCR ($\times 10^{-3}$)
HA 1	30,71	64,91	0,2277	0,1918	0,0377	217,45	0,114	0,4072	0,1318
HA 2	33,6	71,01	0,2491	0,1918	0,0412	237,9	0,1043	0,4453	0,1442
HA 3	32,98	68,99	0,246	0,1863	0,0405	234,05	0,1133	0,4167	0,1415
HA 4	35,81	74,9	0,2672	0,2023	0,0439	254,15	0,1044	0,4523	0,1537
HA 5	45,81	96,82	0,3621	0,2615	0,0562	322,57	0,0761	0,6342	0,1966
HA 6	30,89	65,3	0,2442	0,1764	0,0379	217,55	0,1128	0,4278	0,1326
HA 7	36,89	77,15	0,2751	0,2083	0,0452	261,82	0,1014	0,4657	0,1583
HA 8	28,36	59,32	0,2116	0,1602	0,0348	201,34	0,132	0,3579	0,1218
HA 9	30,71	64,91	0,2277	0,1753	0,0377	217,45	0,114	0,4072	0,1318
HA 10	35,6	71,01	0,2491	0,1918	0,0412	237,9	0,1043	0,4453	0,1442
HA 11	31,18	66,02	0,23	0,178	0,038	220,74	0,112	0,416	0,134
HA 12	32,72	68,98	0,243	0,186	0,04	231,82	0,108	0,429	0,142
HA 13	33,77	70,93	0,249	0,192	0,041	239,67	0,108	0,432	0,145
HA 14	36,53	76,48	0,274	0,207	0,045	259,12	0,102	0,465	0,157
HA 15	46,32	98,09	0,363	0,265	0,057	326,25	0,074	0,643	0,199
HA 16	32,16	68,15	0,256	0,184	0,039	226,12	0,106	0,453	0,138
HA 17	37,22	78,01	0,274	0,211	0,046	264,29	0,102	0,471	0,16
HA 18	29,65	62,33	0,22	0,168	0,036	210,22	0,122	0,383	0,127
HA 19	31,54	66,92	0,232	0,181	0,039	223,33	0,11	0,424	0,135
HA 20	34,36	72,82	0,253	0,197	0,042	243,19	0,101	0,46	0,147
mean	34,34	72,15	0,26	0,20	0,04	242,35	0,11	0,45	0,15
max	46,32	98,09	0,36	0,27	0,06	326,25	0,13	0,64	0,20
min	28,36	59,32	0,21	0,16	0,03	201,34	0,07	0,36	0,12

APPENDIX E: Hazard parameters associated with coastal sediment from Sekondi-Takoradi.

Sample ID	Dr(nGy^{-1})	Raeq	Hin	Hex	AED (mSvy^{-1})	AGD (uSvy^{-1})	RLI	AUI	ELCR ($\times 10^{-3}$)
TK 1	42,21	86,14	0,2886	0,2326	0,0518	303,74	0,1111	0,4341	0,1812
TK 2	45,91	94,49	0,3141	0,2552	0,0563	329,6	0,096	0,4974	0,1971
TK 3	50,05	104,21	0,3401	0,2814	0,0614	358,42	0,0845	0,5766	0,2149
TK 4	47,81	98,74	0,3223	0,2666	0,0586	343,32	0,0927	0,5227	0,2052
TK 5	43,57	89,87	0,3035	0,2427	0,0534	312,2	0,0979	0,4844	0,187
TK 6	39,53	80,75	0,2816	0,2181	0,0485	283,46	0,1176	0,4227	0,1697
TK 7	40,07	81,85	0,2854	0,2211	0,0491	287,33	0,116	0,4285	0,172
TK 8	45,28	93,37	0,2946	0,2522	0,0555	326,12	0,1076	0,478	0,1944
TK 9	49,39	102,9	0,3387	0,2779	0,0606	353,3	0,0837	0,5754	0,212
TK 10	43,5	88,52	0,3215	0,2391	0,0533	311,34	0,1194	0,4682	0,1867
TK 11	33,68	67,52	0,192	0,182	0,041	246,57	0,338	0,263	0,145
TK 12	36,11	73,12	0,203	0,197	0,044	263,92	0,579	0,301	0,155
TK 13	37,37	75,79	0,216	0,205	0,046	272,57	0,291	0,322	0,161
TK 14	39,44	80,42	0,229	0,217	0,048	287,14	0,285	0,354	0,169
TK 15	43,19	88,87	0,303	0,24	0,053	309,49	0,101	0,476	0,185
TK 16	40,93	83,96	0,292	0,227	0,049	293,12	0,109	0,449	0,176
TK 17	40,72	83,44	0,288	0,225	0,058	291,95	0,111	0,441	0,175
TK 18	47,23	97,77	0,312	0,264	0,051	339,43	0,098	0,516	0,203
TK 19	41,84	86,71	0,246	0,234	0,04	303,07	0,259	0,424	0,179
TK 20	32,97	65,96	0,191	0,178	0,037	241,3	0,282	0,256	0,142
mean	42,04	86,22	0,28	0,23	0,05	302,87	0,17	0,43	0,18
max	50,05	104,21	0,34	0,28	0,06	358,42	0,58	0,58	0,21
min	32,97	65,96	0,19	0,18	0,04	241,30	0,08	0,26	0,14

APPENDIX F: Hazard parameters associated with coastal sediment from Axim.

Sample ID	Dr(nGy-1)	Raeq	Hin	Hex	AED ($mSvy^{-1}$)	AGD ($uSvy^{-1}$)	RLI	AUI	ELCR ($\times10^{-3}$)
AX 1	28,82	63,37	0,2179	0,1711	0,0353	201,37	0,1058	0,4644	0,1237
AX 2	29,61	64,95	0,2284	0,1754	0,0363	206,68	0,1001	0,4775	0,1271
AX 3	28,38	62,24	0,2189	0,1681	0,0348	198,08	0,1045	0,4575	0,1218
AX 4	29,81	65,38	0,2301	0,1766	0,0366	208,06	0,099	0,4806	0,1279
AX 5	30,15	66,13	0,2327	0,1786	0,037	210,43	0,0983	0,4862	0,1294
AX 6	28,23	61,92	0,2178	0,1672	0,0346	197,04	0,105	0,4553	0,1212
AX 7	19,5	42,38	0,1564	0,1145	0,0239	136,05	0,1507	0,3091	0,0837
AX 8	29,05	60,74	0,217	0,164	0,0356	206,19	0,1292	0,3664	0,1247
AX 9	35,37	77,68	0,2793	0,2098	0,0434	246,31	0,0815	0,581	0,1518
AX 10	31,47	68,98	0,2439	0,1863	0,0386	219,61	0,0938	0,5073	0,1351
AX 11	30,13	66,37	0,228	0,179	0,037	210,38	0,101	0,489	0,129
AX 12	30,49	66,98	0,234	0,181	0,037	212,78	0,097	0,494	0,131
AX 13	29,87	65,6	0,232	0,177	0,036	208,23	0,098	0,487	0,128
AX 14	29,7	65,03	0,232	0,176	0,039	207,27	0,099	0,478	0,128
AX 15	31,58	69,4	0,245	0,187	0,037	220,28	0,093	0,514	0,136
AX 16	29,82	65,53	0,231	0,177	0,026	207,92	0,098	0,486	0,128
AX 17	21,32	46,54	0,171	0,126	0,037	148,53	0,136	0,344	0,092
AX 18	30,47	63,95	0,23	0,173	0,045	215,91	0,12	0,394	0,131
AX 19	36,6	80,43	0,291	0,217	0,04	254,65	0,078	0,605	0,157
AX 20	32,53	71,4	0,254	0,193	0,053	226,83	0,09	0,529	0,14
mean	29,65	64,75	0,23	0,17	0,04	207,13	0,10	0,47	0,13
max	36,60	80,43	0,29	0,22	0,05	254,65	0,15	0,61	0,16
min	19,50	42,38	0,16	0,11	0,02	136,05	0,08	0,31	0,08

APPENDIX G: Hazard parameters associated with coastal sediment from Beyin.

Sample ID	Dr(nGy^{-1})	Raeq	Hin	Hex	AED (mSvy-^{1})	AGD (uSvy^{-1})	RLI	AUI	ELCR ($\times10^{-3}$)
BN 1	22,68	49,61	0,1853	0,134	0,0278	157,59	0,1258	0,3739	0,0973
BN 2	23,93	52,5	0,1853	0,1418	0,0293	166,96	0,1232	0,3871	0,1027
BN 3	24,88	54,57	0,1928	0,1474	0,0305	173,56	0,1184	0,4024	0,1068
BN 4	22,56	49,49	0,1747	0,1337	0,0277	157,39	0,1307	0,3649	0,0968
BN 5	24,32	53,37	0,1885	0,1441	0,0298	169,71	0,1212	0,3936	0,1044
BN 6	23,37	51,27	0,1812	0,1385	0,0287	163,07	0,126	0,378	0,1003
BN 7	21,83	47,75	0,1784	0,129	0,0268	151,72	0,1307	0,3599	0,0937
BN 8	22,15	48,6	0,1715	0,1313	0,0272	154,58	0,1331	0,3583	0,0951
BN 9	24,26	53,07	0,2028	0,1433	0,0298	168,24	0,1174	0,4053	0,1041
BN 10	30,9	69,02	0,237	0,1864	0,0379	214,61	0,0967	0,5357	0,1326
BN 11	23,72	51,99	0,193	0,14	0,029	164,77	0,12	0,394	0,102
BN 12	25,29	55,61	0,196	0,15	0,031	176,35	0,116	0,413	0,109
BN 13	25,9	56,94	0,201	0,154	0,032	180,67	0,114	0,422	0,111
BN 14	24,56	54,02	0,192	0,146	0,03	171,08	0,118	0,404	0,105
BN 15	25,17	55,26	0,197	0,149	0,031	175,59	0,116	0,41	0,108
BN 16	25,13	55,21	0,197	0,149	0,031	175,03	0,115	0,412	0,108
BN 17	22,29	48,94	0,178	0,132	0,027	155,08	0,128	0,368	0,096
BN 18	23,67	52,02	0,185	0,14	0,029	164,95	0,123	0,388	0,102
BN 19	25,86	56,63	0,218	0,153	0,032	179,16	0,101	0,436	0,111
BN 20	32,13	71,8	0,248	0,194	0,039	222,99	0,092	0,56	0,138
mean	24,73	54,38	0,20	0,15	0,03	172,16	0,12	0,41	0,11
max	32,13	71,80	0,25	0,19	0,04	222,99	0,13	0,56	0,14
min	21,83	47,75	0,17	0,13	0,03	151,72	0,09	0,36	0,09

APPENDIX H: Hazard parameters associated with coastal sediment from Half-Asini

Sample ID	Dr(nGy^{-1})	Raeq	Hin	Hex	AED (mSvy^{-1})	AGD (uSvy^{-1})	RLI	AUI	ELCR ($\times 10^{-3}$)
HA 1	31,24	67,9	0,239	0,1834	0,0383	218,87	0,0976	0,4874	0,1341
HA 2	46,98	98,99	0,352	0,2674	0,0576	332,62	0,075	0,6178	0,2016
HA 3	47,91	100,97	0,3589	0,2727	0,0588	339,26	0,074	0,6301	0,2057
HA 4	48,14	101,45	0,3608	0,274	0,059	340,87	0,0736	0,6333	0,2066
HA 5	58,03	122,29	0,4349	0,3303	0,0712	410,9	0,0611	0,7633	0,2491
HA 6	53,12	111,95	0,398	0,3024	0,0651	376,12	0,0667	0,6989	0,228
HA 7	43,33	90,95	0,3251	0,2456	0,0531	307,15	0,0841	0,5589	0,186
HA 8	40,48	85,97	0,2835	0,2322	0,0496	287,54	0,0926	0,5298	0,1737
HA 9	38,23	81,21	0,268	0,2193	0,0469	271,59	0,0979	0,5007	0,1641
HA 10	43,74	92,89	0,3065	0,2509	0,0536	310,72	0,0856	0,5724	0,1878
HA 11	30,65	66,37	0,239	0,179	0,038	214,58	0,099	0,47	0,132
HA 12	46,83	98,51	0,354	0,266	0,057	331,52	0,076	0,614	0,201
HA 13	47,46	99,81	0,359	0,27	0,058	335,95	0,076	0,622	0,204
HA 14	47,98	100,98	0,363	0,273	0,059	339,95	0,074	0,632	0,206
HA 15	58,84	124,12	0,441	0,335	0,072	416,5	0,06	0,778	0,253
HA 16	54,55	115,2	0,41	0,311	0,067	385,92	0,064	0,726	0,234
HA 17	44,64	93,88	0,337	0,254	0,055	316,06	0,08	0,584	0,192
HA 18	41,76	88,92	0,294	0,24	0,051	296,3	0,088	0,556	0,179
HA 19	39,06	83,04	0,276	0,224	0,048	277,27	0,094	0,516	0,168
HA 20	45,32	96,46	0,32	0,26	0,056	321,53	0,0801	0,603	0,195
mean	45,41	96,09	0,34	0,26	0,06	321,56	0,08	0,60	0,20
max	58,84	124,12	0,44	0,34	0,07	416,50	0,10	0,78	0,25
min	30,65	66,37	0,24	0,18	0,04	214,58	0,06	0,47	0,13

APPENDIX I: Model used for beach sand between all elements.

```
Call:
lm(formula = X228Ra ~ X232Th + X228Th + X40K, data = df)

Residuals:
   Min     1Q Median     3Q    Max
-3.321  0.000  0.000  0.000  3.321

Coefficients:
             Estimate Std. Error t value Pr(>|t|)
(Intercept)  -4.302428   3.898839  -1.104  0.30629
X232Th        1.527277   0.180399   8.466 6.34e-05 ***
X228Th11.2   -0.465564   3.252789  -0.143  0.89022
X228Th13     -1.144784   3.917187  -0.292  0.77857
X228Th13.1    0.051739   3.790611   0.014  0.98949
X228Th14     -4.217106   3.298344  -1.279  0.24181
X228Th14.9   -5.802061   3.282309  -1.768  0.12044
X228Th15.9   -6.532292   3.304508  -1.977  0.08860 .
X228Th16.1    2.207715   3.313588   0.666  0.52658
X228Th16.3   -1.354776   3.724855  -0.364  0.72681
X228Th16.6   -6.436111   3.246226  -1.983  0.08784 .
X228Th16.7   -4.471473   3.242606  -1.379  0.21035
X228Th16.8    1.253977   4.456289   0.281  0.78654
X228Th17.3   -8.190673   3.290101  -2.489  0.04163 *
X228Th17.6   -2.787121   3.289257  -0.847  0.42483
X228Th17.7   -9.716180   4.479433  -2.169  0.06671 .
X228Th17.8   -5.834622   3.252764  -1.794  0.11594
X228Th18     -8.157235   3.373930  -2.418  0.04625 *
X228Th18.4   -7.367163   2.764856  -2.665  0.03225 *
X228Th18.7   -4.040375   3.502339  -1.154  0.28652
X228Th18.8   -5.269742   3.238442  -1.627  0.14771
X228Th18.9   -7.826358   3.255044  -2.404  0.04716 *
X228Th19.1    0.707374   2.824808   0.250  0.80946
X228Th19.2   -8.554722   3.273622  -2.613  0.03475 *
X228Th19.4  -10.391621   2.831234  -3.670  0.00796 **
X228Th19.9   -8.021423   3.405159  -2.356  0.05066 .
X228Th20     -9.032871   3.455120  -2.614  0.03469 *
X228Th20,1   -8.061217   3.440541  -2.343  0.05162 .
X228Th20.1   -8.061217   3.440541  -2.343  0.05162 .
X228Th20.3   -8.172429   3.344059  -2.444  0.04451 *
X228Th20.6   -9.434710   3.500080  -2.696  0.03084 *
X228Th21.3   -6.323579   3.383473  -1.869  0.10384
X228Th21.5    0.693322   3.373342   0.206  0.84301
X228Th21.6   -9.292692   2.973186  -3.125  0.01671 *
X228Th21.8   -8.082959   4.686356  -1.725  0.12822
X228Th22     -9.275633   3.347161  -2.771  0.02765 *
X228Th22.1  -11.739660   5.185233  -2.264  0.05798 .
X228Th22.5   -9.953361   3.434530  -2.898  0.02305 *
X228Th22.8   -0.757175   3.485847  -0.217  0.83424
X228Th23.1  -12.741368   4.882275  -2.610  0.03493 *
X228Th23.4  -13.849953   4.504500  -3.075  0.01795 *
```

```
X228Th23.7  -11.517289   5.140874  -2.240  0.06005 .
X228Th23.8  -10.780919   5.320215  -2.026  0.08235 .
X228Th24.5  -10.806899   5.384330  -2.007  0.08473 .
X228Th25.3  -14.147065   5.955314  -2.376  0.04920 *
X228Th25.5   -2.013372   3.283232  -0.613  0.55912
X228Th25.6   -9.984396   5.145567  -1.940  0.09348 .
X228Th25.9  -10.167813   5.208933  -1.952  0.09190 .
X228Th26.4  -13.660652   3.393852  -4.025  0.00503 **
X228Th26.5  -13.358905   5.518644  -2.421  0.04605 *
X228Th26.8  -10.665532   5.406674  -1.973  0.08914 .
X228Th26.9  -13.997265   3.404350  -4.112  0.00451 **
X228Th27.1  -13.681425   3.428758  -3.990  0.00526 **
X228Th28.1  -11.461937   5.710875  -2.007  0.08474 .
X228Th28.3  -10.080575   5.248916  -1.921  0.09626 .
X228Th28.6  -11.265393   4.367736  -2.579  0.03651 *
X228Th29.5  -13.966251   5.205856  -2.683  0.03141 *
X228Th29.7  -10.297236   4.730929  -2.177  0.06597 .
X228Th30.6  -10.155617   5.783416  -1.756  0.12252
X228Th30.7  -12.690301   4.838701  -2.623  0.03428 *
X228Th30.8  -29.420228   4.899276  -6.005  0.00054 ***
X228Th31.9   -3.514834   3.924383  -0.896  0.40019
X228Th32.3  -17.702212   3.999221  -4.426  0.00306 **
X228Th34.5  -15.537804   4.666616  -3.330  0.01260 *
X228Th41    -17.393115   3.838078  -4.532  0.00269 **
X228Th5.1     4.665790   3.282079   1.422  0.19813
X228Th7       1.676189   3.285713   0.510  0.62564
X228Th7.1     1.491100   3.281454   0.454  0.66329
X228Th7.4     1.389962   3.268333   0.425  0.68340
X228Th7.6     4.074155   3.281920   1.241  0.25444
X228Th8.8     1.470943   3.255299   0.452  0.66504
X228Th9.2     1.742965   3.269314   0.533  0.61044
X40K          0.003505   0.006958   0.504  0.62995
---
Signif. codes:  0 ‘***’ 0.001 ‘**’ 0.01 ‘*’ 0.05 ‘.’ 0.1 ‘ ’ 1

Residual standard error: 2.288 on 7 degrees of freedom
Multiple R-squared:  0.9936,    Adjusted R-squared:  0.9272
F-statistic: 14.98 on 72 and 7 DF,  p-value: 0.0004895
```

APPENDIX J: Beach sand Model between ^{228}Ra and ^{232}Th

```
Call:
lm(formula = X228Ra ~ X232Th, data = df)

Residuals:
    Min      1Q  Median      3Q     Max
-16.363  -3.027  -1.260   3.293  13.144

Coefficients:
            Estimate Std. Error t value Pr(>|t|)
(Intercept) -1.35679    1.82327  -0.744    0.459
X232Th       1.07161    0.08629  12.419   <2e-16 ***
---
Signif. codes:  0 ‘***’ 0.001 ‘**’ 0.01 ‘*’ 0.05 ‘.’ 0.1 ‘ ’ 1

Residual standard error: 4.946 on 78 degrees of freedom
Multiple R-squared:  0.6641,    Adjusted R-squared:  0.6598
F-statistic: 154.2 on 1 and 78 DF,  p-value: < 2.2e-16
```

APPENDIX K: Beach sand Model between ^{40}K and ^{232}Th

```
Call:
lm(formula = X40K ~ X232Th, data = df)

Residuals:
    Min      1Q  Median      3Q     Max
-322.30 -114.89  -31.31   68.25  524.71

Coefficients:
            Estimate Std. Error t value Pr(>|t|)
(Intercept)   99.764     64.972   1.535 0.128708
X232Th        12.178      3.075   3.961 0.000164 ***
---
Signif. codes:  0 ‘***’ 0.001 ‘**’ 0.01 ‘*’ 0.05 ‘.’ 0.1 ‘ ’ 1

Residual standard error: 176.3 on 78 degrees of freedom
Multiple R-squared:  0.1674,    Adjusted R-squared:  0.1568
F-statistic: 15.69 on 1 and 78 DF,  p-value: 0.0001641
```

APPENDIX L: Beach sand Model between ^{228}Th and ^{232}Th

```
Call:
lm(formula = X232Th ~ X228Th, data = df)

Residuals:
   Min     1Q Median     3Q    Max
 -6.35   0.00   0.00   0.00   6.35

Coefficients:
             Estimate Std. Error t value Pr(>|t|)
(Intercept)  1.400e+01  4.327e+00   3.236   0.0102 *
X228Th11.2   1.500e+00  6.119e+00   0.245   0.8119
X228Th13     9.000e+00  6.119e+00   1.471   0.1754
X228Th13.1   7.500e+00  6.119e+00   1.226   0.2514
X228Th14    -3.600e+00  6.119e+00  -0.588   0.5708
X228Th14.9  -2.400e+00  6.119e+00  -0.392   0.7040
X228Th15.9  -1.505e-14  5.299e+00   0.000   1.0000
X228Th16.1   4.000e+00  6.119e+00   0.654   0.5297
X228Th16.3   1.000e+01  6.119e+00   1.634   0.1367
X228Th16.6  -1.400e+00  6.119e+00  -0.229   0.8241
X228Th16.7  -1.200e+00  6.119e+00  -0.196   0.8489
X228Th16.8   1.690e+01  6.119e+00   2.762   0.0220 *
X228Th17.3   1.200e+00  6.119e+00   0.196   0.8489
X228Th17.6   2.800e+00  6.119e+00   0.458   0.6581
X228Th17.7   1.900e+00  6.119e+00   0.310   0.7633
X228Th17.8  -1.900e+00  6.119e+00  -0.310   0.7633
X228Th18     4.000e+00  6.119e+00   0.654   0.5297
X228Th18.4   2.467e+00  4.996e+00   0.494   0.6333
X228Th18.7   6.200e+00  6.119e+00   1.013   0.3374
X228Th18.8  -3.656e-14  6.119e+00   0.000   1.0000
X228Th18.9   1.900e+00  6.119e+00   0.310   0.7633
X228Th19.1   1.250e+00  5.299e+00   0.236   0.8188
X228Th19.2   4.000e-01  6.119e+00   0.065   0.9493
X228Th19.4   1.800e+00  5.299e+00   0.340   0.7419
X228Th19.9   4.700e+00  6.119e+00   0.768   0.4621
X228Th20     2.700e+00  6.119e+00   0.441   0.6695
X228Th20,1   4.600e+00  6.119e+00   0.752   0.4714
X228Th20.1   4.600e+00  6.119e+00   0.752   0.4714
X228Th20.3   4.300e+00  6.119e+00   0.703   0.5000
X228Th20.6   3.200e+00  6.119e+00   0.523   0.6136
X228Th21.3   3.400e+00  6.119e+00   0.556   0.5920
X228Th21.5   5.200e+00  6.119e+00   0.850   0.4175
X228Th21.6   4.533e+00  4.996e+00   0.907   0.3879
X228Th21.8   1.010e+01  6.119e+00   1.651   0.1332
X228Th22     4.700e+00  6.119e+00   0.768   0.4621
X228Th22.1   4.200e+00  6.119e+00   0.686   0.5098
X228Th22.5   5.100e+00  6.119e+00   0.833   0.4262
X228Th22.8   7.000e+00  6.119e+00   1.144   0.2822
X228Th23.1   1.210e+01  6.119e+00   1.977   0.0794 .
X228Th23.4   1.680e+01  6.119e+00   2.745   0.0226 *
X228Th23.7   3.200e+00  6.119e+00   0.523   0.6136
```

```
X228Th23.8   1.570e+01  6.119e+00   2.566   0.0304 *
X228Th24.5   1.610e+01  6.119e+00   2.631   0.0273 *
X228Th25.3   6.900e+00  6.119e+00   1.128   0.2887
X228Th25.5   3.000e+00  6.119e+00   0.490   0.6357
X228Th25.6   1.420e+01  6.119e+00   2.321   0.0454 *
X228Th25.9   1.450e+01  6.119e+00   2.370   0.0419 *
X228Th26.4   5.500e+00  6.119e+00   0.899   0.3922
X228Th26.5   1.215e+01  5.299e+00   2.293   0.0476 *
X228Th26.8   1.550e+01  6.119e+00   2.533   0.0321 *
X228Th26.9   5.900e+00  6.119e+00   0.964   0.3602
X228Th27.1   6.300e+00  6.119e+00   1.030   0.3301
X228Th28.1   1.700e+01  6.119e+00   2.778   0.0215 *
X228Th28.3   1.400e+01  6.119e+00   2.288   0.0479 *
X228Th28.6   1.570e+01  6.119e+00   2.566   0.0304 *
X228Th29.5   1.440e+01  5.299e+00   2.717   0.0237 *
X228Th29.7   1.930e+01  6.119e+00   3.154   0.0117 *
X228Th30.6   1.640e+01  6.119e+00   2.680   0.0252 *
X228Th30.7   9.200e+00  6.119e+00   1.503   0.1670
X228Th30.8   1.840e+01  6.119e+00   3.007   0.0148 *
X228Th31.9   1.260e+01  6.119e+00   2.059   0.0696 .
X228Th32.3   1.060e+01  6.119e+00   1.732   0.1173
X228Th34.5   1.880e+01  6.119e+00   3.072   0.0133 *
X228Th41     1.120e+01  6.119e+00   1.830   0.1004
X228Th5.1   -1.200e+00  6.119e+00  -0.196   0.8489
X228Th7     -3.200e+00  6.119e+00  -0.523   0.6136
X228Th7.1   -3.100e+00  6.119e+00  -0.507   0.6246
X228Th7.4   -2.600e+00  6.119e+00  -0.425   0.6809
X228Th7.6   -8.000e-01  6.119e+00  -0.131   0.8989
X228Th8.8    5.000e-01  6.119e+00   0.082   0.9367
X228Th9.2    1.500e+00  6.119e+00   0.245   0.8119
---
Signif. codes:  0 ‘***’ 0.001 ‘**’ 0.01 ‘*’ 0.05 ‘.’ 0.1 ‘ ’ 1

Residual standard error: 4.327 on 9 degrees of freedom
Multiple R-squared:  0.9487,    Adjusted R-squared:  0.5499
F-statistic: 2.379 on 70 and 9 DF,  p-value: 0.07999
```

APPENDIX M: Sediment Model between all elements

```
Call:
lm(formula = X228Ra ~ X232Th + X228Th + X40K + X226Ra, data = df)

Residuals:
    Min      1Q  Median      3Q     Max
-6.3637 -1.2955 -0.0566  0.9016  7.3977

Coefficients:
             Estimate Std. Error t value Pr(>|t|)
(Intercept) -1.456544   1.348194  -1.080   0.2834
X232Th       1.680992   0.142976  11.757  < 2e-16 ***
X228Th      -0.753465   0.090119  -8.361 2.45e-12 ***
X40K         0.004029   0.001591   2.533   0.0134 *
X226Ra       0.022322   0.036294   0.615   0.5404
---
Signif. codes:  0 ‘***’ 0.001 ‘**’ 0.01 ‘*’ 0.05 ‘.’ 0.1 ‘ ’ 1

Residual standard error: 2.515 on 75 degrees of freedom
Multiple R-squared:  0.7578,    Adjusted R-squared:  0.7449
F-statistic: 58.66 on 4 and 75 DF,  p-value: < 2.2e-16
```

APPENDIX N: Sediment Model between ^{228}Ra and ^{232}Th

```
Call:
lm(formula = X228Ra ~ X232Th, data = df)

Residuals:
    Min      1Q  Median      3Q     Max
-7.9845 -1.2968  0.4254  2.0014 12.7367

Coefficients:
             Estimate Std. Error t value Pr(>|t|)
(Intercept)  1.37374    1.84068   0.746    0.458
X232Th       0.69661    0.08251   8.443  1.3e-12 ***
---
Signif. codes:  0 ‘***’ 0.001 ‘**’ 0.01 ‘*’ 0.05 ‘.’ 0.1 ‘ ’ 1

Residual standard error: 3.622 on 78 degrees of freedom
Multiple R-squared:  0.4775,    Adjusted R-squared:  0.4708
F-statistic: 71.28 on 1 and 78 DF,  p-value: 1.302e-12
```

APPENDIX O: Sediment Model between ^{40}K and ^{232}Th

```
Call:
lm(formula = X40K ~ X232Th, data = df)

Residuals:
    Min      1Q  Median      3Q     Max
-240.25 -168.67  -45.98  187.74  280.92

Coefficients:
            Estimate Std. Error t value Pr(>|t|)
(Intercept)  191.597     92.483   2.072   0.0416 *
X232Th         5.236      4.146   1.263   0.2103
---
Signif. codes:  0 ‘***’ 0.001 ‘**’ 0.01 ‘*’ 0.05 ‘.’ 0.1 ‘ ’ 1

Residual standard error: 182 on 78 degrees of freedom
Multiple R-squared:  0.02004,  Adjusted R-squared:  0.00748
F-statistic: 1.595 on 1 and 78 DF,  p-value: 0.2103
```

APPENDIX P: Sediment Model between ^{228}Th and ^{232}Th

```
Call:
lm(formula = X228Th ~ X232Th, data = df)

Residuals:
     Min       1Q   Median       3Q      Max
-10.0754  -2.2722  -0.3377   1.0385   8.2680

Coefficients:
            Estimate Std. Error t value Pr(>|t|)
(Intercept) -2.55452    1.74552  -1.463    0.147
X232Th       1.35219    0.07824  17.282   <2e-16 ***
---
Signif. codes:  0 ‘***’ 0.001 ‘**’ 0.01 ‘*’ 0.05 ‘.’ 0.1 ‘ ’ 1

Residual standard error: 3.435 on 78 degrees of freedom
Multiple R-squared:  0.7929,    Adjusted R-squared:  0.7903
F-statistic: 298.7 on 1 and 78 DF,  p-value: < 2.2e-16
```